Performance Analysis of a Solar Refrigeration System

A Thesis Submitted To

Nirma University

In Partial Fulfillment of the Requirements For

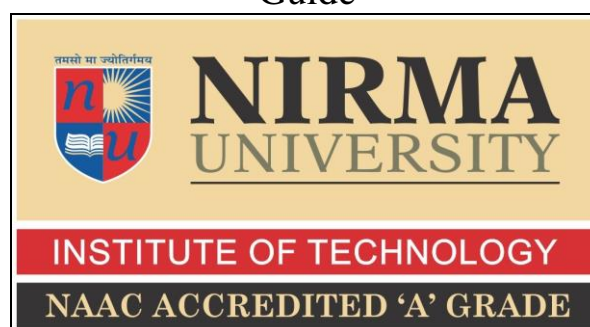The Degree of

Doctor of Philosophy

In

Technology & Engineering

By

Virang Hareshchandra Oza (11EXTPHDE62)

Dr N M Bhatt
Guide

Mechanical Engineering Department
Institute of Technology
Nirma University
Ahmedabad-382481
Gujarat, India
September, 2018

Nirma University
Institute of Technology

Certificate

This is to certify that the thesis entitled **Performance Analysis of a Solar Refrigeration System** has been prepared by **Mr. Virang Hareshchandra Oza** under my supervision and guidance. The thesis is his own original work completed after careful research and investigation. The work of the thesis is of the standard expected of a candidate for Ph.D. Programme in **Technology & Engineering** and I recommend that it be sent for evaluation.

Date: 29\9\2018

Guide Dr N M Bhatt

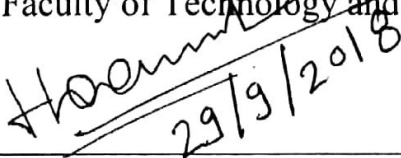Forwarded Through:

(V.J. Lakhera)
(i) Head of the Department

R N PATEL
(ii) Additional Director

(iii) Dean Faculty of Technology and Engineering

29/9/2018
(iv) Dean Faculty of Doctoral Studies and Research

To:
Executive Registrar
Nirma University

Nirma University
Institute of Technology

<u>Declaration</u>

I, **Virang Hareshchandra Oza**, registered as Research Scholar, bearing Registration No. **11EXTPHDE62** for Doctoral Programme under the Faculty of **Technology & Engineering** of Nirma University do hereby declare that I have completed the course work, pre-synopsis seminar and my research work as prescribed under R. Ph.D. 3.5.

I do hereby declare that the thesis submitted is original and is the outcome of the independent investigations / research carried out by me and contains no plagiarism. The research is leading to the discovery of new facts / techniques / correlation of scientific facts already known. (Please tick whichever is applicable). This work has not been submitted to any other University or Body in quest of a degree, diploma or any other kind of academic award.

I do hereby further declare that the text, diagrams or any other material taken from other sources (including but not limited to books, journals and web) have been acknowledged, referred and cited to the best of my knowledge and understanding.

Date: 29|09|2018

Signature of the student

Dr N M Bhatt
Supervisor

ACKNOWLEDGEMENT

I would like to express my sincere gratitude to god, my parents, and family members, whose blessings have made me whatever I am today.

I wish to express my sincere gratitude, regards and thanks to my respected supervisor Dr N M Bhatt for his invaluable guidance, support and encouragement. It is my achievement to be guided under him. He has been a constant source of encouragement & momentum that any intricacy becomes simple. I gained a lot of invaluable guidance & prompt suggestions from him during my Research work. I remain obliged of him forever & I take pride to work under him. I am very much thankful to Nirma University for providing me an opportunity to pursue Doctor of Philosophy and huge support during the tenure of research work. I am very much thankful to Institute of Technology, Nirma University for providing me an opportunity to pursue Doctor of Philosophy and huge support during the tenure of research work. I wish to express my sincere gratitude and thanks to Dr. S A Chaniwala, Member of RPC, Professor, SVNIT, and Dr. R N Patel, member of RPC and Additional Director, School of Engineering, *Institute of Technology,* for their invaluable guidance, suggestions and support during entire work of Doctor of Philosophy. I am thankful to Dr. V J Lakhera, Head of Department, Mechanical Engineering, Institute of Technology, for providing me necessary facility at the Department of Mechanical Engineering and also providing me invaluable guidance and motivation. I am thankful to Dr. Alka Mahajan, Dean, FoTE for her support and encouragement. I am thankful to Dr. Dhaval Pujara, Dean, FDSR for his support and encouragement. I am thankful to all administrative staff of Nirma University for providing me huge support. Further, I am thankful to all the respected faculty members and supporting staff at Department of Mechanical Engineering for their overall support and encouragement.

Oza Virang H.

(11EXTPHDE62)

Abstract

Because of limited sources of fossil fuels and environmental issues like global warming, researchers are focusing on renewable energy sources and mainly solar energy as it is clean, inexhaustible and abundantly and universally available source of renewable energy without any environmental pollution. Along with use of fossil fuels which are the major contributors to the climate change and global warming, the demand of refrigeration and air conditioning has increased drastically. The need of using eco-friendly refrigerants and refrigeration system using low grade energy has increased since long, which eventually increases the need of solar energy for refrigeration system. In present work, thermodynamic analysis of 3 TR ammonia-water absorption refrigeration system with and without ejector was carried out to obtain maximum performance of the system. Thermodynamic analysis of absorption refrigeration system with ejector was carried out for various combinations of condenser temperatures of 45°C and 35°C and evaporator temperatures of 15°C and 5°C and results were compared with conventional absorption refrigeration system. For combined ejector-absorption refrigeration system, effect of the generator temperature on coefficient of performance (COP) was studied for the different value of entrainment ratio in the range of 0.04 to 0.14. COP of combined cycle is improved by 14.66% to 30.1% compared to conventional cycle. Results indicate that combined ejector absorption refrigeration system requires generator pressure of 45 bar for condenser and evaporator temperatures of 45°C and 5°C respectively at the entrainment ratio of 0.14. Even for low entrainment ratio, ejector inlet pressure is twice as compared to conventional absorption refrigeration system for higher condenser and lower evaporator temperatures which causes practical limitations of solution pump. Due to the limitation further development was carried with conventional absorption refrigeration system. First and second law analysis of 3 TR absorption refrigeration system with refrigerant and solution heat exchangers was carried out to obtain maximum performance of the system at optimum generator temperature. Major components of absorption refrigeration system are generator, rectifier, condenser, refrigerant heat exchanger (RHE), expansion device, evaporator, absorber, pump, solution heat exchanger (SHE), and pressure reducing valve. The effect of generator temperature and effectiveness of SHE and RHE on COP, total entropy generation and exergetic efficiency for the different values of evaporator and condenser temperatures was studied. Results show that higher value of evaporator temperature, lower value of condenser temperature and higher values of effectiveness of SHE and RHE gives better performance of the system. The results show that

for Indian weather condition, considering condenser temperature of 50ºC and evaporator temperature of 10ºC for the application of summer air conditioning, maximum COP obtained is 0.525 at optimum generator temperature of 170ºC. Optimization of the parameters of ammonia-water absorption refrigeration system using Taguchi design was also carried out. Multi linear Regression analysis was also carried out to obtain best equations of COP and exergetic efficiency of 3 TR absorption refrigeration system. COP and exergetic efficiency were considered as objective functions and condenser, evaporator, and generator temperatures as well as solution heat exchanger and refrigerant heat exchanger effectiveness were considered as independent parameters. L16 orthogonal array was selected for Taguchi method of design of experiment. Maximum COP is obtained at lower condenser and higher evaporator temperature and maximum exergetic efficiency is obtained at lower condenser and lower evaporator temperature for the selected Taguchi design. Optimum COP was 0.65 and optimum exergetic efficiency was 23.94% for the selected Taguchi design. From signal-to-noise ratio analysis optimum COP calculated was 0.6612 at $T_c = 35ºC$, $T_e = 10ºC$, $T_g = 150ºC$, $\varepsilon_{RHE} = 0.6$ and $\varepsilon_{SHE} = 0.75$ and optimum exergetic efficiency calculated was 24.74% at $T_c = 35ºC$, $T_e = -5ºC$, $T_g = 120ºC$, $\varepsilon_{RHE} = 0.6$ and $\varepsilon_{SHE} = 0.75$. An evacuated glass tube based parabolic trough collector was conceived to supply heat to the absorption refrigeration system. To understand the effect of solar radiation on efficiency and required mass flow rate for desired air outlet temperature in the range of 150 to 190ºC, simulation was carried out for solar radiation between 500 and 1100 W/m^2, assuming air inlet temperature of 35ºC. Simulation results of solar powered absorption refrigeration system are also presented. Effect of generator temperature on solar COP for the different values of concentration ratio (CR) in the range of 2 to 4 of evacuated glass tube based parabolic trough solar collector was studied. Results show that solar COP increases with increase in CR. Solar COP is maximum between 140º and 150ºC generator temperature for the CR in the range of 2 to 4. In present work concentration ratio 3 is selected as it was intended to adjust the tilt of the collector once in a day. With higher CR, acceptance angle decreases which increases incidence losses and solar radiation is effectively utilized only around solar noon if the collector is not tracked continuously. From the simulation results, it was observed that for the concentration ratio of 3, maximum Solar COP is 0.3164 at optimum generator temperature of 150ºC. To validate the simulation results and to evaluate the benefit of using turbulator, two identical collectors, one with turbulator and the other without turbulator were constructed and tested under outdoor field conditions at Rajkot, Gujarat, India (latitude 22.3039ºN, longitude 70.8022ºE). It was intended to achieve air temperature of more than 170ºC for six hours.

Experiments were carried out for the mass flow rate from 4.32 kg/h to 13.68 kg/h. For mass flow rates of 4.32 kg/h and 6.12 kg/h, efficiency of collector with turbulator is about 24% higher compared to that without turbulator, while for mass flow rates of 10.8 kg/h and 13.68 kg/h, efficiency of collector with turbulator is 4.73% and 3.57% higher compared to without turbulator. For mass flow rates of 6.12 kg/h and lower, the collector with turbulator is capable of delivering heat at temperature higher than 170°C for more than 6 h per day. Pressure drop was 2.5 to 4 times higher for collector with turbulator compared to that without turbulator for the mass flow range. It is concluded that evacuated glass tube based parabolic trough collector is technically feasible option to supply heat energy requirement of widely used conventional ammonia-water absorption refrigeration system. This will not only reduce the fast depleting fossil fuel resources but also address the critical environmental issue of global warming.

Contents

List of Figures

List of Tables

Nomenclature

A	area (m^2)
ARS	absorption refrigeration system
COP	coefficient of performance
c	velocity (m/s) {for ARS}
c_p	specific heat (kJ/kg K)
CR	concentration ratio
d	diameter (m)
d_h	hydraulic diameter (m)
$d_{it.o} = d_{abs}$	outer/absorber diameter of outer glass tube (m)
$d_{ot.i}$	inner diameter of outer glass tube (m)
$d_{it.o}$	outer diameter of inner glass tube (m)
$d_{it.i}$	inner diameter of inner glass tube (m)
$d_{at.o}$	outer diameter of air tube (m)
$d_{at.i}$	inner diameter of air tube (m)
e	enhancement factor
ETC	evacuated glass tube
E-W	east-west
f	specific rich solution circulation
f'	specific poor solution circulation
h	enthalpy (kJ/kg) {for ARS}
h	convective heat transfer coefficient {for solar system}
HE	heat exchanger
I_t	solar insolation (W/m^2)
k	thermal conductivity (W/ m K)
l_u	useful length of glass tube (m)
$\dot{m}$	mass flow rate (kg/s) (for ARS)
m	mass flow rate (kg/s) (for EGTSC)
n	number

N-S	north-south
Nu	nusselt number
p	pressure (kPa) {for ARS}
p	perimeter (m) {for solar systrm}
PCM	phase change material
Pr	Prandtl number
Q	heat transfer rate (W)
Q_a	heat absorbed (W) {For solar collector}
Q_i	solar radiation intercepted (W)
Q_r	heat reflected (W) {For solar collector}
Q_{rl}	radiation losses (W)
Q_u	useful heat gain (W)
R	resistance
Re	Reynold's number
RHE	refrigerant heat exchanger
s	entropy (kJ/kg K)
S_{gen}	entropy generation rate (W/K)
SHE	solution heat exchanger
SN	signal-to-noise
T	temperature (ºC)
t	thickness (m)
T_m	bulk mean temperature (ºC)
TR	ton of refrigerant
v	specific volume (m^3/kg) {for ARS}
v	velocity (m/s) {for solar collector}
vol	volume flow rate (m^3/kg) {for solar collector}
W	work (W)
w	width (m)
x	ammonia mass fraction (kg/kg of solution)
Yi	measured value of quality characteristics (COP or exergetc efficiency)
α	absorptivity

ε	heat exchanger effectiveness {for ARS}, and emissivity {for solar system}
η	efficiency
γ	reflectivity
μ	entrainment ratio
σ	stefan boltzmann constant (W/ m^2 K^4)
ρ	density (kg/m^3)

Subscripts

a	absorber {for ARS}
abs	absorber {for evacuated glass tube solar collector}
$abs.av$	average absorber
amb	ambient
anu	annulus
ap	aperture
at	air tube
av	average
$bl.hwt$	blockage due to helical wiry turbulator
c	condenser
cs	cross section
e	evaporator
eff	effectiveness
exe	exergetic
$\exp$	expansion
fi	fluid inlet
fm	flow meter
fo	fluid outlet
g	generator
gc	glass cover
$gc.av$	average glass cover
hs	holding spring

hwt	helical wiry turbulator
in	inlet
n	nozzle
out	outlet
p	pump
para	parabola
r	rectifier
ref	reflector
RHE	refrigerant heat exchanger
sc	solar collector
SHE	solution heat exchange
sky	sky
tot	total
u	useful
*v*1	pressure reducing valve
*v*2	throttle valve
w	wind
0	ambient condition

Chapter 1

Introduction

1.1 General

Development of any country depends on energy consumption rate in the country. In case of developing countries, the energy sector assumes an acute significance in view of ever-increasing energy needs demanding huge investments to meet them. Globalization and increase in the standard of living have caused in the peak demand for electrical energy [1]. Energy consumption of a nation is mostly divided into the following sectors:

- Agriculture sector
- Domestic sector
- Industry sector
- Transport sector

Per capita energy consumption of a country is an index of the standard of living of the people of that country. Therefore, energy has become an important and one of the basic foundations for economic development of a country. Energy sources can be classified based on following criteria:

- Primary and Secondary energy source
- Commercial and Noncommercial energy sources
- Renewable and Non-Renewable energy sources

1.1.1 Primary and secondary energy sources

Primary energy sources are those which are either found or stored in nature. Some of the common primary sources are coal, oil, natural gas etc. Some other available primary energy sources are nuclear energy from radioactive substances, thermal energy stored in earth's interior, and potential energy due to earth's gravity. The energy converted mostly from primary energy for industrial utilities are called secondary energy.

1.1.2 Commercial and noncommercial energy sources

The energy source which is available in the market with some price is called commercial energy like electricity, coal and refined petroleum products etc. The energy source which is not available in the market for a price is known as noncommercial energy sources like firewood, agro waste in rural areas; solar energy for water heating etc.

1.1.3 Renewable and non-renewable energy sources

Renewable energy is the energy obtained from sources that are essentially inexhaustible like solar energy, wind energy, bio energy, geothermal energy, tidal energy and hydro energy. Non-renewable energy are likely to exhaust with time like fossil fuels such as coal, oil and gas.

Today's climate change is recognized as one of the biggest threats to nature and humanity. Our dependence and excessive use of fossil fuels are the most important contributors to climate change; thus addressing the energy issue is fundamental to undertaking climate change. Following points may be considered with this connection.

- The demand of energy is increasing by leaps and bounds due to rapid industrialization and population growth, and hence the conventional source of energy will not be sufficient to meet the growing demand.

- Conventional sources (except hydro) will finish up one day.

- Conventional sources also cause pollution; thereby their use degrades the environment.

- Large hydro resources affect wildlife, cause deforestation and posture various social problems.

The renewable energy sources such as solar, wind, tidal, biomass, geothermal are environment friendly and present in nature provide a potential way in reducing emissions while meeting future energy needs of both developed and developing countries.

1.2 Need of solar energy

To meet the future demand of energy and pollution free environment it is required to adopt renewable source of energy like solar, wind, tidal, biomass, geothermal etc. Wind energy is used to generate the electricity by turning blades on a wind turbine. Wind energy is an important resource; it is safe, clean, and ample. It is non-polluting and freely available in many areas. It is appeared as most economical of all renewable energy sources. Biomass energy is energy resources available from animal and vegetarian. It is important resource especially in rural areas. Biomass material may be transformed by biological process to produce biogas, producer gas, ethanol and charcoal. It depends on the enough quantity of waste material and it requires huge space. Tidal energy is the energy generated due to water waves generated in the ocean. It is available at coastal areas only. Geothermal energy is derived from the huge amount of thermal energy underneath the earth. This heat is brought to the surface of earth and can be used for power generation. Geothermal is not feasible everywhere on earth surface. Solar energy can be a major source of power. The energy reaching the earth is approximately 1.8×10^{11} MW which is many thousands of time greater than the present consumption rate on the earth. The solar energy receives on the surface of the earth on a bright sunny day at noon is approximately up

to 1 kW/m^2. The earth continuously intercepts solar energy. But, so far it is not developed on large scale. Sun remains most important supplies of energy especially when other sources are exhausting. It gives nonpolluting environmental friendly output and available throughout the year in plenty in India.
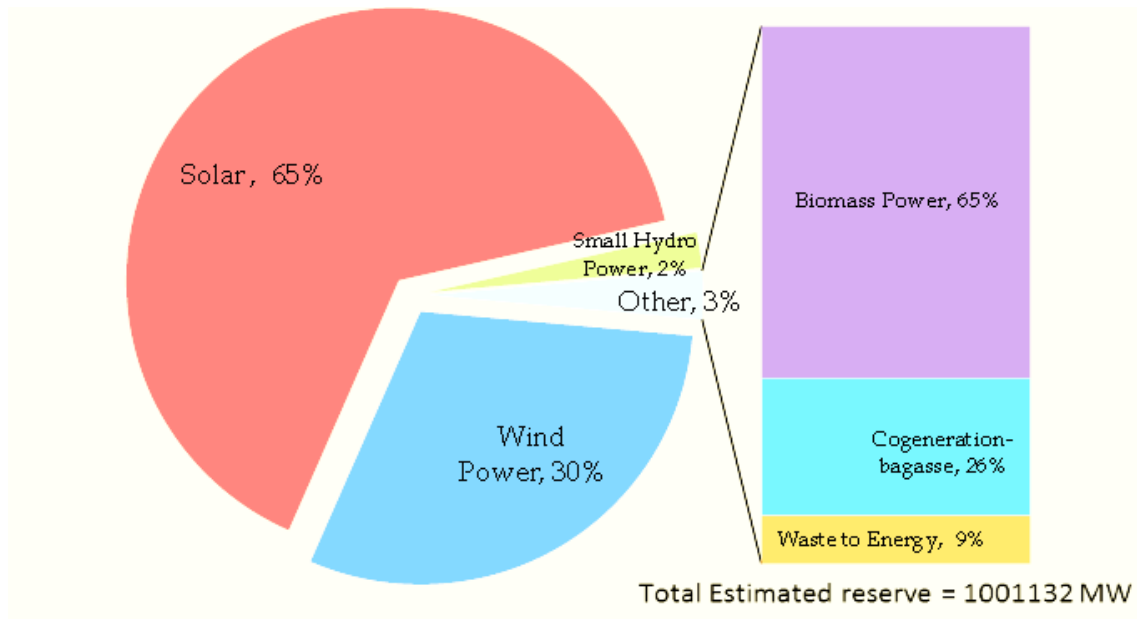
Fig 1.1 Source wise estimated potential of renewable power in India as on 31.03.2017 [2]

Fig 1.1 shows the source wise estimated potential of renewable energy in India as on 31.03.2017, which indicates that solar energy has maximum (65%) potential out of all other renewable energy sources. The total potential of solar energy generation in India on 31.03.2017 was 649342 MW, which is 64.86% of total renewable energy generation [2]. Fig. 1.2 shows the overall renewable energy capacity and future estimate in India [3]. It indicates that renewable energy capacity will increase by approximately 6.3 times in the year 2030 compared to it in the year 2017. Between 2017 and 2030, the share of renewables is expected to reach over 43% in capacity terms. Out of which maximum increase in capacity in India is of solar energy as per Fig 1.2.
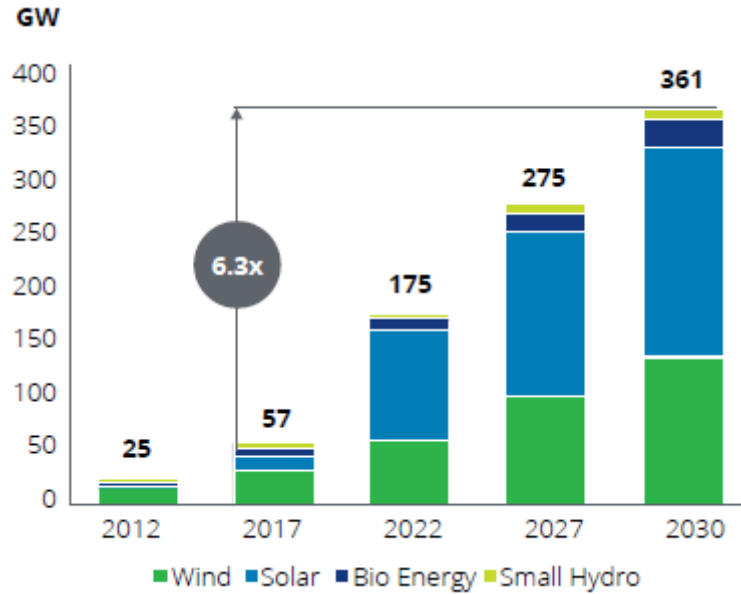
Fig 1.2 The overall renewable energy capacity in India [3]

Table 1.1 shows the global renewable energy scenario by 2040. By 2040 approximately half of energy will develop by renewable energy. As compared to present, approximately 10 times solar thermal energy will develop by 2040. Therefore solar thermal source will be more significant source in future [1].

It can be concluded that from all renewable energy sources, solar energy is the most reliable for the future use in tropical zone of India as well as globally where sufficient solar radiations are available. The sun radiates energy uniformly in all directions in the form of electromagnetic waves. It is a clean, inexhaustible, abundantly and universally available source of renewable energy. The drawbacks of solar energy are that it is dilute form of energy, which is available intermittently and uncertainly, and not steadily and continuously.

Peak incident solar radiation frequently accords with peak daytime demand and therefore it can be well matched to suit commercial power needs. Solar energy can be utilized directly in two ways: (1) by collecting the radiant heat and using it in a thermal system, or (2) by collecting and converting it directly to electrical energy using a photovoltaic system [4].

5

Table 1.1 Global renewable energy scenario by 2040 [1]

Particular	2001	2010	2020	2030	2040
Total consumption					
[in Million ton of oil equivalent (Mtoe)]	10038	10549	11425	12352	13310
Biomass	1080	1313	1791	2483	3271
Large hydro	22.7	266	309	341	358
Geothermal	43.2	86	186	333	493
Small hydro	9.5	19	49	106	189
Wind	4.7	44	266	542	688
Solar thermal	4.1	15	66	244	480
Photovoltaic	0.2	2	24	221	784
Solar thermal electricity	0.1	0.4	3	16	68
Tidal/Wave/Ocean)	0.05	0.1	0.4	3	20
Total renewable energy sources	1366	1746	2694	4289	6351
Renewable energy sources contribution (%)	8.3	10.6	16.4	26.1	38.6

1.3 Solar energy for refrigeration system

In hot and dry climate, processes such as evaporative cooling can offer energy conservation prospects. Only low energy cooling technologies can't satisfy the total required cooling demand of domestic residences in summer time due to high temperature. Therefor active cooling systems are required. Vapour compression refrigeration systems are generally powered by electricity, which is expensive. Its production mainly depends on fossil fuels. In such condition solar energy can be used to power an active solar cooling system based on absorption cycle. Initial cost of solar absorption machine is higher than that of vapour compression refrigeration system but its running cost is very less. Solar absorption refrigeration systems are not readily available in the small capacity range applicable to domestic cooling applications. Less use of conventional vapour compression system will also reduce their effect on both global warming and ozone layer depletion [5].

Solar energy can be used for refrigeration required for preserving food, chilling applications, heating applications, etc. Solar cooling looks like an attractive technique due to fact that when the cooling demand is more, the sunshine is robust. Considerable work on solar cooling systems have been done in last four decades. The utilization and commercialization of solar cooling is not as well-known as other solar energy applications like solar water heating and solar space heating.

There are several ways of using solar energy for cooling such as:

- Absorption cycle with liquid absorbents such as LiBr – H_2O, H_2O-NH_3, NH_3–NaSCN etc.
- Absorption cycle with solid absorbents such as $CaCl_2$-NH_3.
- Adsorption cycle with solid adsorbents such as Silica gel- H_2O, Zeolite-H_2O.
- Vapour compression cycle using a solar powered Rankine cycle.
- Vapour compression cycle with the compressor driven by electricity from photovoltaic panels.

The performance of cooling process is judged from its COP, which is the ratio of cooling produced to energy input. The overall COP for a Rankine cycle operated solar cooling system is of about 0.3 to 0.4, which very much dependent on solar collector efficiency. The vapour compression cooling process operated by photovoltaic panels gives a COP in the range of 0.25 to 0.35 due to lower solar cell efficiency. A single stage chiller has a COP of about 0.6 for ammonia-water and about 0.7 for LiBr-H_2O system, while double effect chiller have COP's in the range of 0.8 to 1.2. The cooling system based on closed absorption cycle gives a Solar COP of about 0.10 to 0.20 depending on the collector efficiency and based on adsorption cycle operates at Solar COP of about 0.2 [6].

1.4 Objectives of present work

The main objective of present research work is to carry out first and second law analysis of solar powered ammonia-water absorption refrigeration system as well as experimental investigation of evacuated glass tube based parabolic trough collector with helical wiry

turbulator for the solar absorption refrigeration system. The specific objectives of present research work are as below:

- To carry out thermodynamic analysis of ammonia-water absorption refrigeration system with and without ejector of 3 TR capacity to obtain performance at optimum generator temperature and to determine the effect of generator temperature on COP, total entropy generation and exergetic efficiency.
- To study the effect of generator temperature on Solar COP for the different values of concentration ratio (CR) of evacuated glass tube based parabolic trough solar collector with helical wiry turbulator and hence to determine maximum Solar COP at optimum generator temperature.
- To develop thermal model of the evacuated glass tube based parabolic trough collector to predict the thermal efficiency and useful heat gain of the collector under different operating conditions.
- To evaluate the performance of evacuated glass tube based parabolic trough collector with and without helical wiry turbulator for concentration ratio of 3 under outdoor field conditions at Rajkot, Gujarat, India (latitude 22.3039ºN, longitude 70.8022ºE).

1.5 Outline of thesis

Chapter 1 presents the basic introduction and need of solar cooling system. Chapter 2 presents literature survey of vapour absorption systems (VASs), solar collectors which can cater the heat requirement of the VASs and various solar refrigeration systems. Chapter 3 describes thermodynamic analysis and optimization of ammonia-water absorption refrigeration system with and without ejector. Absorption refrigeration system is then considered to be powered by evacuated glass tube based parabolic trough collector with helical wiry turbulator. Analysis of absorption refrigeration system coupled with evacuated glass tube based parabolic trough collector with helical wiry turbulator is outlined in chapter 4. The details of experimental set up, experimental procedure, experimentation and validation of results are given in chapter 5. Chapter 6 summarizes the conclusions drawn from present research work and scope for future work.

Chapter 2

Literature review

The aim of this chapter is to present a review of state of the art in the field of absorption refrigeration systems, high temperature solar collectors which can cater the need of the absorption refrigeration systems and solar refrigeration systems based on absorption cycles. Absorption refrigeration system is evaluated using energy and exergy analysis which are based on first and second law of thermodynamics respectively. While assessing various solar absorption refrigeration systems, COP and solar COP of the systems play a vital importance in comparing these systems.

2.1 Necessity of solar cooling techniques

Our dependence and excessive use of fossil fuels are the most important contributors to the today's climate change, which is recognize as one of the biggest threats to nature and humanity.

Therefore to meet the future demand of energy and pollution free environment it is necessary to adopt renewable energy sources. Along with use of fossil fuels which are the major contributor to the climate change and global warming, the demand of refrigeration and air conditioning have increased drastically. Since many decades vapour compression refrigeration systems have been operated with CFC, HCFC, and HFC refrigerants. These refrigerants deplete ozone layer and cause global warming. Solar powered cooling systems are the best alternative of conventional refrigeration systems as a green cold production [7]. Through the application of phase change material (PCM) in solar thermal systems, CO_2 emission could be reduced by 3.43% by 2020 [8]. The significance and demand of using eco-friendly refrigerants and refrigeration systems using low grade energy eventually increase the need of solar energy for refrigeration system. Solar energy can be used for refrigeration required for preserving food, chilling applications, heating applications etc. It is estimated that about 45% of household energy consumption is used for cooling. Likewise, 10-20% of all electricity produced is consumed for refrigeration and air conditioning. Solar cooling looks like an attractive option due to fact that when the cooling demand is more, the sunshine is robust. Conventional vapour compression refrigeration system are dominating electricity consumers and their operation cause high electricity peak loads during the summer, especially in the countries of tropical climate [9]. Solar thermal energy can be easily captured all over the world, because of constant availability of sunshine. Solar thermal energy has been used since last few decades in all over the world for industrial use as well as residential cooling purposes, but mainly it can be used in remote areas or islands where conventional cooling is difficult [10]. Because of the risk of a global energy scarcity, researchers have progressively paid more attention to solar energy [11].

2.2 Absorption refrigeration system

Absorption refrigeration is one of the oldest refrigeration technologies, which began in 1700s. Ice was produced by evaporating pure water within the evacuated container with sulfuric acid [12]. In 1859, a French engineer named Ferdinand Carre developed machine using ammonia-water as working fluid pair, while in 1950, a new system using LiBr-H_2O as working fluid pair was introduced for commercial purposes [12]. In absorption refrigeration system mechanical compressor is replaced by an absorber, a generator and a pump. Main components of absorption refrigeration system are a condenser, a refrigerant heat exchanger, an expansion valve, an

evaporator, an absorber, a pump, a solution heat exchanger, a generator, a pressure reducing valve, and a rectifier. Attractive features of absorption refrigeration system are: it can work on low grade energy like solar energy, waste heat etc., except pump no moving parts are there means no chance of leakage, it can work on low evaporator pressure without affecting the COP, it is not affected by load variation, and it does not required electricity. Different researchers have worked on absorption refrigeration system (ARS). Literature in present section is of ARS using ammonia-water as working fluid pair as it is selected for analytical work.

Ataer and Gogus [13] carried out comparative study of irreversibility in ammonia-water absorption refrigeration by second law analysis. Their results showed that high exergy loss was observed in evaporator and absorber at the given operating conditions. Their results also showed that the exergy loss of the condenser was drop to 5% of the total exergy loss at low evaporator and condenser temperatures as well as at least 15% of the total exergy loss was observed in the absorber with the operating conditions. Dincer and Dost [14] carried out energy analysis of an ammonia-water absorption refrigeration system. They developed a model of absorption refrigeration system. The same was verified with an experimental data taken from the literature. Their results showed that the differences observed between the experimental results taken from the literature and the computed values of heat load and COP are within 5.3% and 9.6% respectively. These values were bit higher because they included the pump load in the definition of COP. Chua et al. [15] carried out thermodynamic modeling of an ammonia-water absorption chiller at the design point. Contribution of heat and mass transfer in the vapour phase within the rectifier and regenerative heat transfer was dominated to the internal losses; about 30% of the theoretical energy inputs dissipated jointly by this two mechanisms. They also found that liquid phase mass transfer within the absorber contributed typically 6% to the 1/COP of the chiller. Their results also showed that heat and mass transfer in the vapour region within the absorbers accounts for approximately 3% of the dissipative losses. Sahoo et al. [16] carried out exergoeconomic optimization of an ammonia-water absorption refrigeration system. They worked to minimize overall operation and paying back cost by using the theory of exergetic cost of an ammonia-water absorption refrigeration system for air conditioning application. Their results showed 14.5% reduction in product cost, with a small 1.81% increment in investment cost. Adewusi and Zubair [17] studied single-stage and two-stage ammonia-water absorption refrigeration systems based on second law of thermodynamic analysis by varying some input design parameters. They calculated COP, total entropy generation of both the

systems as well as entropy generation of each component of ammonia-water absorption refrigeration systems using thermodynamic properties of the working fluids. Second law analysis via entropy generation showed that the single stage system has less energy dissipation of 0.1973 kW/K compared to 0.4627 kW/K for the two stage system. However their results showed that the two-stage system was more efficient with a COP of 0.734 compared to 0.598 for the single stage system. Ezzine et al. [18] performed a second law analysis of an ammonia-water double-effect, double-generator absorption chiller. They determined irreversibility in each component and contribution of each component to the overall system efficiency. Their simulation results indicated that greatest irreversibility found in the absorber, the solution heat exchanger, and the condenser.

Dieter et al. [19] analyzed ammonia-water absorption cooling cycle based on the exergy and structural analysis. They studied how the selection of efficiency parameters affected the results comparing coefficient of structural bonds of heat exchangers obtained from the minimum temperature difference or the product of overall heat transfer coefficient and heat transfer area values. They concluded that for the purpose of a thermo-economic optimization of the cycle, the product of overall heat transfer coefficient and heat transfer area (UA) values are more appropriate, as fixing the UA value of a component its capital cost is approximately constant. Kim and Park [20] performed dynamic simulation of a single-effect ammonia-water absorption chiller. They developed a model based on the continuity of species constituting the ammonia-water mixture and the conservation of energy for each component of absorption chiller. They investigated time constant of the ammonia-water solution. They suggested that mass of the solution filled should be small for rapidly attaining its rated cooling capacity. The best combination of the bulk concentration and the mass of the solution filled for attaining the maximum cooling capacity for the shortest time constant without damaging the cooling capacity significantly is a low mass of the solution of a stronger concentration in a larger generator.

Hasabnis and Bhagwat [21] simulated ammonia-water absorption refrigeration system based on exergetic COP for comparing energy efficiency. They studied effect of various operating parameters to operate absorption refrigeration system at optimum conditions. They compared simulation results with conventional ammonia absorption refrigeration system as well as vapour compression refrigeration system on the basis of COP. Ammonia absorption refrigeration cycle with partial condenser was optimized by varying the percentage of the total cooling load. The

performance was optimum when 21% of the total cooling load was achieved in the partial condenser and 79% cooling load was achieved in the main condenser. According to the results exergetic COP reflected that it was beneficial if low grade heat was available for ammonia absorption refrigeration cycle with intermediate reboiler. Darwish et al. [22] carried out performance analysis and evaluation of a commercial ammonia-water absorption refrigeration system. They found very good agreement between the Aspen plus simulator's results and the experimental measurements. Their results obtained for the effect of the generator heat duty on the COP agreed well with the reported experimental data with a maximum percentage deviation of 1.8%. Their results showed that introducing a throttling process directly before the separator (generator) can ease the separator heat load and improve the COP by up to 20%. Sathyabhama, & Ashokbabu [23] presented polynomial equations used to study the effect of operating variables on the performance of ammonia-water absorption refrigeration system. Their results showed that for condenser and absorber temperature of 25°C, 30°C, and 40°C the maximum COP was 0.75, 0.67, and 0.57 respectively. The corresponding generator temperature were 65°C, 77°C and 97°C respectively. Barhoumi et al. [24] presented exergy analysis of an ammonia-water absorption system for cooling application. They evaluated exergy destruction rate and heat rate in each component of the system. They concluded that the evaporator and condenser heat loads and exergy destruction rates were less than those of the absorber and generator due to the heat of mixing in the solution. Kong et al. [25] carried out thermodynamic and experimental analysis of an ammonia-water absorption chiller. They designed an apparatus for a cooling capacity of 2814 W, which was obtained using electric heater. Their experimental results showed that cooling capacity of apparatus was found between 1900 and 2200 W with the actual COP between 0.32 and 0.36. The actual results were found to lie between 75% and 85% of the calculated values. Their results also showed that the larger irreversibility was caused by spanning the largest temperature and dissipated thermal energy by heat transfer losses at the generator and evaporator.

Matawala and Prabhakaran [26] carried out exergoeconomic analysis of Industrial brine chilling unit using ammonia-water absorption refrigeration system. They analyzed system based on Tsatsaronis's thermo-economic evaluation and optimization method. They selected generator, condenser and evaporator temperatures, pump efficiency and heat exchanger effectiveness as decision variables. They obtained optimum configuration aiming the design improvement for minimum product cost and the overall cost effective system. Ouadha and Youcef [27] examined

through thermodynamic analysis the feasibility of using waste heat from marine diesel engines to drive an ammonia-water absorption system. They carried out thermodynamic study of the cycle for various operating conditions by varying generator, condenser, absorber and evaporator temperatures. Higher performance of the system was obtained at higher generator and evaporator temperature and at low condenser and absorber temperatures. Rashidi et al. [28] studied absorption machine for an ammonia-water system decentralized trigeneration. They investigated effects of evaporator, absorber and boiler temperature on the COP of the cycle. Their results showed that COP of the cycle was increased with increase in evaporator and boiler temperatures, and was decrease with condenser and absorber temperatures. Their simulation showed that generator, absorber and evaporator obtained the highest exergy loss. The system operating with relatively higher evaporator temperatures had better cooling COP and smaller exergetic efficiency as well as increasing the generator temperature improved the cooling COP of the system, but COP left off as the heat source temperature further increased. Anand et al. [29] analyzed the performance of a process steam operated ammonia-water vapour absorption system for cooling and heating applications based on first and second law of thermodynamics. They concluded that cooling and heating COP as well as second law efficiency was increased with the heat source temperature at constant evaporator, condenser, and absorber temperature. They also concluded that COP as well as exergy efficiency was increased with an increase in the evaporator temperature at constant generator, condenser, and absorber temperature.

2.3 Solar absorption refrigeration system

In the 1970s when world suffered from oil crises, solar refrigeration received great concern. There were many projects for the expansion of solar refrigeration technologies, and solar refrigeration sustained to be a significant issue in the 1980s [30]. Many of the solar refrigeration technologies have been developed and available in the market, with cheaper prices than ever as well as with better performance. In present section solar absorption refrigeration system and its literature is discussed.

2.3.1 Single-effect solar absorption system

Resent statistic shows that a single effect absorption refrigeration system is most commonly used and the simplest. Single effect absorption refrigeration system consists of a single absorber and generator as shown in Fig 2.1 Heat is provided in the generator by using solar energy to separate out refrigerant from absorbent. The separated vapour refrigerant passes through condenser, where it is condensed. The condensed refrigerant passes through expansion valve, where its pressure and temperature reduces. This low pressure low temperature refrigerant enters to evaporator, where it absorbs heat from space to be cooled and gets evaporated. This vapour refrigerant absorbed in the absorber by using absorbent and it forms strong solution. This strong solution pumped to generator. The solution heat exchanger can be used to improve the efficiency of the cycle [7].
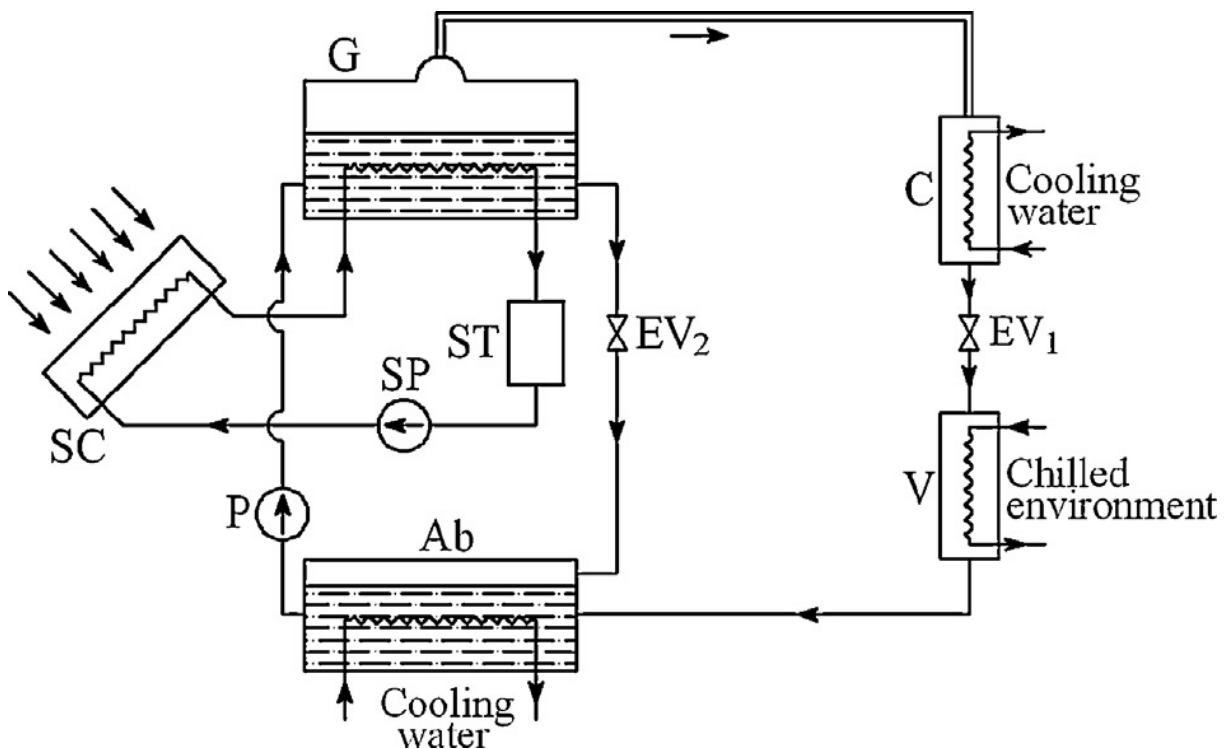
(G: Generator, C: Condenser, EV_1: Expansion valve, V: Evaporator, Ab: Absorber, P: Solution pump, EV_2: Pressure reducing valve, SC: Solar collector)

Fig 2.1 Schematic diagram of single effect solar absorption cooling system [31]

Solar energy can be used to separate out refrigerant from absorbent in the generator. The poor solution separated from refrigerant is returned back to absorber after passing through pressure reducing valve. The system gives better performance when non-volatile working fluid pair like LiBr-H_2O is used, but when it uses volatile working fluid pair like ammonia-water, it requires a rectifier before condenser to provide pure refrigerant to condenser [12].

2.3.2 Double effect solar absorption system

For developing system performance at higher temperature, double effect absorption cooling technology was launched in 1956 [31]. Fig 2.2 shows the double effect solar absorption refrigeration system. Double effect system has two generators. Generator-I (G-I) provides heat to Generator-II (G-II). Working fluid from G-I enters to condenser, where heat is rejected and it enters to evaporator after passes through expansion valve. In evaporator heat is absorbed from the space to be cooled and refrigeration occurs. This working fluid is absorbed in the absorber then it is pumped to G-I after passing through Heat Exchanger-I (HE-I) and Heat Exchanger-II (HE-II). Through this process, HE-II can pass the fluids to G-II and then G-II passes fluid to HE-I. The entire cycle works on three different pressure levels: high, medium and low. Solar collectors provide heat to G-I.
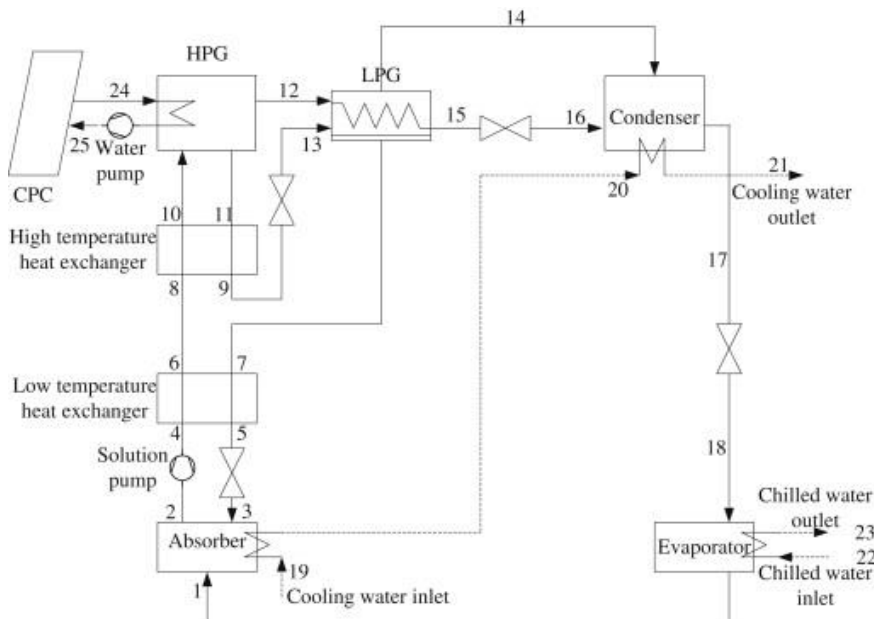
Fig 2.2 Double effect solar absorption refrigeration system [32]

2.3.3 Solar ejector-absorption refrigeration system

A combined solar assisted ejector-absorption refrigeration system using ammonia-water as working fluid pair is illustrated in Fig 2.3. The primary fluid in vapour form at high pressure from generator enters the nozzle of ejector. In the nozzle high velocity fluid creates high vacuum at inlet of mixing chamber and entrain secondary vapour into the chamber from evaporator. The two streams mix in the mixing chamber and then pressure increases to condenser pressure in the diffuser part of the ejector. This mixed stream condenses in the condenser by rejecting heat to atmosphere. The liquid refrigerant enters to evaporator after passing through expansion valve. The liquid refrigerant vaporizes in evaporator by absorbing heat from space/material being cooled, in absorber this low pressure vapour is absorbed by absorbent and produces strong solution. Then it is pumped to generator at high pressure. In the generator low grade solar energy is used to separate out refrigerant from absorbent. This refrigerant rectifies in the rectifier and enters to ejector. The remaining solution called weak solution flows back to the absorber through pressure reducing valve, thus completes the cycle [33]. Sirwan et al. [34] studied effect of adding flash tank on evaporator's thermal load of the combined ejector-absorption cooling system. Their results showed that the cooling effect and evaporator capacity improved by adding flash tank (Fig 2.4).
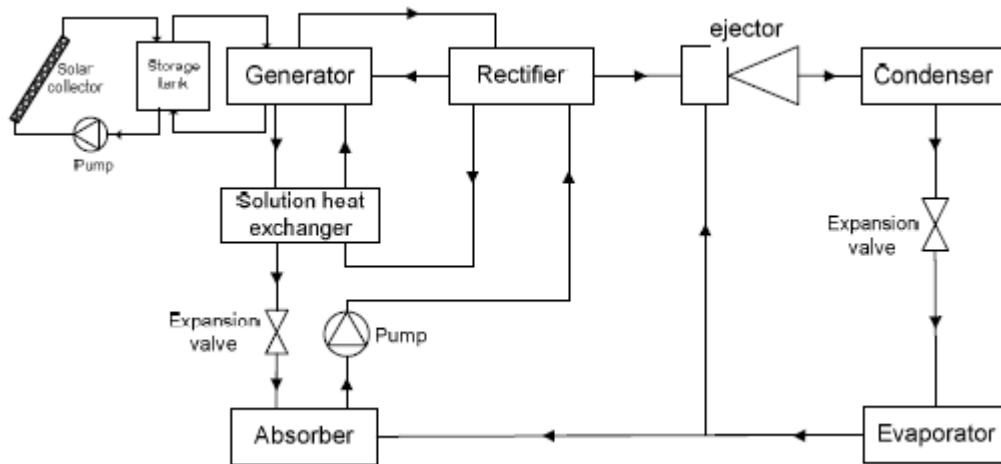
Fig 2.3 Schematic of solar ejector-absorption refrigeration [33]
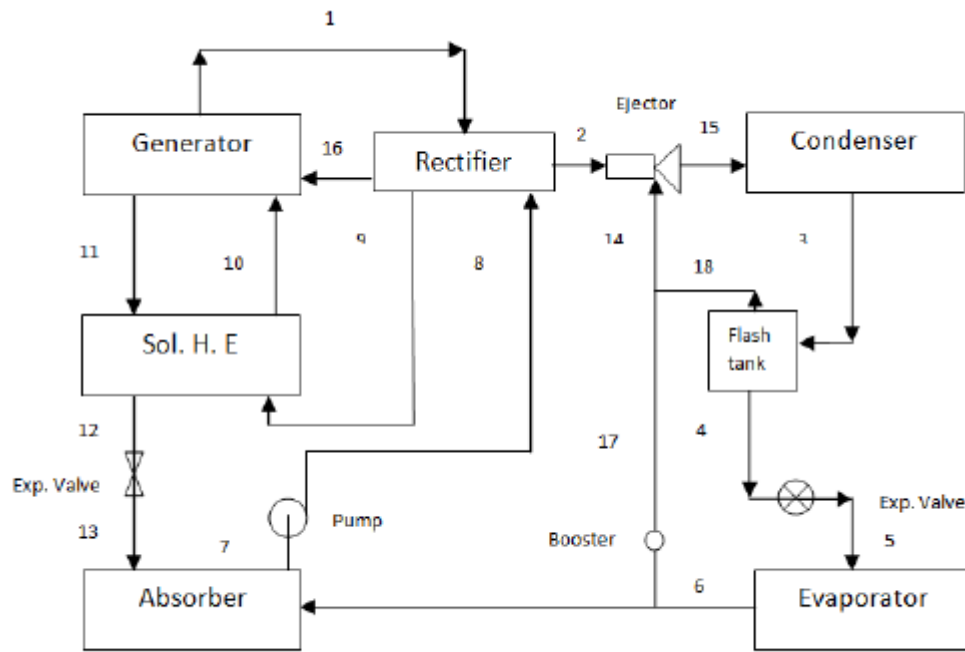
Fig 2.4 Schematic of combined ejector-absorption refrigeration with flash tank [34]

2.3.4 Absorption refrigeration cycl with Generator Absorber heat exchanger (GAX)

An absorber and generator may be considered as counter flow heat exchanger. At absorber, weak solution from generator and vapour refrigerant from evaporator enters at top section. Heat is provided by solar collector to the generator. Rich solution from the absorber enters at top section of generator. Here, the refrigerant become dry out from solution as it is heated by using heat rejected from the top section of absorber. Therefore, a single-effect absorption system can provide as high COP as compared to double effect absorption system by using GAX [35].
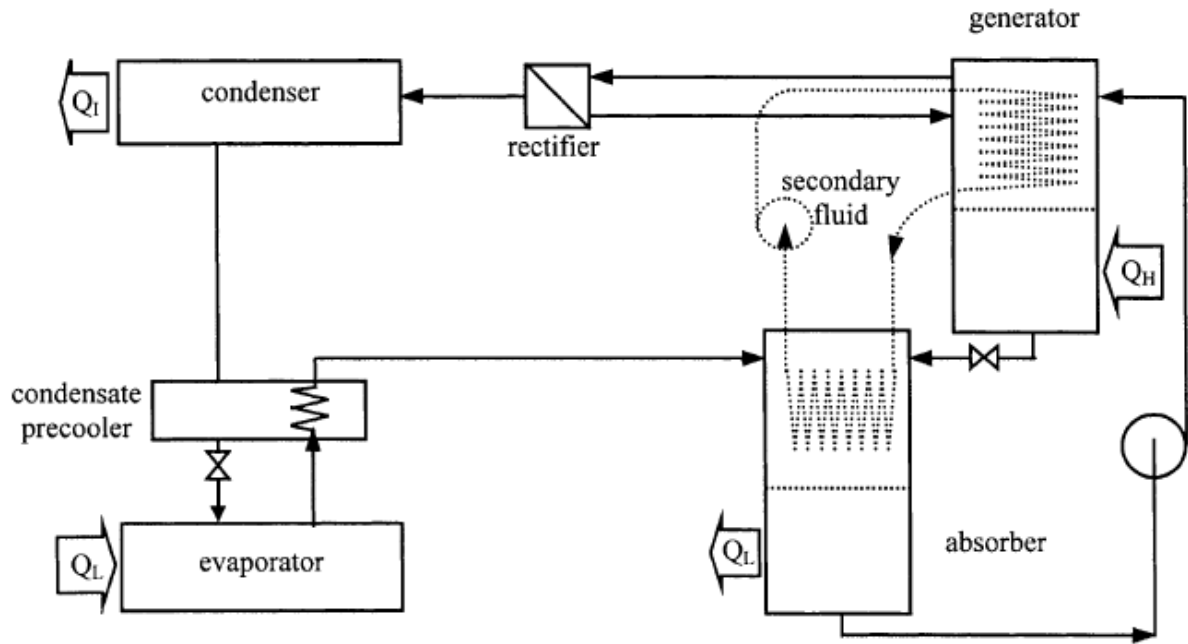
Fig 2.5 Absorption refrigeration cycle with GAX [13]

Staicovici [36] discovered the feasibility of intermittent single-stage solar assisted ammonia-water absorption system for ice production. Intermittent single stage ammonia-water solar absorption system of 46 MJ/cycle was described. Their results indicates that system COP varies from 0.152 to 0.09 in the period of May-September. Alvares and Trepp [37] performed theoretical analysis of ammonia-water refrigeration cycle coupled with solar water heating system using CPC collectors. They worked on ammonia-water refrigeration system starting from basic cycle consisting of generator, condenser, evaporator, absorber, pump and throttle device to the complete cycle with all mentioned components as well as SHE, RHE and rectifier to achieve maximum COP. They also attempted to minimize the solar collector area. Kaushik et al. [38] presented dynamic simulation of solar powered ammonia-water absorption cooling system. The refrigerant mass was not sufficient to meet the cooling load demand during off generation hours hence provision was required to evaluate the additional mass of refrigerant. The concept of refrigerant mass storage was feasible, but it was necessary to integrate it with other storage options. Francisco et al. [39] designed a 2 kW solar power ammonia-water absorptions refrigeration equipment for isolated rural areas. The system operated with a concentration solar power system to obtain the required temperature. According to the results, with small scale equipment, the system can be more efficient if the generator can operate on its own solar power collector. The temperature obtained by solar system was above 150ºC, which was sufficient to operate absorption system. Thermal oil circuit was used to transmit heat to the

19

generator. Adel and Nasiaf [40] worked on solar assisted ammonia-water absorption refrigeration system. The range of maximum generator temperature was 92 - 97ºC and the minimum evaporator temperature was 5 - 10ºC. The range of COP was 0.1096 to 0.2396.

Shankar and Srinivas [41] developed a system which combines the refrigeration cycle and power generation cycle using solar energy. They investigated a system to get duel benefit of system cooling and power from a single system. They concluded that by combining power and cooling system based on solar energy, the performance of cycle was increased by getting the maximum power and cooling output. They obtained maximum power of 58.75 kW and 91.57 kW of cooling with turbine exit temperature of 267.58 K for the mass of 1 kg/s at exit of absorber. Anand et al. [42] presented a numerical study of an evacuated glass tube collector based ammonia-water absorption system. Their results indicated that COP for cooling and COP for heating were lies in the range of 0.012-0.498 and 1.012-1.498 respectively at maximum available solar intensity of 0.9 kW/m^2 corresponds to collector area of 431.7 m^2. It was also observed that maximum exergy loss was in the generator and lowest in the condenser. Siddiqui et al. [43] presented exergoeconomic analysis of a 5 kW ammonia-water absorption refrigeration system with hybrid storage system. They performed the analysis to compare the components of the refrigeration system based on the costs of initial capital investment and the costs of irreversibility. They studied the effect of generator, condenser and evaporator temperature on the exergetic efficiency of the system. Pump and generator showed the highest exergetic efficiencies among the system components for Dhahran region. They concluded that exergetic efficiency of hybrid storage absorption refrigeration cycle was increased with increase in effectiveness value of solution heat exchanger and its performance was better for low temperature cooling effect at reduced condenser temperature. Khan et al. [44] carried out performance assessment of a 10 kW solar powered ammonia-water absorption refrigeration system with storage units. They considered two alternative storage units in the form of child water and ice installed at Dhahran, Saudi Arabia. Their experimental results indicated that a mean chiller COP for cooling the space and chilling the water was found to be 0.8 at generator temperature of 120ºC and average condenser and evaporator temperature of 34.5ºC and -2.2ºC respectively, whereas it was 1.3 for only making ice. Stanciu et al. [45] analyzed one stage ammonia-water absorption cooling system fueled by solar energy. Their simulation emphasized that any change in parabolic trough collector or fully mixed storage tank dimensions would reduce the operation time of the absorption cooling system. They concluded that with 0.19 m^3

storage tank capacity, absorption cooling system operation period was reduced by 40 min from the best exergetic efficiency point of view.

Nakahara et al. [46] developed a single-effect 7 kW cooling capacity LiBr-H_2O absorption chiller supported by a 32.2 m^2 array of flat plate solar collectors. Their results showed that during the summer period the cooling capacity was 6.5 kW. COP of the absorption system was in range of 0.4 to 0.8 at the generator temperature of 70ºC to 100ºC. Hammad and Audi [47] simulated the performance of a non-storage solar assisted LiBr-H_2O absorption system without storage tank. Their results showed that maximum ideal COP of the system was 1.6 while the peak actual COP was 0.55. Hammed and Zurigat [48] studied the performance of 1.5 TR solar assisted LiBr-H_2O absorption system. The system comprises 14 m^2 flat plate solar collector and five shell and tube heat exchangers. The test was carried in Jordan during April and May. Their test results showed actual COP around 0.55. Chen and Hihara [49] evaluated LiBr-H_2O absorption refrigeration cycle which was driven by solar energy and electricity. Their results showed that their cycle had steady refrigeration capacity, a lower heat load of condenser and higher COP. Syed et al. [50] investigated LiBr-H_2O absorption system consisting of 49.9 m^2 of flat plate collector. Their system performed cooling within generator temperatures of 65ºC to 90ºC, maintaining a capacity of 35 kW. Arora et al. [51] analyzed evacuated tube solar collector. The performance characteristic of the collector was analyzed and compared with commercially available brands to power the generator of a LiBr- H_2O absorption chiller. Approximately 20 tubes were required to power the generator of an absorption machine with 1 kW capacity. Raja and Shanmugam [52] reviewed a new approach of solar assisted absorption cooling system to minimize the cost. Single effect absorption cooling method using LiBr-H_2O as working fluid pair was more suitable for domestic purpose as well as flat plate and evacuated glass tube collectors were more reliable and economical for their system.

Wu et al. [53] derived relationship between solar collector temperature, COP, and cooling load. A completely reversible solar absorption refrigerator system does not provide any cooling but it has highest COP. They calculated optimum operating solar collector temperature and corresponding overall COP for the endoreversible system. Abdulateef et al. [54] worked on solar absorption refrigeration system using new working fluid pairs. Performance of ammonia-water, ammonia-lithium nitrate and ammonia-sodium thiocyanate solar absorption cycle were compared. Their results showed that the ammonia-lithium nitrate and ammonia-sodium

thiocyanate cycle performance was better than the ammonia-water absorption cycle. Due to possibility of crystallization, ammonia-sodium thiocyanate cycle cannot be used below -10ºC. Kim and Ferreira [55] presented a state-of-the-art review of the different technologies which are available for solar refrigeration. Their review covers solar electric, solar thermal and some new emerging technologies. They observed that solar electric and thermo-mechanical systems appear to be more expensive than thermal sorption systems. Absorption and adsorption systems are comparable in terms of COP but adsorption systems are more expensive and bulkier than absorption systems.

2.4 Solar collectors

Solar collectors are mechanical device which captures radiant energy, convert it in to heat and transfer this heat to the fluid mainly air, water or oil, flowing through the collector. Mainly there are two types of solar collectors: non-concentrating which is also called stationary collectors and concentrating collectors. For intercepting and absorbing solar energy, non-concentrating solar collector has the same area, while concentrating solar collector has concave reflecting surfaces to intercept and focus the sun's beam radiation to a smaller receiving area. Concentrating collectors are used for high temperature applications. Flat plate collectors are the most common type, which consists a top glass cover, insulated sides and absorber plate. Evacuated tube collectors consists of a vacuum sealed glass tube and performs better at high temperature. In the concentrating collectors, parabolic trough collectors has light structure and low cost which effectively produces heat at temperature between 50ºC to 400ºC. Parabolic dish reflector is a point focus collector, that concentrating solar energy on a receiver located at focal of the dish which can be used to obtain temperatures above 1500ºC [5, 6]. Many types of solar collectors are available in the market. An inclusive list of solar collectors is shown in Table 2.1 [56]. Now a days, double glass evacuated tube collectors have become popular due to vacuum insulation and its capacity to absorb normal radiation throughout the day. Therefore various designs of such collectors presented by various researchers are reviewed in this section.

Table 2.1 Solar collectors

Motion	Collector type	Absorber type	Concentration ratio	Indicative temperature range (ºC)
Stationary	Flat plate collector (FPC)	Flat	1	30-80
	Evacuated tube collector (ETC)	Flat	1	50-200
	Compound parabolic collector (CPC)	Tubular	1-15	60-240
Single axis tracking	Linear Fresnel reflector (LFR)	Tubular	10-40	60-250
	Parabolic trough collector (PTC)	Tubular	15-45	60-300
	Cylindrical trough collector (CTC)	Tubular	10-50	60-300
Two axis tracking	Parabolic dish reflector (PDR)	Point	100-1000	100-500
	Heliostat field collector (HFC)	Point	100-1500	150-2000

In present section some of the solar collector literature is presented. Mohammad et al. [57] simulated evacuated solar water heating system with natural circulation under the climate condition in Tehran with TRNSYS software. The regression linear curve of the efficiency of evacuated tube solar domestic hot water system against heat loss of the system in spring and summer seasons with the solar irradiation and mean and ambient temperature on each selected day was obtained. Millani and Abbas [58] carried out modelling and performance analysis of evacuated tube collectors for solar water heaters using diffuse flat reflectors. Inclusive model to estimate the annual energy savings and small scale technology certificates which was applied to four major Australian cities representing four Australian solar zones was developed. Tilt and azimuth angle for the four zones were optimized. Pei et al. [59] carried out experimental analysis of evacuated tube solar water heater systems with and without a mini compound parabolic concentrating reflector in China. It was concluded that to attain low temperature water, the evacuated tube solar water heater system without a mini CPC reflector has higher thermal and exergy efficiency than the system with a mini CPC reflector. Ong and Tong [60] carried out short and long term system performance tests on natural and forced convection of U tube and heat pipe evacuated tube solar water heaters. From experimentation it was concluded that the natural convection heat pipe system was capable of heating water up to 100ºC and performed the best among the systems tested. Ayompe and Duffy [61] analyzed the thermal performance of a solar water heating system with heat pipe evacuated tube collector using data

from a field trial over a year in Dublin, Ireland. It was concluded that maximum outlet fluid temperature was 70.3ºC and water temperature at the bottom of the hot water tank was 59.5ºC.

Chow et al. [62] carried out optimization of evacuated tubular solar collector arrays with diffuse reflectors. Study was carried out on optical efficiencies of arrays of evacuated tubular collectors incorporating plane, triangular and semicircular shaped reflectors coated with flat-white and gloss white paint. It was concluded that the plane reflector was the optimum design. Ma et al. [63] analyzed heat loss coefficient and heat efficiency factor of the individual evacuated glass tube solar collector using one dimensional solution. Influence of air layer between the absorber tube and the copper fin on the heat efficiency was also studied. Sharma and Diaz [64] numerically carried out thermal performance of a novel evacuated tube solar collector based on mini-channels consist of U-shaped flat tube absorber with a selective coating on its external surface. Performance and pressure drop for different inlet temperatures and flow rates of working fluid were evaluated. Their results showed that gain in efficiency for their model when compared to a similar sized evacuated tube solar collector without mini-channels, obtained from the literature under identical operating conditions. Demianiuk and Sorko [65] analyzed temperature distribution on the absorber plate and in the pipe system of evacuated tube collectors. Energy efficiency of the device and phenomena of flow and convective heat transfer in the systems of pipes of circular cross section were determined. Jradi and Riffat [66] reviewed and analyzed medium temperature concentrators for solar thermal applications. For improving the overall performance of the concentrator and to decrease the convective losses as well as long wave radiation emissions, the design of the absorbing receiver line plays a significant role. They concludes that no concentrating collector can be considered as ultimate favorable technology and hence selection and design of optimal concentrating solar collector was depend on specific characteristics and nature of application. Sabiha et al. [67] reviewed evacuated tube collector, their structure, applications and challenges. Collector efficiency of different types of evacuated collectors and their performance based on different working fluids was studied. It was concluded that an evacuated tube collector has higher efficiency than the other collectors and very efficient to be used at higher operating temperature. Naik et al. [68] presented mathematical model and carried out performance analysis of a U type evacuated tube solar collector using different working fluids like LiCl-H_2O, water and air. Effect of working fluid flow rate, inlet temperature, ambient temperature and solar intensity on the performance of the system was investigated. It was observed that collector length, working fluid flow rate and solar

24

intensity had higher impact on performance of collector. Nunez et al. [69] determined structure of solar collector networks for the supply of thermal energy to low energy intensity industrial processes. It was observed that inlet temperature had major impact on size of collector for given solar radiation intensity.

Kim and Seo [70] investigated the thermal performance of the glass evacuated tube solar collectors numerically and experimentally with air as working fluid. Performance of solar collector was affected by the shape of the absorber, incidence angle of solar irradiation and arrangement of collector tubes. It was also concluded that number of collector tubes installed decreases, as center distance increases because width of the collector was fixed and with the short center distance absorbing area increases and therefore performance of the collector was increased. Performance of the collector increases because of increase in absorbing area due to large shadow effect as center distance becomes short. Zambolin and Del Col [71] tested glazed flat plate collector and an evacuated tube collector by installing them parallel at the same working conditions. It was observed that in the flat plate collector due to more reflection losses, the optical efficiency of the collector in the morning and in the afternoon decreases where as these efficiency losses were reduced in evacuated tube collector because of its geometry, the most of absorber area is exposed to quasi-normal incidence radiation for a longer period of the day. Hayeka et al. [72] carried out experimental investigation of the overall performance of two kinds of evacuated tube solar collectors, namely, the water-in-glass tubes and the heat-pipe designs under Eastern Mediterranean climate conditions. In their experimental set up, the collectors were made of a row of 20 evacuated tubes, a tank, and a circulation system. It was found that the heat pipe based collectors were better than the water in glass designs and their efficiency was 15 to 20% higher. Nkwetta and Smyth [73] analyzed two profiles of concentrated evacuated tube heat pipe solar collectors made of single sided and double sided absorber. These collectors were experimentally tested at a tilt angle of 60º to the horizontal. Their results showed that at a transverse angle of 0º, an overall improvement of 3.6ºC i.e. 42.4% in average outlet and inlet fluid temperature difference was recognized by truncated double side absorber CPC compared to truncated single side absorber CPC.

Sundari et al. [74] carried out design and fabrication of a solar dryer with evacuated tube collector with and without heat storage material for drying chili under the meteorological condition of Thanjavaur and Tamilnadu, India. Li et al. [75] developed U-shape evacuated tube

collector with external CPC and tested for two different concentration ratios of 3.06 (3x) and 6.03 (6x) for practical solar process heat applications. Their experimental results indicated that the tilt angle of 3x CPC needs to adjust once in a day while that for 6x CPC needs to adjust five times in a day due to its small half acceptance angle. Under the given operating conditions, the daily thermal efficiency of 3x collector was 40% and that for 6x collector was 46% at the collecting temperature of 200ºC. Ricci et al. [76] performed experimental tests on evacuated tube solar thermal collectors with parallel and series configuration. Efficiencies for different flow rates and different inflow water temperatures were evaluated. Their experimental results indicated that parallel configuration had higher performance than the series one. It was concluded that prototypes in optimized configuration can lead to a system improvement, either by increasing the overall energy production or giving the same energy production with smaller collector area. Ghoneim et al. [77] presented experimental and numerical study for assessing the performance of evacuated tube solar water collector in hot climate at Kuwait. Their simulation results were found in well agreement with experimental results. Results showed that optimum ETC area of the solar fraction for space heating and domestic water heating was approximately 44 m^2 of a typical house in Kuwait.

Cabanillas et al. [78] presented experimental results which were obtained by means of a device specially designed in order to measure the distribution of incident solar radiation on tubular solar collector. Their results showed that experimentally measured distribution agrees with that obtained by the ray tracing method. Ghoneim et al. [79] developed a numerical model to study the effect of different collector parameters and operating conditions on performance of parabolic trough solar collector in Kuwait climate. Their results indicated that at noon time, parabolic trough solar collector has the smallest angle of incidence and maximum efficiency. It was also observed that collector efficiency decreases from 0.55 to 0.35 at angle of incidence 0º and 45º respectively at 150ºC temperature. Bellos et al. [80] carried out a detailed working fluid investigation for most mature concentrating technology, the parabolic trough collector for a temperature range from 300 K to 1300 K. Pressurized water, Therminol VP-1, nitrate molten salt, sodium liquid, air, carbon dioxide and helium were examined in the proper temperature range. Their results proved that the liquid working fluids had higher performance than the gas working fluids. Pressurized water up to 550 K, for higher temperature sodium liquid up to 1100 K, while for extremely high temperature carbon dioxide and helium after 1100 K were the most

suitable working fluids. The maximum exergetic performance of air, carbon dioxide, and helium was found 40.12%, 42.06%, and 42.21% respectively.

2.5 Working fluid pair

The selection of operating pair plays an important role on performance of vapour absorption refrigeration system. Thermo-physical properties of selected refrigerant and absorbent are explained in present section. Some desirable characteristics of refrigerant-absorbent pair are low viscosity, low freezing point, better thermal and chemical stability, the refrigerant should have more than Raoult's law solubility in the absorbent, and large difference between their normal boiling points [81].

In ammonia-water absorption system, ammonia is the refrigerant and water is the absorbent. Ammonia has good solubility in water, but difference is the boiling point of ammonia and water is 133.3ºC, so vapour leaving the generator contains some amount of water. Therefore rectifier is required for ammonia-water absorption refrigeration system. In LiBr-H_2O system, water is the refrigerant and lithium bromide is the absorbent. Water has good solubility in the lithium bromide. LiBr being a salt exerts no vapour pressure, therefore vapour leaving the generator is pure refrigerant. LiBr-H_2O absorption system is corrosive and works under high vacuum [81]. The most common working fluid pairs which are used in absorption system are NH_3-H_2O where ammonia is used as refrigerant and water as absorbent and LiBr-H_2O where water is refrigerant and LiBr is absorbent. Different thermodynamic characteristics and properties of these working fluid pairs have been described in various studies and experimental work [82-87]. Still researchers are looking for new working fluid pairs like Glycerol-water [88], water-lithium chloride [89], LiBr+$ZnBr_2$-CH_3OH [90], ammonia-lithium nitrate [91], NH_3-$LiNO_3$ and NH_3-NaSCN [54]. Ammonia-water pair has high affinity, high stability, absence of crystallization zone, positive system pressure, ability to produce subzero temperature, non-corrosive, and evaporator temperature can go down even up to -60ºC, therefore it is suitable for air conditioning, industrial refrigeration, and freezing applications.

2.5.1 Properties of ammonia and water

Important thermo-physical properties of ammonia and water are presented in Table 2.2. Ammonia is color less, alkaline gas at ambient pressure and temperature with odor. Ammonia and water both have hydrogen bonding. Ozone depletion potential of ammonia is zero and its global warming potential is less than 1 [92].

Table 2.2 Thermo-physical properties of ammonia and water [92]

Properties	Ammonia	Water
Chemical formula	NH_3	H_2O
Molecular mass (kg/kmol)	17.03	18.015
Boiling point temperature (K)	239.823	373.124
Freezing point temperature (K)	195.495	273.16
Critical temperature (K)	405.4	647.1
Critical pressure (bar)	113.33	220.64

2.6 Conclusion of literature review

From the literature it is observed that due to high latent heat, excellent heat and mass transfer properties, absence of crystallization zone, positive system pressure, ability to produce subzero temperature, and non-corrosive nature, ammonia-water is the most suitable working fluid pair for vapour absorption refrigeration system. LiBr-H_2O absorption refrigeration system gives better performance but it works under vacuum pressure. To away from vacuum pressure, in present study ammonia-water working fluid pair is selected for absorption refrigeration system. Out of all solar collectors, parabolic trough collector has light structure and low cost which effectively produces heat at temperature between 50ºC to 400ºC. Evacuated tube collector gives better performance than flat plate collector for the same operating conditions. Therefore, in present work evacuated glass tube parabolic trough collector has been selected. Air has been selected as working fluid to extract heat from the collector. It is evident that heat transfer coefficient for air is lower and hence use of turbulator with the evacuated glass tube collector is advantageous. The turbulator increases heat transfer coefficient between absorber and air and thereby reduces absorber temperature for same air average temperature. This increases the

efficiency of the collector. It is observed that generally theoretical and experimental studies were carried out for large capacity absorption system. Few studies have been observed regarding performance improvement and energy savings of solar absorption refrigeration system, however no study was found in the literature where commercially available evacuated glass tube was used with external parabolic trough to powered ammonia-water absorption refrigeration system. It is proposed to use helical wiry turbulator to augment the heat removal rate from the collector and thereby improving its efficiency.

Chapter 3

Thermodynamic analysis and optimization of absorption refrigeration system

Thermodynamic analysis of ammonia-water absorption refrigeration system with and without ejector was carried out. Optimization of ammonia-water absorption refrigeration system (ARS) was also carried out. The function of compressor in vapour compression refrigeration system is to continuously extract the refrigerant from the evaporator and to increase its pressure and hence temperature. Therefore the heat absorbed in the evaporator along with the work of compression may be rejected in the condenser to the surrounding. In vapour absorption refrigeration system the compressor is replaced by three components: absorber, pump, and generator. The function of absorber is to absorb the refrigerant vapour by weak or poor solution and forms a rich or strong solution. The function of pump is to pump the strong solution and increasing its pressure up to condenser pressure. The function of generator is to separate out refrigerant vapour from the strong solution. Therefore, a simple vapour absorption refrigeration system consist of a

condenser, an expansion device, and an evaporator as in vapour compression system and in addition an absorber, a pump, a generator, and a pressure reducing valve to replace the compressor [81].

3.1 Thermodynamic analysis of absorption refrigeration system with ejector

Fig 3.1 shows the schematic diagram of absorption refrigeration system with ejector. The ammonia vapour condenses in the condenser. High-pressure liquid ammonia refrigerant from the condenser is allowed to expand through expansion valve which reduces the pressure of the refrigerant and then passes into the evaporator
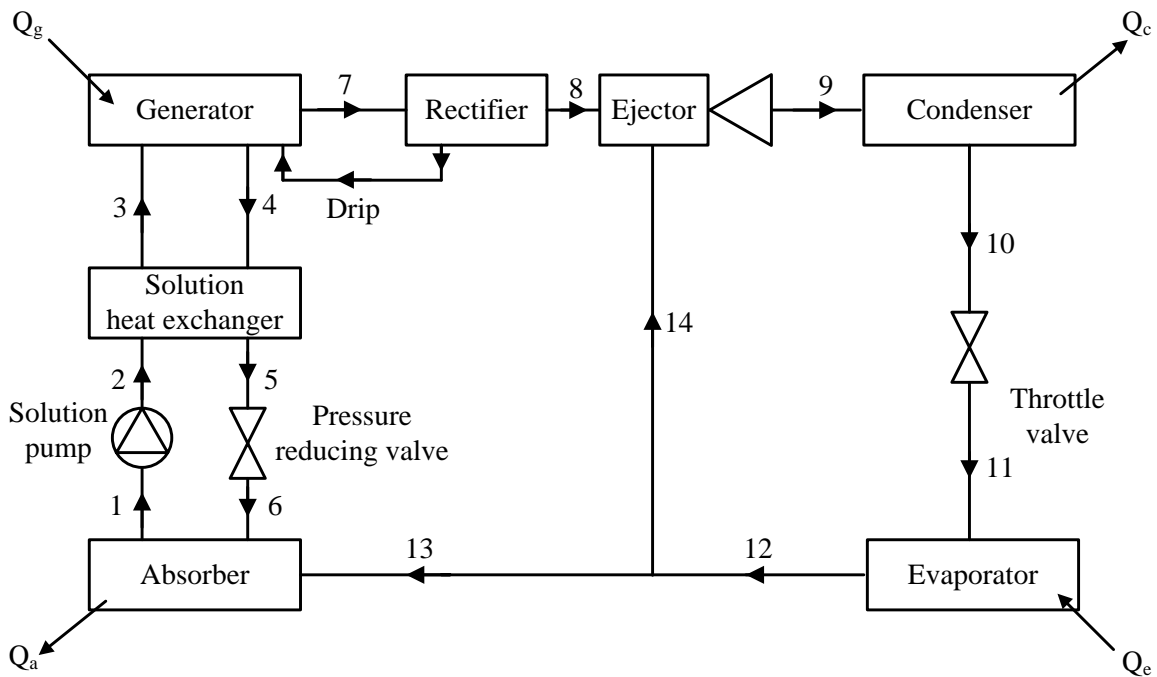
Fig 3.1 Schematic diagram of combined ejector-absorption refrigeration system

The liquid refrigerant vaporizes in the evaporator by absorbing heat from the material/space being cooled and the resulting low-pressure vapour passes to the absorber, where it is absorbed by the poor solution returning from the generator after being cooled in solution heat exchanger and throttled by pressure reducing valve. The strong solution is pumped to the generator. Heat added to the generator brings the separation of ammonia vapour accompanied with small

fraction of water vapour. A rectifier needs to be added to remove water vapour from the mixture leaving the generator before reaching the condenser through the fact that water is volatile. The ordinary combined cycle added an ejector after rectifier and before condenser. On the ejector, suction vapour coming from the evaporator mixes with the motive ammonia vapour coming from the rectifier and flow to the condenser.
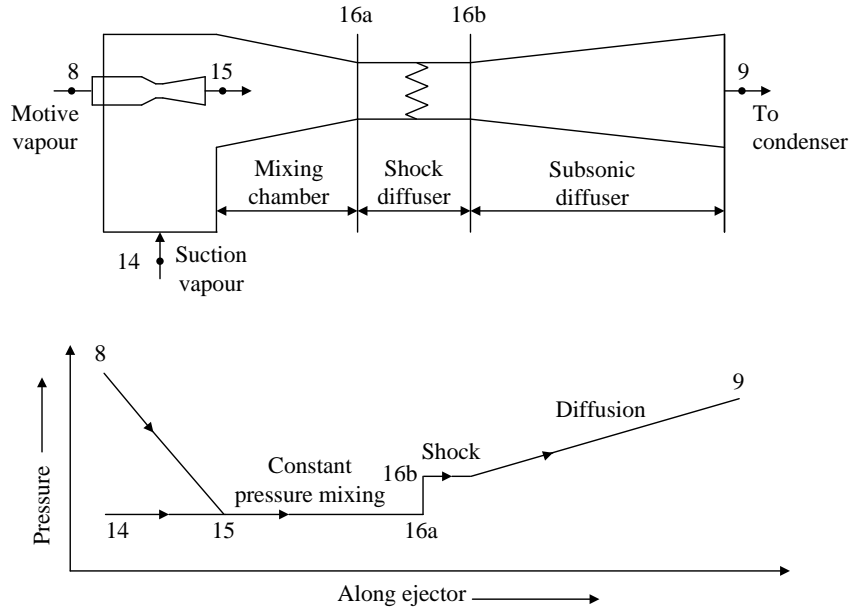
Fig 3.2 Pressure variation along ejector [81]

Fig 3.2 shows the schematic diagram of ejector and pressure variation in the ejector. The high pressure refrigerant vapour expands to a pressure slightly lower than the pressure of suction vapour. The high velocity jet entrains the suction vapour and mixing takes place at constant pressure. Normal shock may occur in the constant area section after the mixing chamber due to which slight increase in pressure takes place. After the shock the fluid is compressed to condenser pressure in the diffuser section.

3.1.1 Assumptions

The analysis of the cycle is carried out under the following assumptions [17,18,59].

- Refrigerant leaving the rectifier is saturated vapour with a mass fraction of 99.96% ammonia.
- The liquid leaving the condenser is saturated liquid at condenser temperature.

- The solution heat exchanger effectiveness is 0.7
- The refrigerant vapour leaving the evaporator is saturated vapour at evaporator temperature.
- The strong solution leaving the absorber is saturated at absorber temperature.
- The weak solution leaving the generator is saturated at generator temperature.
- Pressure drops in the system are neglected.

3.1.2 Governing Equations

Major equations used to calculate COP of combined ejector-absorption refrigeration system shown in Fig 3.1 are as follows [81]. Various properties and mass flow rates at salient points are denoted as suffice as per numbers given in Fig 3.1 and 3.2.

Refrigerant mass flow rate can be calculated as

$$\dot{m}_{ref} = \frac{Q_e}{h_{12} - h_{11}} \tag{3.1}$$

Mass balance for ejector can be written as

$$\dot{m}_1 = \dot{m}_{14} + \dot{m}_6 \tag{3.2}$$

Entropy after expansion in the nozzle of ejector

$$s_{15} = s_{f15} + \left(x \times s_{fg15}\right) \tag{3.3}$$

Where, x is the dryness fraction

Enthalpy after expansion in the nozzle of ejector

$$h_{15} = h_{f15} + \left(x \times h_{fg15}\right) \tag{3.4}$$

Velocity of refrigerant at outlet to nozzle

$$c_{15} = \sqrt{2 \times \eta_n \times \left(h_8 - h_{15}\right)} \tag{3.5}$$

The momentum equation in mixing section of ejector

$$\eta_e \times c_{15}^2 = \left(1 + \mu\right) \times c_{16a}^2 \tag{3.6}$$

Where entrainment ratio (μ) is defined as the ratio between suction vapour to the motive vapour. It is given by

$$\mu = \frac{\dot{m}_{14}}{\dot{m}_8} \tag{3.7}$$

The energy equation of ejector

$$h_8 + \left(\mu \times h_6\right) = \left(1 + \mu\right) \times \left(h_{16a} + \left(\frac{c_{16a}^2}{2}\right)\right) \tag{3.8}$$

Dryness fraction after mixing section in ejector

$$x_{16a} = \left(\frac{h_{16a} - h_{f15}}{h_{fg15}}\right) \tag{3.9}$$

Specific volume after mixing section in ejector

$$v_{16a} = \left(x_{16a} \times v_{g15}\right) + \left(\left(1 - x_{16a}\right) \times v_{f15}\right) \tag{3.10}$$

The continuity, momentum and energy equations for shock diffusers can be written as equations (3.11), (3.12) and (3.13).

$$\frac{\dot{m}_{16}}{A} = \frac{c_{16a}}{v_{16a}} = \frac{c_{16b}}{v_{16b}} \tag{3.11}$$

$$p_{16b} = p_{16a} + \left(c_{16a} - c_{16b}\right) \times \frac{\dot{m}_{16}}{A} \tag{3.12}$$

$$h_{16b} = h_{16a} + \frac{c_{16a}^2}{2} - \frac{c_{16b}^2}{2} \tag{3.13}$$

Equations (3.11), (3.12) and (3.13) are to be iteratively solved for the four variables p_{16b}, v_{16b}, h_{16b} and c_{16b}.

The kinetic energy at '16b' is converted into enthalpy in the subsonic diffuser, which can be obtained from following equation.

$$\frac{c_{16b}^2}{2} = \frac{h_1 - h_{16b}}{\eta_d} \tag{3.14}$$

Specific rich solution circulation

$$f = \frac{c_9 - c_4}{c_3 - c_4} \tag{3.15}$$

Specific poor solution circulation

$$f' = f - 1 \tag{3.16}$$

Heat exchange in the solution heat exchanger

$$f' \times \left(h_4 - h_5\right) = f \times \left(h_3 - h_2\right) \tag{3.17}$$

Heat added in the generator

$$Q_g = \dot{m}_{13} \times \left[h_7 + \left(\left(f - 1\right) \times h_4 - \left(f \times h_3\right)\right)\right] \tag{3.18}$$

Pump work

$$W_p = \frac{\dot{m}_{ref} \times f \times v_1 \times (p_2 - p_1)}{\eta_p} \quad\quad (3.19)$$

Coefficient of Performance (COP)

$$COP = \frac{Q_e}{W_p + Q_g} \quad\quad (3.20)$$

3.1.3 Results and discussion

Thermodynamic analysis of combined ejector absorption refrigeration system with NH_3-H_2O as working fluid pair was carried out. Calculations of conventional system was also carried out for the comparison. Following parameters are considered for thermodynamic analysis [17,18,93].

- Condenser temperature: 35°C, 45°C
- Evaporator temperature: 5°C, 15°C
- Nozzle efficiency: 0.85
- Diffuser efficiency: 0.85
- Entrainment efficiency: 0.95
- Pump efficiency = 50%
- System capacity = 3 TR
- Condenser temperature = Absorber temperature

Properties of ammonia-water solution were taken from Markel's diagram [94]. Fig 3.3 shows the effect of generator temperature on COP for conventional system with different condenser and evaporator temperature.
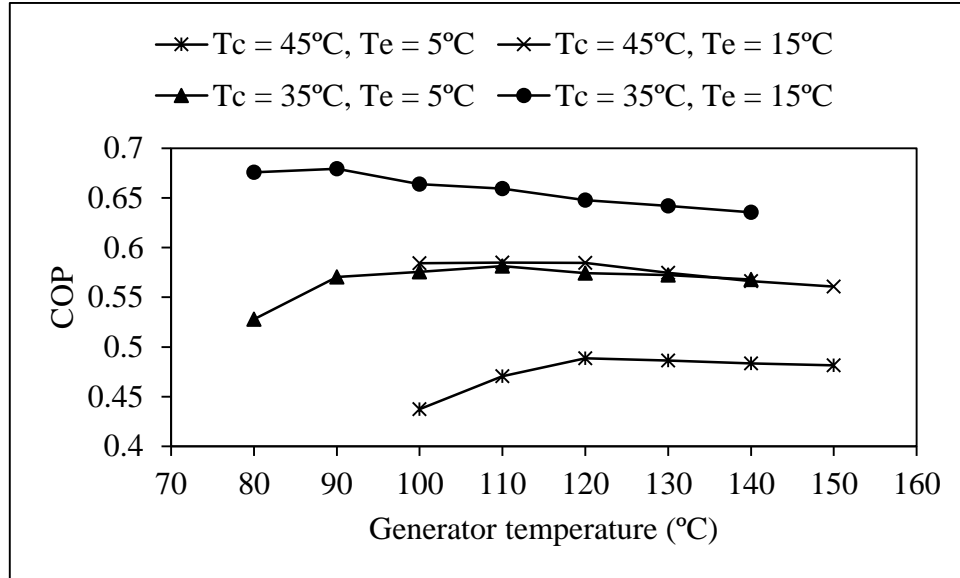
Fig 3.3 Variation of COP with generator temperature for conventional system

It can be seen that COP first increases with increase in generator temperature, reaches an optimum value and then starts decreasing as a result of increase in irreversibility at higher generator temperatures. Results of conventional absorption refrigeration system at optimum generator temperature are shown in Table 3.1.

Table 3.1 Optimum generator temperature and COP of conventional absorption system for different operating conditions.

T_c (°C)	T_e (°C)	Optimum T_g (°C)	COP
35	15	90	0.6794
35	5	110	0.5815
45	15	110	0.5849
45	5	120	0.4886

For combined ejector-absorption refrigeration system, effect of the generator temperature on COP was studied for the different value of entrainment ratio in the range of 0.04 to 0.14. Fig 3.4 shows the variation of COP with generator temperature with condenser and evaporator temperatures of 45°C and 5°C respectively. Maximum COP of 0.638 was calculated at generator temperature 140°C with entrainment ratio of 0.14. As the generator temperature increases with given evaporator and condenser temperature, COP of the system first increases, reaches to its maximum value and then start to decrease as irreversibility in the system increase at higher generator temperature for entrainment ratio from 0.04 to 0.08. For the entrainment

37

ratio of 0.1 and above, concentration of refrigerant in strong and weak solutions are almost same at generator temperature below 140°C. As the generator temperature increases COP reduces above 140°C for entrainment ratio 0.1 and above. It is observed that COP increases with entrainment ratio at same generator temperature. It is also observed that optimum generator temperature remains almost same at different entrainment ratio in the range of 0.04 to 0.14 for given set of evaporator and condenser temperature.

Fig 3.5 shows the effect of generator temperature on COP when condenser and evaporator temperatures are 45°C and 15°C respectively. Maximum COP of 0.6815 was calculated at generator temperature 130°C with entrainment ratio of 0.14. The evaporator temperature affects the low pressure of the system. With the increase in evaporator temperature the concentration of weak solution increases while solution circulation rates reduce. It causes a decrease in thermal load on generator and absorber and ensure a higher COP. As the generator temperature further increases above 130°C COP reduces. It is also observed that for given set of evaporator and condenser temperature the optimum generator temperature is almost independent of entrainment ratio in the range of 0.04 to 0.14.
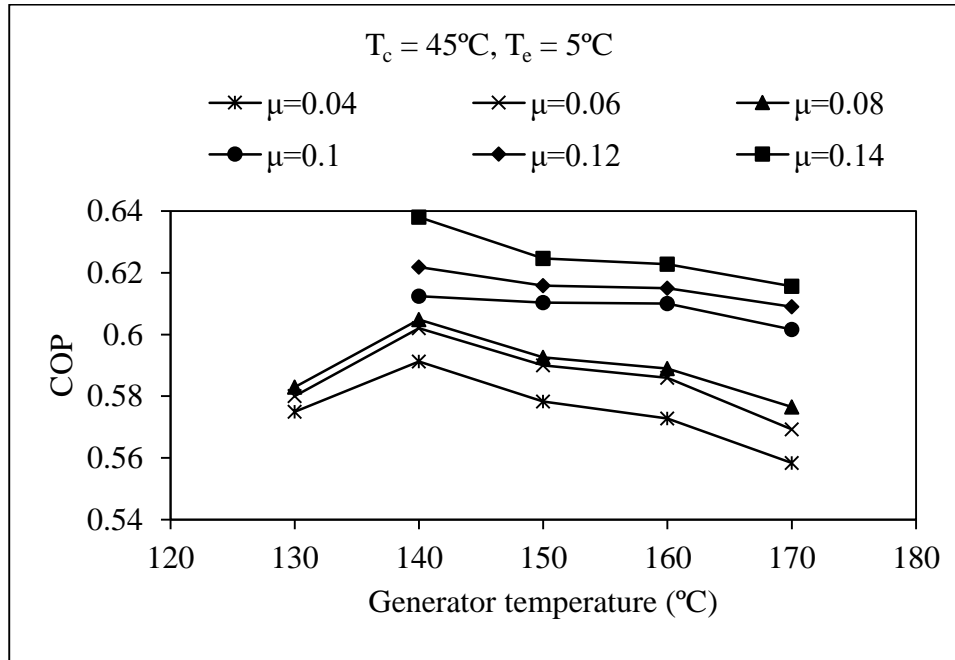
Fig 3.4 Variation of COP with generator temperature for combined ejector absorption refrigeration system at T_c=45°C and T_e=5°C
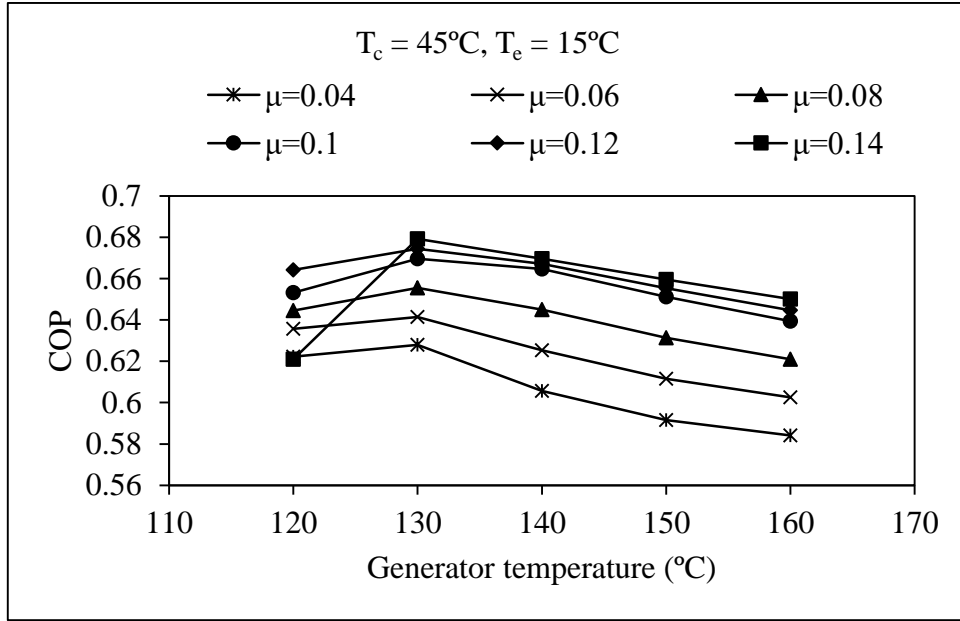
Fig 3.5 Variation of COP with generator temperature for combined ejector absorption refrigeration system at T_c=45°C and T_e=15°C

Fig 3.6 shows the effect of generator temperature on COP when condenser and evaporator temperatures are 35°C and 5°C respectively. Maximum COP of 0.675 was calculated at generator temperature 110°C. The condenser temperature affects the high pressure of the system. With the decrease in condenser temperature the saturation liquid enthalpy leaving the condenser decreases, this eventually decrease in mass flow rate of refrigerant through evaporator for the same capacity. This reduces solution circulation rate through generator which eventually decreases heat supplied to generator and thus it leads to higher COP at lower condenser temperature. With decrease in condenser temperature, generator pressure also decreases, which results in lower concentration of weak solution. This reduces solution circulation rate through generator which eventually decreases heat supplied to generator and thus it leads to higher COP at lower condenser temperature.
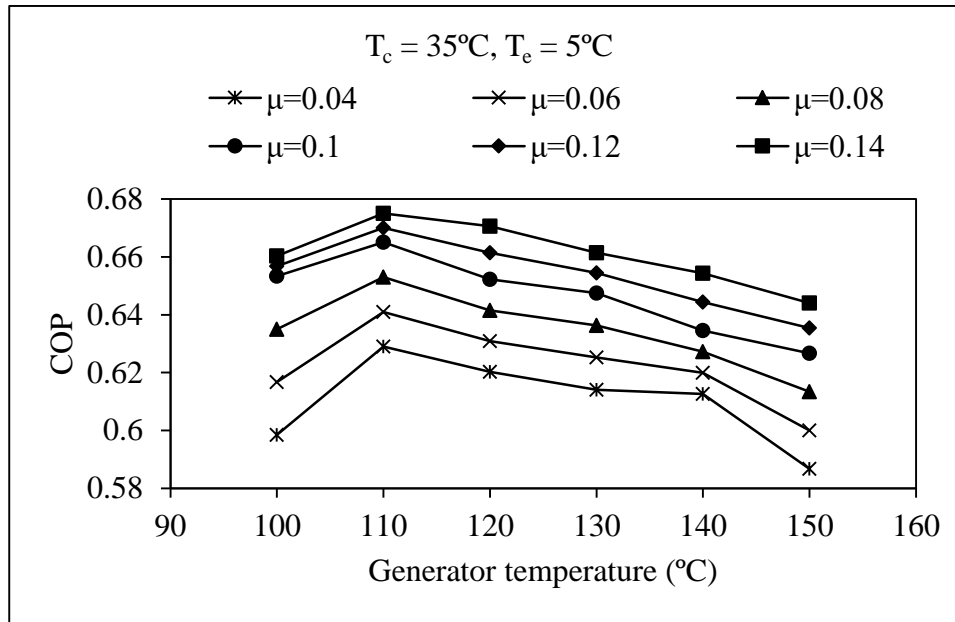
Fig 3.6 Variation of COP with generator temperature for combined ejector absorption refrigeration system at $T_c=35°C$ and $T_e=5°C$

Fig 3.7 shows the effect of generator temperature on COP when condenser and evaporator temperatures are 35°C and 15°C respectively. Maximum COP of 0.779 was calculated at generator temperature 100°C. It is also observed that higher COP is obtained for lower condenser temperature at same generator and evaporator temperatures and entrainment ratio.
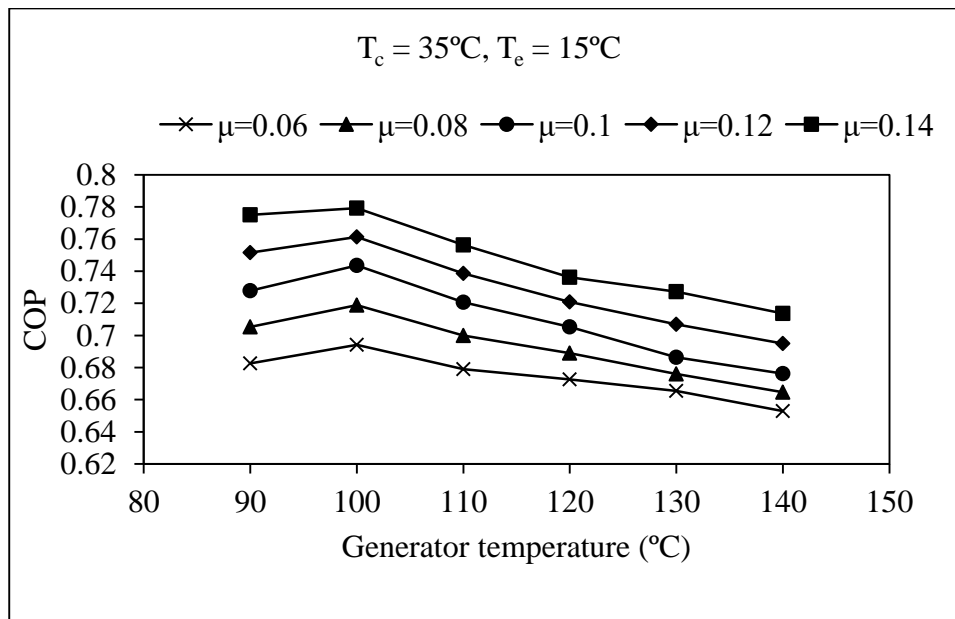
Fig 3.7 Variation of COP with generator temperature for combined ejector absorption refrigeration system at $T_c=35°C$ and $T_e=15°C$

It can be noted that COP increases with increase of entrainment ratio as it leads to increase in mass flow rate of the suction refrigerant for fixed mass flow rate of the motive refrigerant. Since mass flow rate through condenser and evaporator is increased, solution circulation rate through generator and absorber decreases which eventually reduces heat supplied in generator and hence COP increases. It was also observed that at higher condenser and lower evaporator temperature ejector inlet pressure was more than twice of that of conventional ammonia-water absorption refrigeration system even for lower entrainment ratio. For entrainment ratio of 0.14, the ejector inlet pressure was as high as 45 bar for condenser and evaporator temperatures of 45°C and 5°C respectively. Therefore a solution pump with higher pressure ratio is required for combined ejector-absorption refrigeration cycle which is presently not available in the market.

Results of combined ejector-absorption refrigeration system at optimum generator temperature are tabulated in Table 3.2. Last column indicates percentage increase in COP of combined ejector-absorption refrigeration system compared to conventional system at same condenser and evaporator temperatures.

Table 3.2 Optimum generator temperature and COP of combined ejector-absorption refrigeration system for different operating conditions.

T_c (°C)	T_e (°C)	Optimum T_g (°C)	COP	% increase in COP
35	15	100	0.779	14.66
35	5	110	0.675	16.1
45	15	130	0.679	16.52
45	5	140	0.638	30.1

Based on analysis of absorption refrigeration system it is concluded that ejector absorption refrigeration system works with very high generator pressure. Which requires large size solution pump. This cause practical limitations of solution pump. Therefore, further work is carried out on absorption refrigeration system without ejector.

3.2 Thermodynamic analysis of ammonia-water vapour absorption refrigeration system

First and second law analysis of ammonia-water absorption refrigeration system were carried out. The first law of thermodynamics deals with the quantity of energy and states that energy can neither be created nor be destroyed but it can transfer from one form to another form. The second law deals with the quality of energy. It is concerned with the degradation of energy during a process, the entropy generation and the lost opportunities to do work; and it deals with large space for improvement.

3.2.1 Exergy and exergy destruction

It is necessary to reconsider energy policies and take strong measures in reducing waste due to limited energy resources of the world. It has new challenge for science and technology to take a closer look at the energy conversion device and to develop new techniques to utilize the existing limited resources in better ways [95].

There are basically two related tactics that we can use to compute the irreversible nature of real processes and to perform analysis based on the combined first and second law of thermodynamics commonly called second law analysis. One method is concept of entropy generation and lost work and second method is the concept of availability (exergy) and irreversibility (loss of availability or exergy destruction). Exergy is defined as the maximum useful work that can be obtained from the system at a given state in definite environment. Reversible work is defined as the maximum useful work that can be obtained as a system undergoes a process between two identified states. Irreversibility called as the exergy destruction or lost work which is the waste work potential during a process. The exergy equation may be looked upon as a statement of the principle of degradation of energy, which may be simply stated as:

Exergy in – Exergy out = Change in stored exergy + Exergy destruction   (3.21)

Where, exergy destruction is a positive nonzero quantity for any real process [96].

Any difference between the reversible work and useful work is due to irreversibility present during the process. It is expressed as

$$I = W_{rev} - W_u \qquad (3.22)$$

Irreversibilities like friction, mixing of fluids, chemical reactions, and heat transfer through a finite temperature difference, unrestrained expansion, non-quasi-equilibrium compression or expansion generates entropy and anything that generates entropy always destroys exergy. The exergy destroyed is proportional to the entropy generated, and is expressed as [95]

$$X_{destroyed} = T_0 S_{generation} \qquad (3.23)$$

Initial state is specified and it is not a variable, in exergy analysis. The maximum work output is obtained when the process between two specified states performed in a reversible manner. Therefore, all the reversibility's are overlooked in determining the work potential. Finally, the system must be in a dead state at the end of process to maximize the work output. A system is said to be in the dead state when it is in thermodynamic equilibrium with the environment. At the dead state, a system is at the pressure and temperature of its environment; it has no kinetic or potential energy relative to the environment; and it does not react with the environment. Also there are no unbalanced magnetic, electrical and surface tension effects between the system and its surroundings. A system has zero exergy at dead state [95].

Second law efficiency: To measure the performance of any process, device or system concept of efficiency is used. The figure of merit extensively used in thermodynamics is generally based on the concept of energy, in which no effort is made to differentiate low quality energy and high quality energy. A simple example is COP of a refrigeration system which is defined as the ratio between refrigerating effect to the work input. Another example is thermal efficiency of a heat engine. Thermal efficiency of heat engine is defined as the ratio of network output to the amount of heat addition. In this definition, heat and work are given the same weight. These types of efficiencies do serve some useful purposes but they do not give an accurate measure of thermodynamic performance. Since it is exergy, not an energy that is consumed in producing changes, it would be more reasonable to have an efficiency based on the concept of exergy. Second law efficiency is based on concept of exergy and exergy destruction and is also called exergetic efficiency [95].

3.2.2 System description and mathematical modeling

A single stage ammonia-water absorption refrigeration system with solution and refrigerant heat exchanger is considered. Fig 3.8 shows the schematic diagram of the system. The system uses ammonia as refrigerant and water as absorbent. The main component of the system are a generator, a condenser, an absorber, an evaporator, a SHE, a RHE, a throttling device, a pressure reducing valve, a rectifier and a pump.
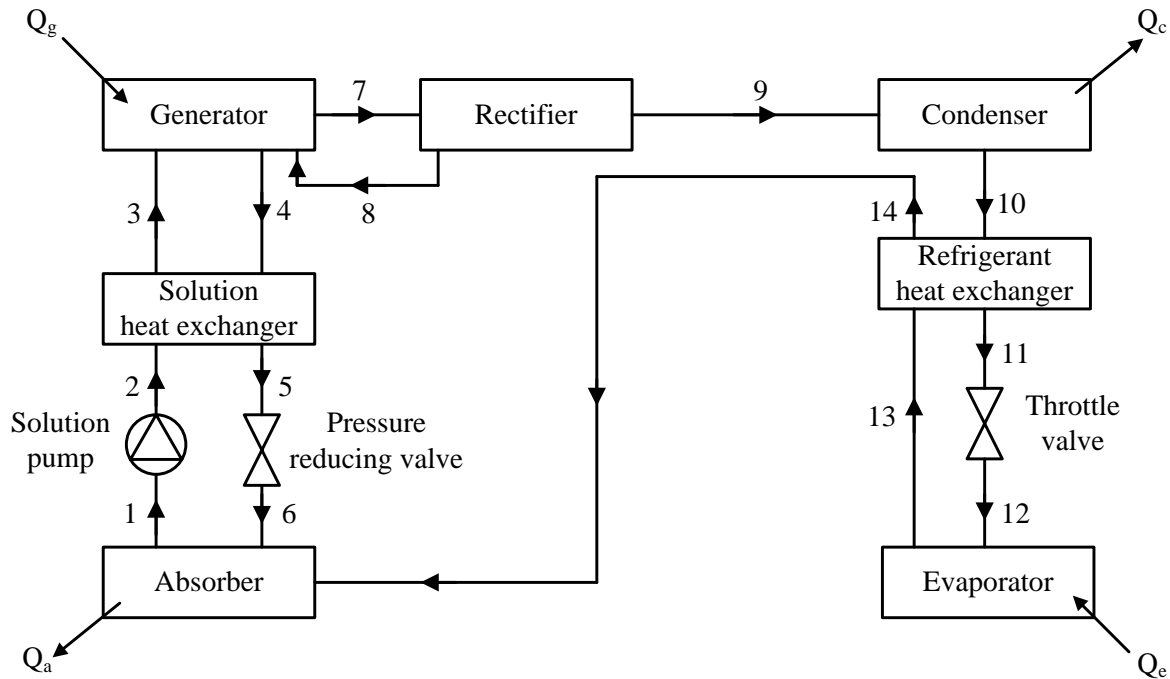
Fig 3.8 Schematic diagram of absorption refrigeration system

Low pressure, rich ammonia solution from absorber is pumped in to the SHE and gets heated by weak solution coming out of generator. Heated refrigerant rich solution then enters the generator. The generator separates the binary solution of water and ammonia by causing ammonia to vaporize using solar energy (low grade energy), and the rectifier purifies the ammonia vapour and remaining solution called as weak solution moves back to the absorber after passing through the pressure reducing valve. High pressure ammonia vapour is condensed in condenser and the condensate is then passed through RHE and the throttling valve to the evaporator as low pressure liquid ammonia. The refrigerant passing through evaporator is used to cool the space by absorbing heat from the space being cooled. During the cooling process, the liquid ammonia vaporizes and enters to the absorber after passing through the RHE. In the absorber, refrigerant is absorbed by the weak solution and rich solution is formed.

44

Assumptions

The analysis of the ammonia-water absorption refrigeration system described above is carried out with the following assumptions [17,18].

- Refrigerant leaving the rectifier is saturated vapour with a mass fraction of 99.96% ammonia.
- The liquid leaving the condenser is saturated liquid at condenser temperature.
- The refrigerant vapour leaving the evaporator is saturated vapour at evaporator temperature.
- The strong solution leaving the absorber is saturated at absorber temperature.
- The weak solution leaving the generator is saturated at generator temperature.
- Pump efficiency is 50%.
- Pressure drops in the system are negligible.
- Condenser and absorber temperatures are equal.

Mathematical Model

Major equations used to calculate COP, entropy generation of each component as well as total entropy generation and exergetic efficiency are as follows [15,18,81]. Various properties and mass flow rates at salient points are denoted as suffice as per numbers given in Fig. 3.8.

Absorber:
Solution mass balance, refrigerant mass balance, energy equation and entropy balance for absorber can be written as

$$\dot{m}_1 = \dot{m}_6 + \dot{m}_{14} \tag{3.24}$$

$$\dot{m}_1 x_1 = \dot{m}_6 x_6 + \dot{m}_{14} x_{14} \tag{3.25}$$

$$Q_a = \dot{m}_6 h_6 + \dot{m}_{14} h_{14} - \dot{m}_1 h_1 \tag{3.26}$$

$$S_{gen.a} - \dot{m}_1 s_1 + \dot{m}_6 s_6 + \dot{m}_{14} s_{14} - \frac{Q_a}{T_0} = 0 \tag{3.27}$$

Pump:

The work transfer and entropy balance equation for pump can be written as

$$W_p = \frac{\dot{m}_1 v_1 (p_2 - p_1)}{\eta_p} \tag{3.28}$$

$$W_p = \dot{m}_2 h_2 - \dot{m}_1 h_1 \tag{3.29}$$

$$S_{gen.p} + \dot{m}_1 s_1 - \dot{m}_2 s_2 = 0 \tag{3.30}$$

Solution heat exchanger:

Effectiveness, energy equation and entropy balance equation for SHE can be written as

$$\varepsilon_{shx} = \frac{T_4 - T_5}{T_4 - T_2} \tag{3.31}$$

$$\dot{m}_2 h_2 + \dot{m}_4 h_4 = \dot{m}_3 h_3 + \dot{m}_5 h_5 \tag{3.32}$$

$$S_{gen.she} - \dot{m}_5 s_5 - \dot{m}_3 s_3 + \dot{m}_4 s_4 + \dot{m}_2 s_2 = 0 \tag{3.33}$$

Generator:

Solution mass balance, refrigerant mass balance, energy equation and entropy balance for generator can be written as

$$\dot{m}_3 + \dot{m}_8 = \dot{m}_4 + \dot{m}_7 \tag{3.34}$$

$$\dot{m}_3 x_3 + \dot{m}_8 x_8 = \dot{m}_4 x_4 + \dot{m}_7 x_7 \tag{3.35}$$

$$Q_g = \dot{m}_4 h_4 + \dot{m}_7 h_7 - \dot{m}_3 h_3 - \dot{m}_8 h_8 \tag{3.36}$$

$$S_{gen.g} - \dot{m}_7 s_7 - \dot{m}_4 s_4 + \dot{m}_3 s_3 + \dot{m}_8 s_8 + \frac{Q_g}{T_4} = 0 \tag{3.37}$$

Pressure reducing valve:

Solution mass balance, refrigerant mass balance, energy equation and entropy balance for pressure reducing valve can be written as

$$\dot{m}_6 = \dot{m}_5 \tag{3.38}$$

$$x_6 \dot{m}_6 = x_5 \dot{m}_5 \tag{3.39}$$

$$h_6 = h_5 \tag{3.40}$$

$$S_{gen.v1} - \dot{m}_6 s_6 + \dot{m}_5 s_5 = 0 \tag{3.41}$$

Condenser:

Solution mass balance, refrigerant mass balance, energy equation and entropy balance for condenser can be written as

$$\dot{m}_9 = \dot{m}_{10} \; ; \; x_9 = x_{10} \tag{3.42}$$

$$Q_c = \dot{m}_9 h_9 - \dot{m}_{10} h_{10} \tag{3.43}$$

$$S_{gen.c} - \dot{m}_{10} s_{10} + \dot{m}_9 s_9 - \frac{Q_c}{T_0} = 0 \tag{3.44}$$

Refrigerant heat exchanger:

Effectiveness, energy equation and entropy balance equation for RHE can be written as

$$\varepsilon_{rhe} = \frac{T_{10} - T_{11}}{T_{10} - T_{13}} \tag{3.45}$$

$$\dot{m}_{10} h_{10} + \dot{m}_{13} h_{13} = \dot{m}_{11} h_{11} + \dot{m}_{14} h_{14} \tag{3.46}$$

$$S_{gen.rhe} - \dot{m}_{11} s_{11} - \dot{m}_{14} s_{14} + \dot{m}_{10} s_{10} + \dot{m}_{13} s_{13} = 0 \tag{3.47}$$

Throttle valve:

Refrigerant mass balance, energy equation and entropy balance for throttle valve can be written as

$$\dot{m}_{11} = \dot{m}_{12} \; ; \; x_{11} = x_{12} \tag{3.48}$$

$$h_{11} = h_{12} \tag{3.49}$$

$$S_{gen.v2} - \dot{m}_{12} s_{12} + \dot{m}_{11} s_{11} = 0 \tag{3.50}$$

Evaporator:

Refrigerant mass balance, energy equation and entropy balance for evaporator can be written as

$$\dot{m}_{12} = \dot{m}_{13} \; ; \; x_{12} = x_{13} \tag{3.51}$$

$$Q_e = \dot{m}_{13} h_{13} - \dot{m}_{12} h_{12} \tag{3.52}$$

$$S_{gen.e} - \dot{m}_{13} s_{13} + \dot{m}_{12} s_{12} + \frac{Q_e}{T_e} = 0 \tag{3.53}$$

Rectifier:

Solution mass balance, refrigerant mass balance, energy equation and entropy balance for rectifier can be written as

$$\dot{m}_7 = \dot{m}_8 + \dot{m}_9 \tag{3.54}$$

$$\dot{m}_7 x_7 = \dot{m}_8 x_8 + \dot{m}_9 x_9 \tag{3.55}$$

$$Q_r = \dot{m}_7 h_7 - \dot{m}_8 h_8 - \dot{m}_9 h_9 \tag{3.56}$$

$$S_{gen.r} - \dot{m}_8 s_8 - \dot{m}_9 s_9 + \dot{m}_7 s_7 - \frac{Q_r}{T_0} = 0 \tag{3.57}$$

Total entropy generation in the ARS can be written as

$$S_{gen.tot} = S_{gen.a} + S_{gen.p} + S_{gen.she} + S_{gen.g} + S_{gen.v1} + S_{gen.c} + S_{gen.rhe} + S_{gen.v2} + S_{gen.e} + S_{gen.r} \tag{3.58}$$

COP of the ARS can be calculated by using equation (3.20).

Exergetic efficiency of the ARS can be written as

$$\eta_{exe} = \frac{-Q_e \times \left(1 - \dfrac{T_0}{T_e}\right)}{\left(Q_g \times \left(1 - \dfrac{T_0}{T_g}\right)\right) + W_p} \tag{3.59}$$

Results and discussion

Thermodynamic analysis of ammonia-water absorption system with refrigerant and solution heat exchanger was carried out to obtain maximum performance of the system and hence optimum value of generator temperature. The effect of generator temperature on COP, total entropy generation and exergetic efficiency for the different values of evaporator and condenser temperatures is studied. Calculations are also carried out to understand the effect of solution heat exchanger (SHE) and refrigerant heat exchanger (RHE) effectiveness on COP, total entropy generation and exergetic efficiency.

Fig 3.9, 3.10 and 3.11 shows the variation of COP, total entropy generation and exergetic efficiency with generator temperature respectively at different evaporator temperatures for the fixed value of condenser temperature of 35°C and effectiveness of SHE & RHE as 0.7.
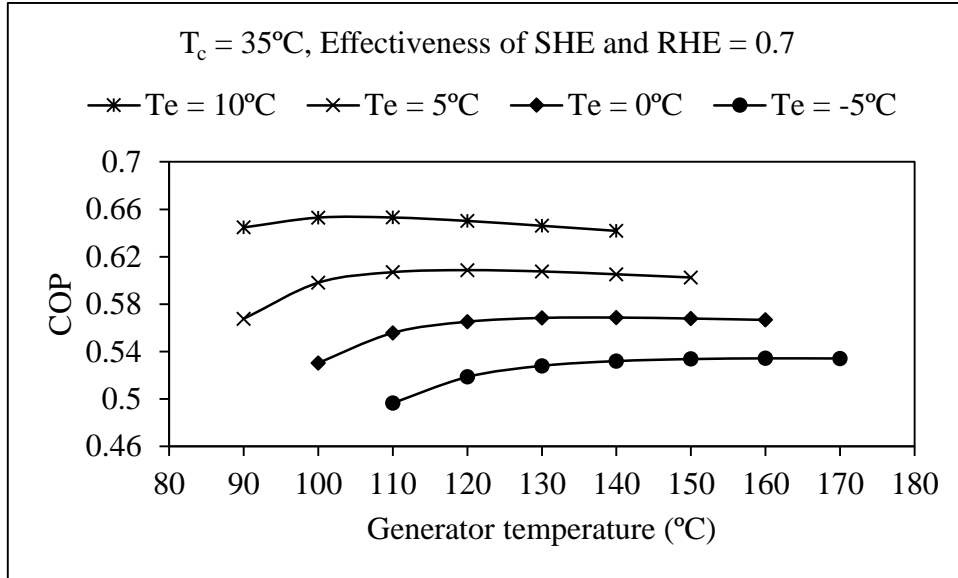
Fig 3.9 Effect of generator temperature on COP for the different evaporator temperature

The evaporator temperature is varied from -5°C to 10°C at the interval of 5°C. It can be seen that COP first increases with increase in generator temperature, reaches an optimum value and then starts decreasing as a result of increase in irreversibility at higher generator temperatures. Total entropy generation increases and exergetic efficiency decreases, with increase in generator temperature.
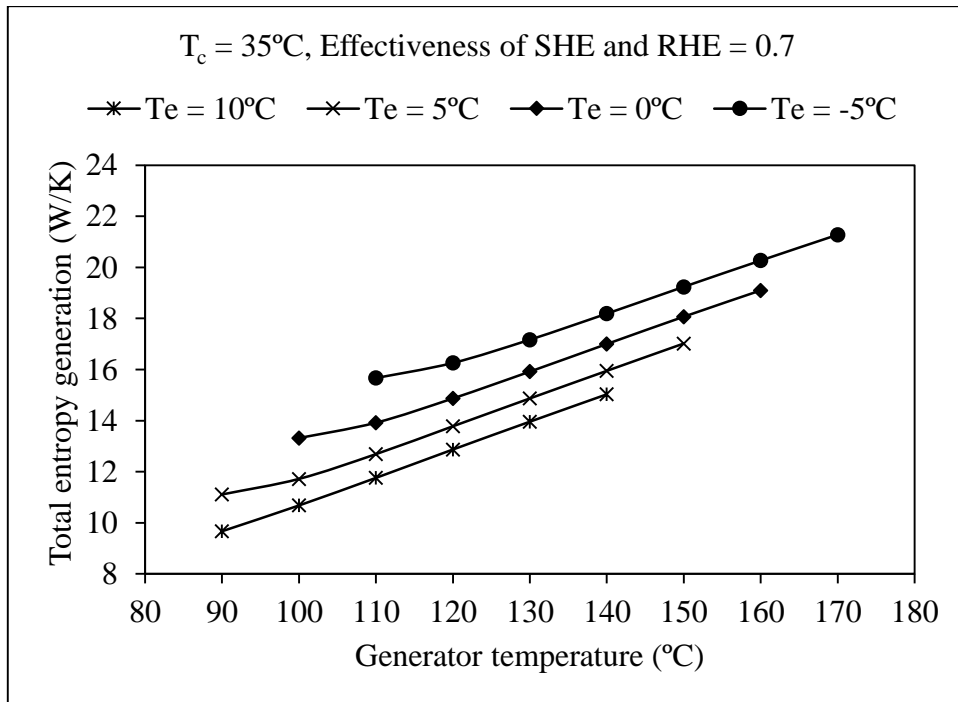
Fig 3.10 Effect of generator temperature on total entropy generation for the different

evaporator temperature
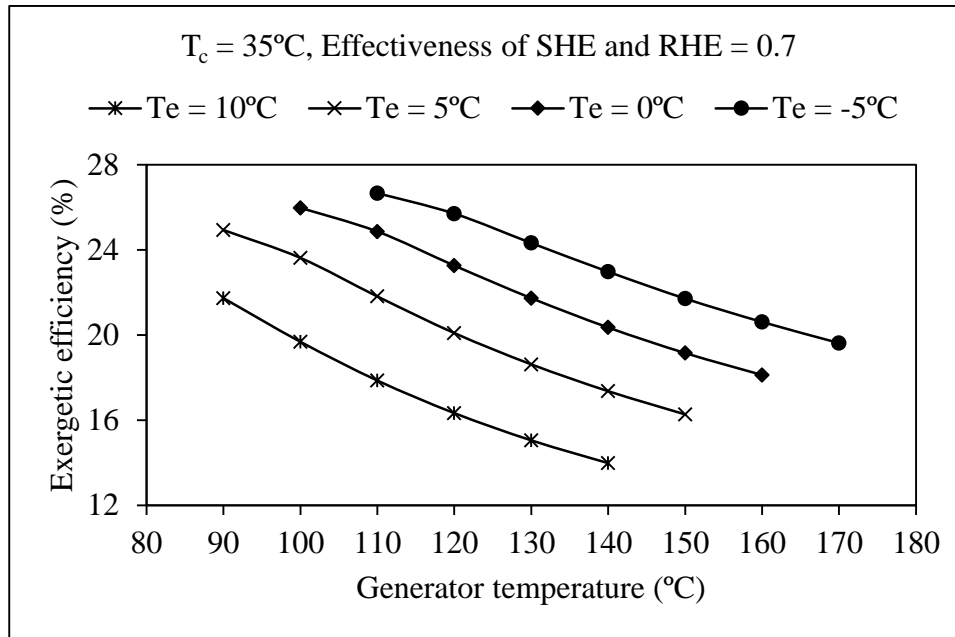
Fig 3.11 Effect of generator temperature on exergetic efficiency of the system for different evaporator temperature

The evaporator temperature affects the low pressure of the system. With increase in evaporator temperature, the concentration of rich solution increases which reduces the solution circulation rate and increases degasing range. It causes a decrease in thermal load on generator and absorber which ensure higher COP. It can be seen that total entropy generation and exergetic efficiency is higher at the low evaporator temperature for the same generator temperature. Results shows that total entropy generation increases and exergetic efficiency decreases with increase in generator temperature.

Fig 3.12, 3.13 and 3.14 shows the variation of COP, total entropy generation and exergetic efficiency with generator temperature respectively at different condenser temperatures for the fixed value of evaporator temperature of 10°C and effectiveness of SHE & RHE as 0.7. The condenser temperature is varied from 35°C to 50°C at the interval of 5°C. The condenser temperature affects the high pressure of the system. With the decrease in condenser temperature the saturation liquid enthalpy leaving the condenser decreases, this eventually decrease in mass flow rate of refrigerant through evaporator for the same capacity. With decrease in condenser temperature, generator pressure also decreases, which results in lower concentration of weak solution. This reduces solution circulation through generator which eventually decreases heat supplied to generator and thus it leads to higher COP at lower condenser temperature. It can

also be seen that total entropy generation is higher and exergetic efficiency is lower at high condenser temperature at the same value of generator temperature.
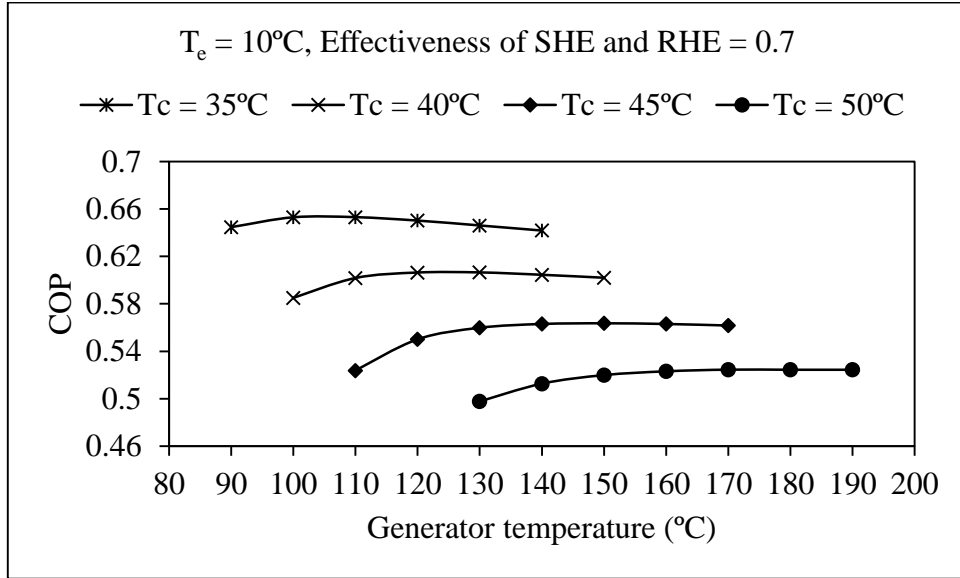
Fig 3.12 Effect of Generator temperature on COP for the different condenser Temperature
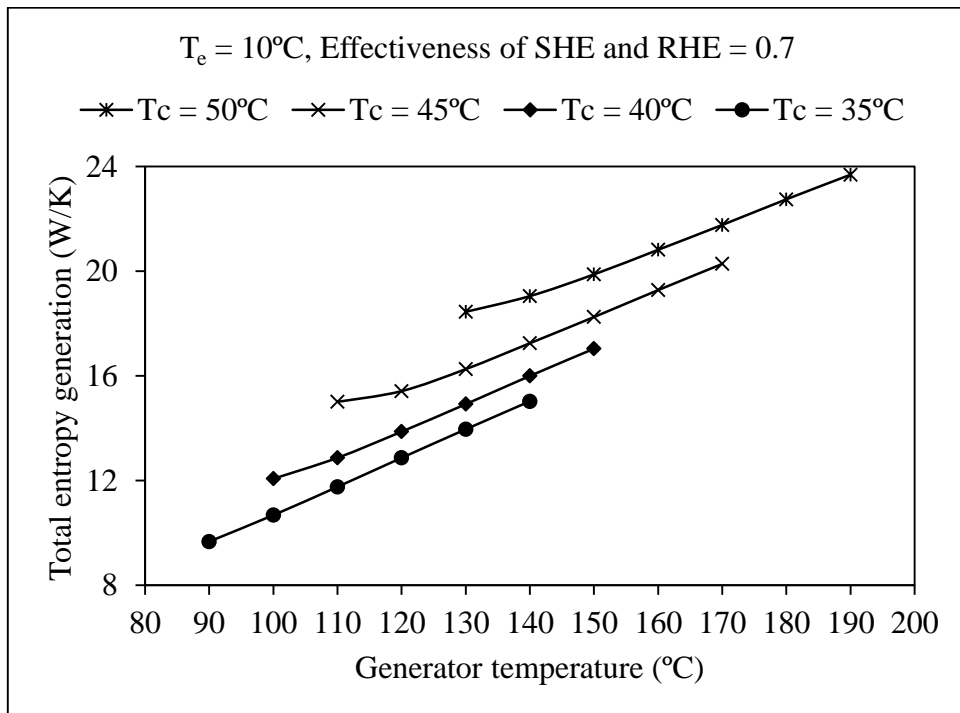
Fig 3.13 Effect of generator temperature on total entropy generation for different condenser temperature
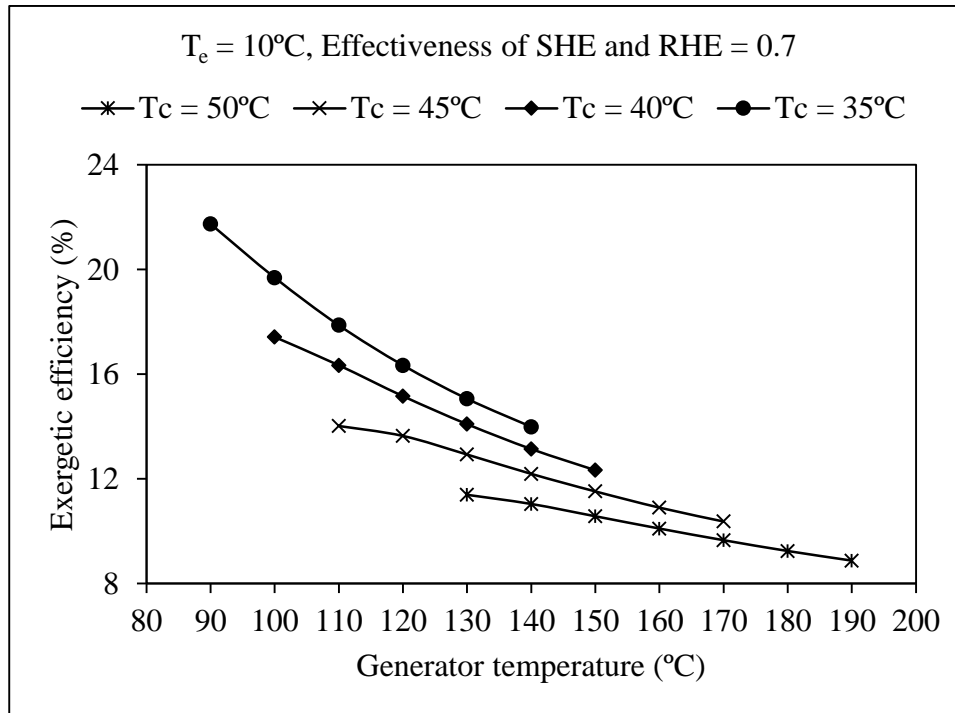
Fig 3.14 Effect of generator temperature on exergetic efficiency for different condenser temperature

Fig 3.15 to 3.17 show the effect of effectiveness of SHE and RHE on COP, total entropy generation and exergetic efficiency. When effect of effectiveness of SHE on COP, total entropy generation, and exergetic efficiency is studied, effectiveness of RHE is considered as 0.7 and similarly when effect of effectiveness of RHE on COP, total entropy generation, and exergetic efficiency is studied, effectiveness of SHE is considered as 0.7.
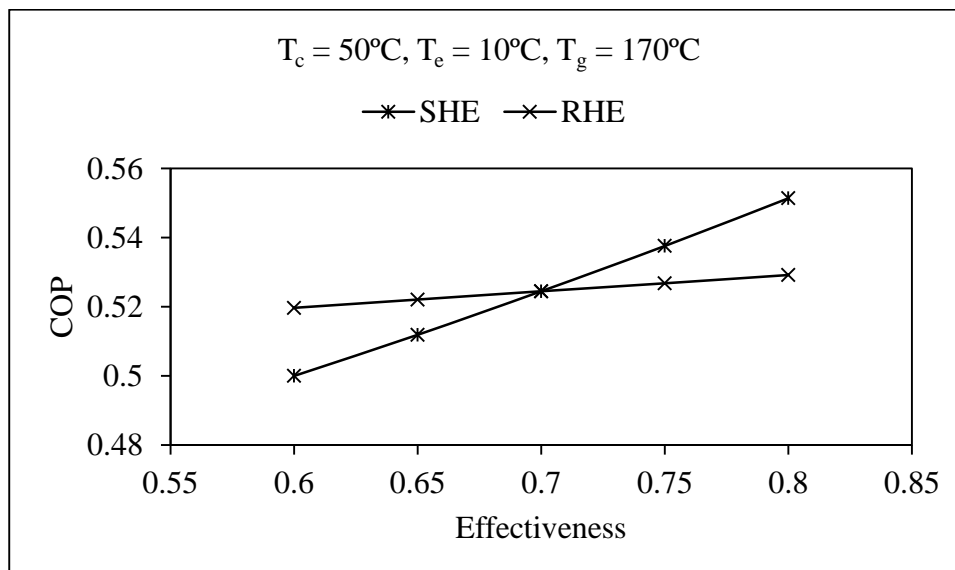
Fig 3.15 Effect of effectiveness of SHE and RHE on COP
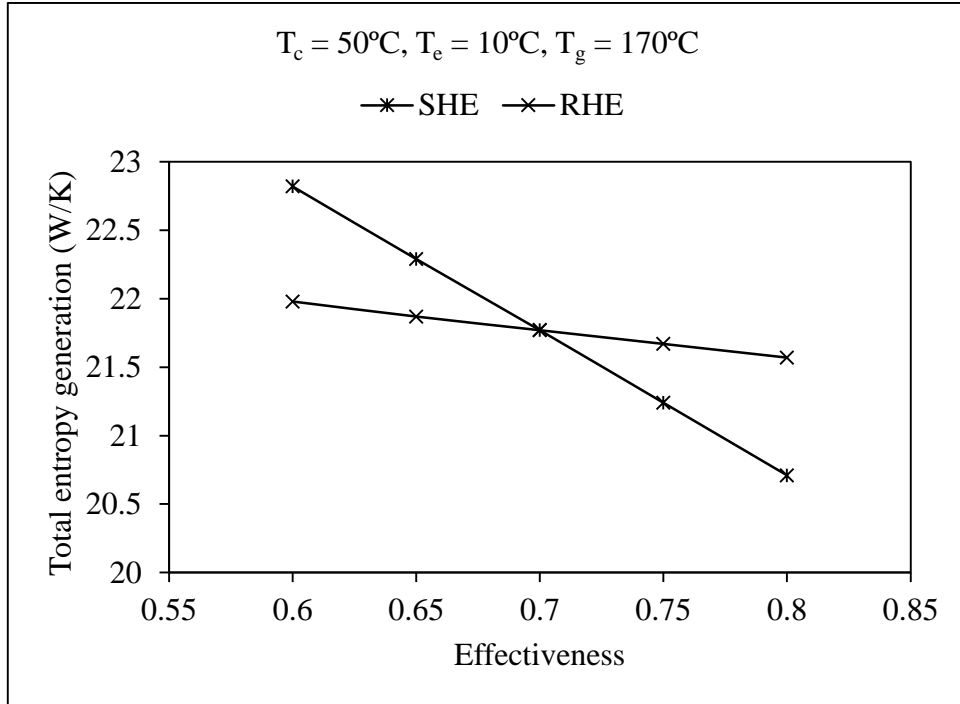
Fig 3.16 Effect of effectiveness of SHE and RHE on total entropy generation
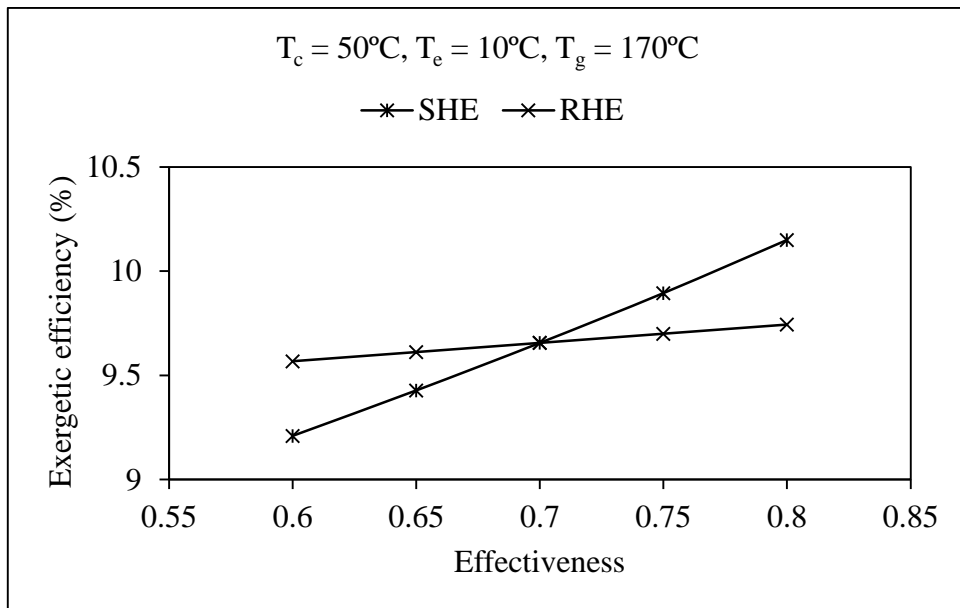
Fig 3.17 Effect of effectiveness of SHE and RHE on exergetic efficiency

With the increase in effectiveness of SHE and RHE, COP and exergetic efficiency increases while total entropy generation decreases for the fix value of condenser, evaporator, generator temperatures and effectiveness of RHE or SHE (as the case may be). However the effect of SHE effectiveness is higher on performance of the system compared to RHE effectiveness.

Table 3.3 shows the results of COP, total entropy generation and exergetic efficiency for the different values of generator temperature for Indian weather condition, considering condenser temperature of 50ºC, evaporator temperature of 10ºC for the application of summer air conditioning and considering effectiveness as 0.7 for SHE and RHE. It is seen that maximum COP is 0.525 at optimum generator temperature of 170ºC. With increase in generator temperature degree of irreversibility increases due to mixing of refrigerant and absorbent with fix value of evaporator, condenser and absorber temperatures, which causes increase in total entropy generation and decrease in exergetic efficiency.

Table 3.4 shows the entropy generation in the different system components for condenser temperature of 50ºC, evaporator temperature of 10ºC, generator temperature of 170ºC and effectiveness of SHE and RHE as 0.7. Maximum entropy generation is associated with the absorber and generator of the vapour absorption refrigeration system. Entropy generation in absorber and generator is 39.64% and 16.55% of total entropy generation respectively. While minimum entropy generation is calculated for the refrigerant heat exchanger and pressure reducing valve.

Table 3.3 Results of COP, total entropy generation and exergetic efficiency for the different values of generator temperature at condenser temperature of 50ºC, evaporator temperature of 10ºC, and effectiveness of SHE and RHE as 0.7

T_g (ºC)	COP	S_{tot} (W/K)	η_{exe} (%)
130	0.498	18.45	11.39
140	0.513	19.05	11.04
150	0.52	19.88	10.57
160	0.523	20.82	10.1
170	0.525	21.77	9.656
180	0.524	22.75	9.243
190	0.524	23.69	8.875

Table 3.4 Entropy generation in different system components at condenser temperature of 50ºC, evaporator temperature of 10ºC, generator temperature of 170ºC and effectiveness of SHE and RHE as 0.7

System Component	Entropy Generation (W/K)	% of total
Evaporator	2.557	11.74
Generator	3.603	16.55
Condenser	2.387	10.96
Absorber	8.631	39.64
Rectifier	1.444	6.63
SHE	2.524	11.59
RHE	0.07403	0.34
Pump	0.1583	0.73
Expansion Valve	0.3073	1.41
Pressure Reducing Valve	0.08715	0.40

3.3 Optimization of the system

Optimization is finding an alternative with most cost effectiveness or highest possible performance under the given constraints, by maximizing desired or minimizing undesired factors. Design of experiment (DOE) is a systematic method to regulate the relationship between factors affecting a process and output of the process. It is used to manage process inputs in order to optimize the output. Design of experiment can be used at the point of ultimate influence to reduce design costs by speeding up the design process, reducing late engineering design changes, and reducing product material and labor difficulty. DOE is suitable to combine the factors at suitable levels, each with the respective satisfactory range, to produce the best results and yet exhibit minimum variation around the optimum results [97]. The design of an experiment involves the following steps.

- Selection of independent variables
- Selection of number of level settings for each independent variable
- Selection of orthogonal array
- Assigning the independent variables to each column

- Conducting the experiments
- Analyzing the data
- Inference

The methods of Design of Experiment are as follows:

- Full factorial method
- Taguchi method
- Response surface method
- Mixture method

In the present work, the Taguchi method has been used to optimize the ammonia-water absorption refrigeration system.

3.3.1 Taguchi method

Taguchi method is a statistical method developed by Genichi Taguchi for optimizing design parameters. Taguchi method was formerly proposed as a means of improving the quality of products through the application of statistical and engineering concepts. The main objective of the Taguchi method is to design robust systems that are reliable under uncontrollable conditions. In parameter design, there are two types of factors that affect a product's functional characteristic: signal factors and noise factors. Signal factors can easily be controlled while noise factors are difficult or impossible or highly expensive to control [97]. Orthogonal Arrays (OA) are employed in Taguchi's approach to systematically vary and test the different levels of each of the control parameters. Commonly used OA are L4, L9, L16, L18, and L25 etc. Orthogonal Arrays provide a set of well balanced (minimum) experiments and Taguchi's Signal-to-Noise (SN) ratios are log functions of desired output, serve as objective functions for optimization, help in data analysis and prediction of optimum results. The SN ratio takes both the mean and the variable into account. The SN ratio is the ratio of the mean (Signal) to the standard deviation (Noise). The SN ratio depends on the quality characteristics of the product/process to be optimized. Taguchi specified three situations: Larger is better, Nominal is Better, and Smaller is better [97].

3.3.2 Taguchi method of design of experiments for COP and exergetic efficiency of the absorption refrigeration system

COP and exergetic efficiency of ARS mainly depends on six parameters i.e. condenser temperature, absorber temperature, evaporator temperature, generator temperature, solution heat exchanger effectiveness, and refrigerant heat exchanger effectiveness.

Table 3.5 Factors and their levels

Factor	Level 1	Level 2	Level 3	Level 4
Condenser temperature, T_c (°C)	35	40	45	50
Evaporator temperature, T_e (°C)	-5	0	5	10
Generator temperature, T_g (°C)	120	130	140	150
Effectiveness of refrigerant heat exchanger, ε_{RHE}	0.6	0.65	0.7	0.75
Effectiveness of solution heat exchanger, ε_{SHE}	0.6	0.65	0.7	0.75

Table 3.6 Orthogonal array L16 of Taguchi method

1	1	1	1	1
1	2	2	2	2
1	3	3	3	3
1	4	4	4	4
2	1	2	3	4
2	2	1	4	3
2	3	4	1	2
2	4	3	2	1
3	1	3	4	2
3	2	4	3	1
3	3	1	2	4
3	4	2	1	3
4	1	4	2	3
4	2	3	1	4
4	3	2	4	1
4	4	1	3	2

In present study condenser and absorber temperatures are considered as the same. Therefore, total five parameters are considered as independent variables. All 1024 possible combinations of five independent variables are developed based on selected range of each parameters as shown in Table 3.5. All parameters are selected in ascending order to make all possible combinations. Condenser temperatures are selected for the possible Indian weather conditions. Evaporator temperatures are chosen for air conditioning applications. Due to marginal increase in COP above 150°C, generator temperature is considered up to 150°C. Range of effectiveness of RHE and SHE is selected based on the literature. L16 orthogonal array is selected for present analysis and sixteen different combinations of four level and five factors are shown in Table 3.6.

Table 3.7 Results of COP and exergetic efficiency for Taguchi design

T_c (°C)	T_e (°C)	T_g (°C)	ε_{RHE}	ε_{SHE}	COP	η_{exe} (%)
35	-5	120	0.6	0.6	0.4825	23.94
35	0	130	0.65	0.65	0.5527	21.15
35	5	140	0.7	0.7	0.6052	17.36
35	10	150	0.75	0.75	0.6500	13.34
40	-5	130	0.7	0.75	0.4904	22.44
40	0	120	0.75	0.7	0.5079	20.74
40	5	150	0.6	0.65	0.5495	14.82
40	10	140	0.65	0.6	0.5787	12.59
45	-5	140	0.75	0.65	0.4084	17.45
45	0	150	0.7	0.6	0.4564	15.31
45	5	120	0.65	0.75	0.507	16.44
45	10	130	0.6	0.7	0.5554	12.83
50	-5	150	0.65	0.7	0.3743	14.99
50	0	140	0.6	0.75	0.4186	14.68
50	5	130	0.75	0.6	0.3950	11.86
50	10	120	0.7	0.65	0.4390	10.72

The columns in the OA indicate the factor and its corresponding levels and each row in the OA founds an analysis which should conducted using the combination of levels for each independent factor. It has 16 rows and 5 columns as shown in Table 3.6. This orthogonal array

is chosen due to its capability to check the relations among factors. The columns of Table 3.6 are assigned to condenser temperature, evaporator temperature, generator temperature, effectiveness of RHE, and effectiveness of SHE respectively. COP and exergetic efficiency are considered as objective functions. Based on Taguchi design, sixteen different combinations of five different independent variables are developed as shown in Table 3.7. COP and exergetic efficiency are evaluated for all sixteen combinations.

Multi linear regression analysis provides best equations of COP and exergetic efficiency, which are as under.

The regression equation of COP is

$$COP = 0.709 - 0.0109 \, T_c + 0.00762 \, T_e + 0.000747 \, T_g - 0.0779 \, \varepsilon_{RHE} + 0.277 \, \varepsilon_{SHE} \qquad (3.60)$$

$$S = 0.0133185 \quad R^2 = 98.2\% \quad R^2 \, (adj) = 97.2\%$$

The regression equation of exergetic efficiency is

$$\eta_{exe} = 0.489 - 0.00396 \, T_c - 0.00497 \, T_e - 0.00116 \, T_g - 0.0399 \, \varepsilon_{RHE} + 0.0569 \, \varepsilon_{SHE} \qquad (3.61)$$

$$S = 0.00593086 \quad R^2 = 98.5\% \quad R^2 \, (adj) = 97.8\%$$

SN ratio analysis

Simulation results are transferred in to SN ratio. SN ratio response determines the effect of control parameters such as T_c, T_e, T_g, ε_{RHE}, and ε_{SHE} on COP and exergetic efficiency.

Highest values of COP and exergetic efficiency are desirable. Therefore, 'Larger is the better' type category of the performance characteristic for COP and exergetic efficiency are selected to analyze the SN ratio as shown in Tables 3.8 and 3.9. Following equation of SN ratio is used for larger is better to maximize the response.

$$SN = -10 \log_{10} \left[\frac{1}{n} \sum_{i=1}^{n} \frac{1}{Yi^2} \right] \qquad (3.62)$$

Table 3.8 SN ratio for COP

T_c (°C)	T_e (°C)	T_g (°C)	ε_{RHE}	ε_{SHE}	COP	SN
35	-5	120	0.6	0.6	0.4825	-6.3301
35	0	130	0.65	0.65	0.5527	-5.1502
35	5	140	0.7	0.7	0.6052	-4.362
35	10	150	0.75	0.75	0.6500	-3.7417
40	-5	130	0.7	0.75	0.4904	-6.189
40	0	120	0.75	0.7	0.5079	-5.8844
40	5	150	0.6	0.65	0.5495	-5.2006
40	10	140	0.65	0.6	0.5787	-4.7509
45	-5	140	0.75	0.65	0.4084	-7.7783
45	0	150	0.7	0.6	0.4564	-6.8131
45	5	120	0.65	0.75	0.507	-5.8998
45	10	130	0.6	0.7	0.5554	-5.1079
50	-5	150	0.65	0.7	0.3743	-8.5356
50	0	140	0.6	0.75	0.4186	-7.564
50	5	130	0.75	0.6	0.395	-8.0681
50	10	120	0.7	0.65	0.439	-7.1507

Table 3.9 SN ratio for exergetic efficiency

T_c (°C)	T_e (°C)	T_g (°C)	ε_{RHE}	ε_{SHE}	η_{exe}	SN
35	-5	120	0.6	0.6	23.94	27.5825
35	0	130	0.65	0.65	21.15	26.5062
35	5	140	0.7	0.7	17.36	24.791
35	10	150	0.75	0.75	13.34	22.5031
40	-5	130	0.7	0.75	22.44	27.0205
40	0	120	0.75	0.7	20.74	26.3362
40	5	150	0.6	0.65	14.82	23.417
40	10	140	0.65	0.6	12.59	22.0005
45	-5	140	0.75	0.65	17.45	24.8359
45	0	150	0.7	0.6	15.31	23.6995
45	5	120	0.65	0.75	16.44	24.318
45	10	130	0.6	0.7	12.83	22.1645
50	-5	150	0.65	0.7	14.99	23.516
50	0	140	0.6	0.75	14.68	23.3345
50	5	130	0.75	0.6	11.86	21.4817
50	10	120	0.7	0.65	10.72	20.6039
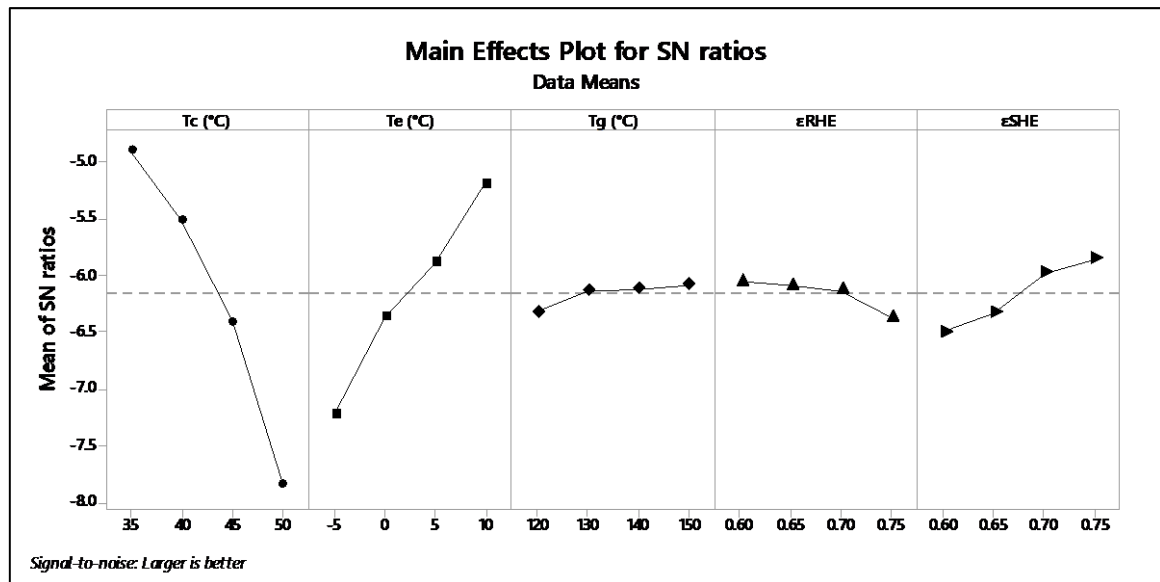
Fig 3.18 Main effect plot of SN ratio for COP

Fig 3.18 and 3.19 shows the main effect plot of mean of SN ratio and mean of means for COP respectively. From Fig 3.18 it is observed that $T_c = 35°C$, $T_e = 10°C$, $T_g = 150°C$, $\varepsilon_{RHE} = 0.6$ and $\varepsilon_{SHE} = 0.75$ are suitable parameters for maximum COP and from Fig 3.19 it can be seen that $T_c = 35°C$, $T_e = 10°C$, $T_g = 150°C$, $\varepsilon_{RHE} = 0.65$ and $\varepsilon_{SHE} = 0.75$ are suitable parameters for maximum COP. From predicted values of Taguchi analysis, COP is 0.6612 for mean value of $T_c = 35°C$, $T_e = 10°C$, $T_g = 150°C$, $\varepsilon_{RHE} = 0.6$, and $\varepsilon_{SHE} = 0.75$.
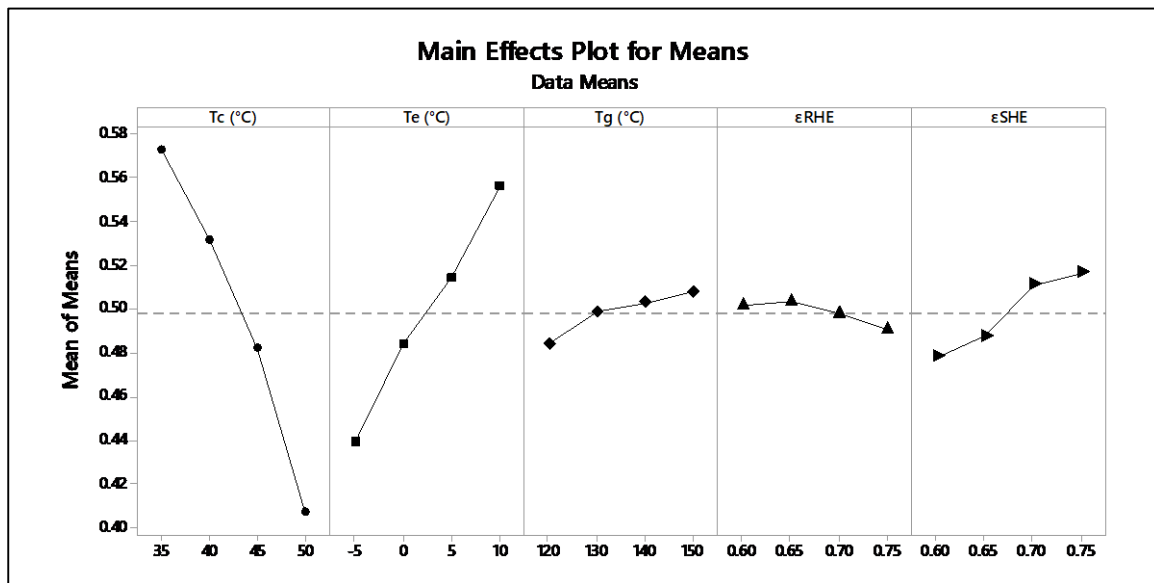
Fig 3.19 Main effect plot of mean of means for COP
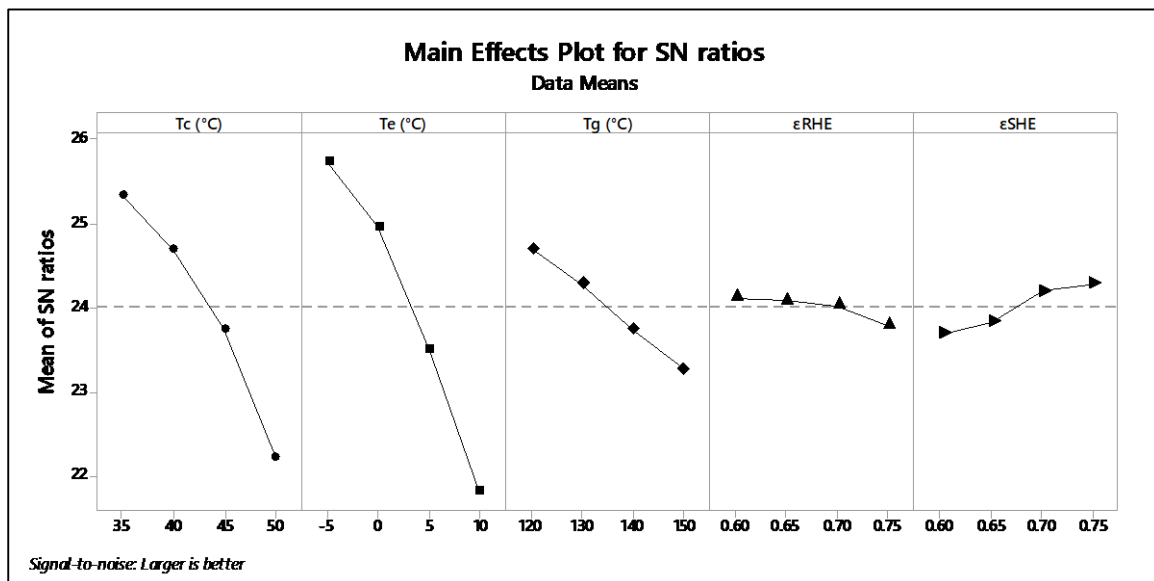
Fig 3.20 Main effect plot of SN ratio for exergetic efficiency

Fig 3.20 and 3.21 shows the main effect plot of mean of SN ratio and mean of means for exergetic efficiency respectively. From predicted values of Taguchi analysis, prediction for exergetic efficiency is 24.74% for mean value of $T_c = 35°C$, $T_e = -5°C$, $T_g = 120°C$, $\varepsilon_{RHE} = 0.6$ and $\varepsilon_{SHE} = 0.75$.
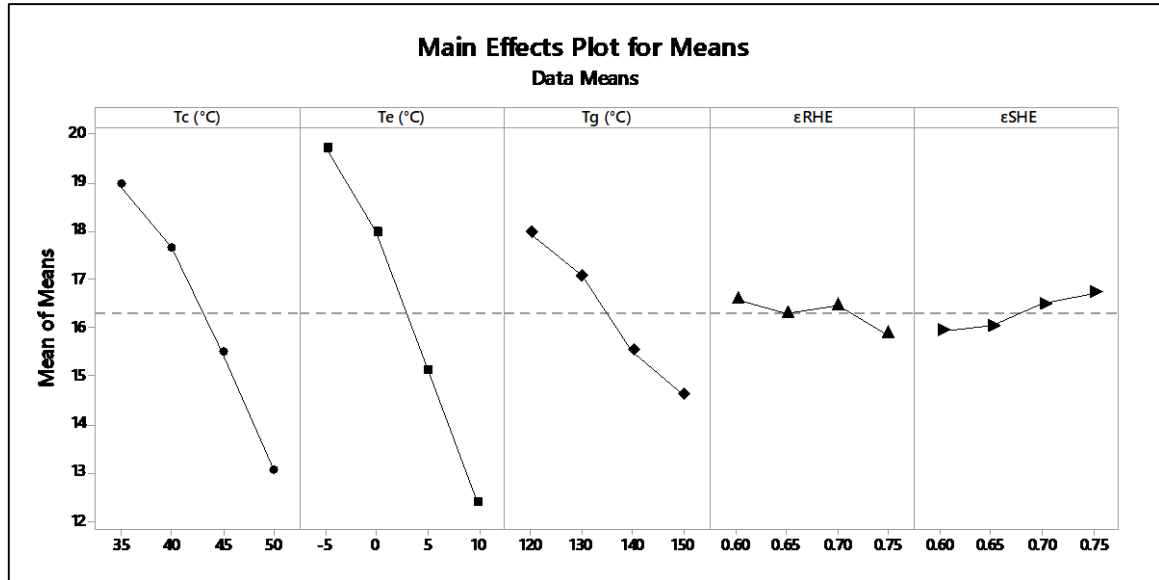
Fig 3.21 Main effect plot of mean of means for exergetic efficiency

Results of SN ratio analysis

Tables 3.10 and 3.11 shows the response of SN ratio and means for COP respectively.

Table 3.10 Response of SN for COP

Level	T_c (°C)	T_e (°C)	T_g (°C)	ε_{RHE}	ε_{SHE}
1	-4.896	-7.208	-6.316	-6.051	-6.491
2	-5.506	-6.353	-6.129	-6.084	-6.320
3	-6.400	-5.883	-6.114	-6.129	-5.972
4	-7.830	-5.188	-6.073	-6.368	-5.849
Delta	2.934	2.020	0.243	0.317	0.642
Rank	1	2	5	4	3

Table 3.11 Response of Means for COP

Level	T_c (°C)	T_e (°C)	T_g (°C)	ε_{RHE}	ε_{SHE}
1	0.5726	0.4389	0.4841	0.5015	0.4781
2	0.5316	0.4839	0.4984	0.5032	0.4874
3	0.4818	0.5142	0.5027	0.4977	0.5107
4	0.4067	0.5558	0.5075	0.4903	0.5165
Delta	0.1659	0.1169	0.0234	0.0128	0.0384
Rank	1	2	4	5	3

From both the tables it can be seen that condenser temperature has maximum influence on COP of all selected parameters. Tables 3.12 and 3.13 shows the response of SN ratio and means for exergetic efficiency respectively. It is observed form both the tables that evaporator temperature has maximum influence on exergetic efficiency of all selected parameters.

Table 3.12 Response of SN for exergetic efficiency

Level	T_c (°C)	T_e (°C)	T_g (°C)	ε_{RHE}	ε_{SHE}
1	25.35	25.74	24.71	24.12	23.69
2	24.69	24.97	24.29	24.09	23.84
3	23.75	23.50	23.74	24.03	24.20
4	22.23	21.82	23.28	23.79	24.29
Delta	3.11	3.92	1.43	0.34	0.60
Rank	2	1	3	5	4

Table 3.13 Response of Means for exergetic efficiency

Level	T_c (°C)	T_e (°C)	T_g (°C)	ε_{RHE}	ε_{SHE}
1	18.95	19.70	17.96	16.57	15.93
2	17.65	17.97	17.07	16.29	16.04
3	15.51	15.12	15.52	16.46	16.48
4	13.06	12.37	14.62	15.85	16.73
Delta	5.89	7.33	3.35	0.72	0.80
Rank	2	1	3	5	4

Chapter 4

Analysis of absorption refrigeration system coupled with evacuated glass tube based parabolic trough collector

From thermodynamic analysis of ammonia-water absorption refrigeration system maximum COP of 0.525 was calculated at optimum generator temperature of 170ºC for the condenser temperature of 50ºC, evaporator temperature of 10ºC, and effectiveness of RHE and SHE of 0.7. In a typical absorption refrigeration system, ammonia and water is separated by providing heat to the generator. ARS can work on low grade energy like waste heat, solar energy etc. In present work solar energy is used. To provide required heat to the generator it is necessary to select proper solar collector. Evacuated glass tube collector has many advantages compared to flat plate collector.

Weathering influences cause early deterioration of materials, resulting in performance reduction and system failure of flat plate collectors. Efficiency of evacuated tube collector is

higher at low incidence angle. Therefore, evacuated tube collector has an advantage over flat plate collector in terms of day long performance. In evacuated tube collector water or any other fluid can be used, which flows through the collector in either U-shape tube or coaxial pipe. Nowadays, Dewar type evacuated tube collectors are most commercialized which has low cost and more lifetime. The advantages of these type of collectors are that it is made entirely of glass and not necessary to penetrate the glass envelope to remove heat from the tube, eliminating leakage losses and cheaper than the single envelope system. Evacuated tube collectors are available in the market in a variety of sizes, with outer diameters ranging from 30 mm to about 100 mm and usual length of these collectors is about 2 m [5]. Commercially available evacuated glass tube has stagnation temperature around 200°C and can deliver heat efficiently at around 100°C. Therefore to harvest the heat at higher temperatures, it is necessary to use external reflectors to concentrate the solar radiation on to the evacuated glass tube. Parabolic trough reflector can be used with evacuated glass tube to deliver heat at higher temperature with better efficiency. Parabolic trough collectors can be used for process heat applications up to 400ºC. It is made by bending a sheet of reflective material into a parabolic shape. Parallel rays of solar radiation incident on the reflector are reflected to the receiver tube, when the parabola is pointed towards the sun. The concentrated radiation, which transfers to the receiver tube, heats the fluid that circulates through U-shape or coaxial pipe. Thus it transforms solar radiation into useful heat [56]. In present work, parabolic trough reflector is used with evacuated glass tube. Helical wiry turbulator is placed in the annulus of a coaxial tube and evacuated glass tube to enhance heat removal from the collector. Thus evacuated glass tube based parabolic trough collector with helical wiry turbulator is conceived to harvest solar energy to supply heat to the generator of ARS at required temperature.

4.1 Evacuated glass tube based parabolic trough collector with helical wiry turbulator

Cross sectional view of evacuated glass tube based parabolic trough collector with helical wiry turbulator is shown in Fig 4.1. Two views of the collector are shown in Fig 4.2 where reflector is not shown intentionally. The solar collector consists of an evacuated glass tube, a metal tube, helical wiry turbulator and a reflector. A two layered evacuated glass tube is fused together at one end, and the selective coating is deposited on the outer surface of the inner tube which is

also called an absorber tube. Air is withdrawn from the space between two glass tubes and vacuum is formed. Due to combined effect of vacuum insulation and high selective absorbing coating, solar energy can be absorbed well and the thermal loss is very small, so it is possible to achieve higher working fluid temperature.
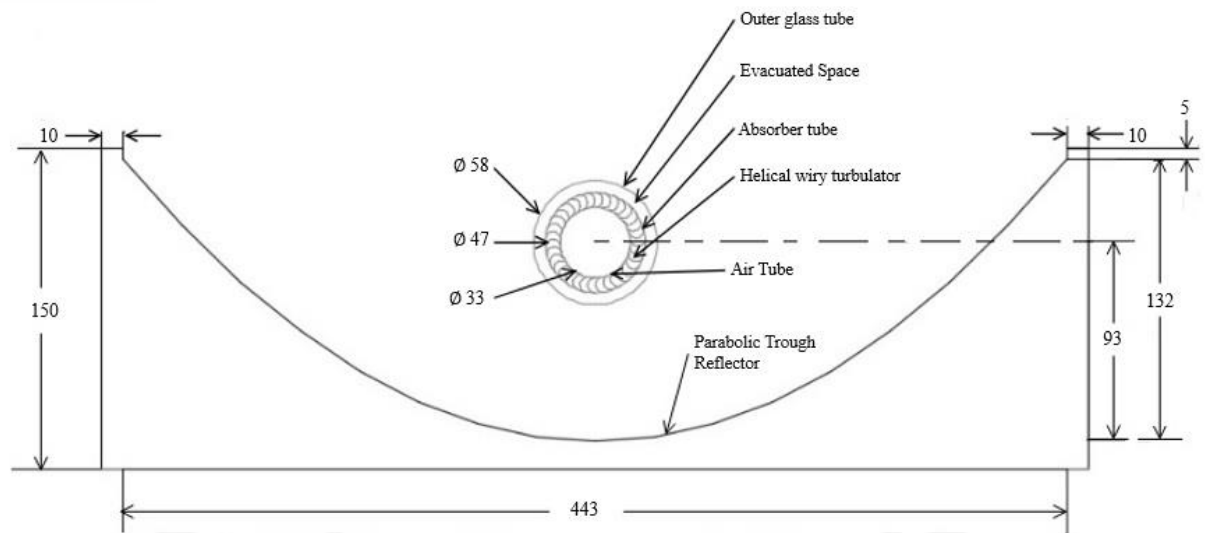
Fig 4.1 Sectional view of the solar collector
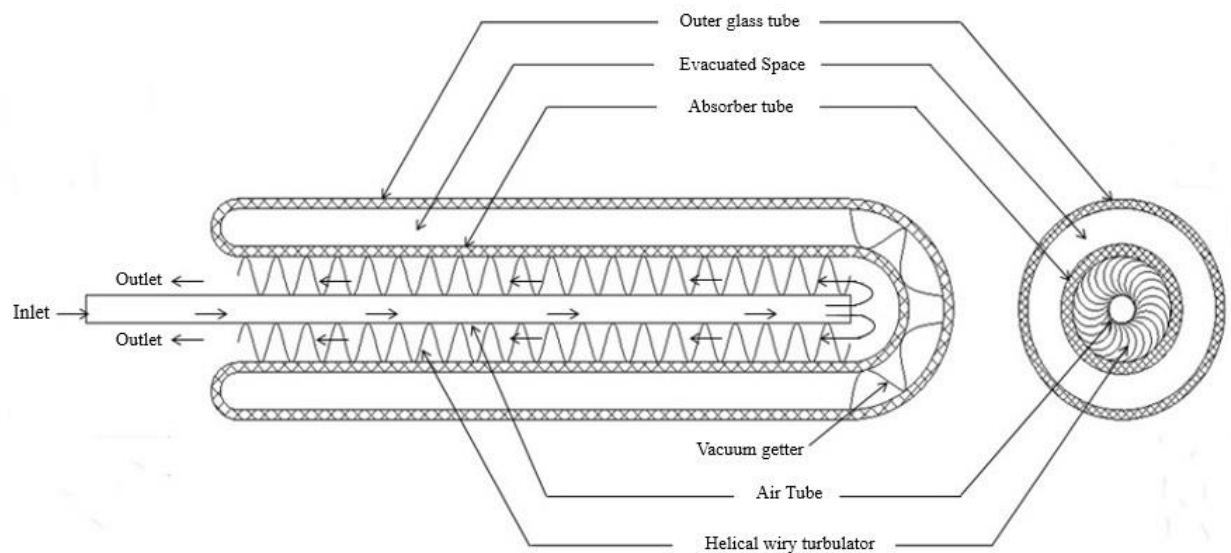
Fig 4.2 Schematic diagram of evacuated glass tube based parabolic trough collector with helical wiry turbulator

A metal tube is located concentrically inside the inner glass tube to create fluid passage. Air is used as heat transfer fluid in present study and hence metal tube is also referred as air tube.

Helical wiry turbulator is located in the annulus of the inner glass tube and the metal tube. Turbulator augments the heat transfer between absorber and the air flowing through the annulus and thus reduces temperature difference between absorber and air, which eventually helps to achieve higher collector efficiency for same air outlet temperature.

Table 4.1 Materials, parameters, and properties of evacuated glass tube based parabolic trough collector with helical wiry turbulator

Component (Material)	Parameters and properties	Dimensions	Units
Evacuated glass tube (borosilicate glass tube with outer surface of inner glass tube coated with selective coating)	Outer tube outer diameter	58	mm
	Outer tube inner diameter	54.4	mm
	Absorber tube outer diameter	47	mm
	Absorber tube inner diameter	43.8	mm
	Effective length of glass tube	1710	mm
	Transmissivity of glass cover	0.91	-
	Absorptivity of glass cover	0.04	-
	Reflectivity of glass cover	0.05	-
	Absorptivity of absorber	0.9	-
	Emissivity of glass cover	0.92	-
	Emissivity of absorber	0.1	-
	Conductivity	1	W/m K
Metal tube (SS304)	Outer diameter	33	mm
	Inner diameter	30	mm
	Conductivity	16.2	W/m K
	Total length	2000	mm
Turbulator (SS304)	Wire diameter	0.5	mm
	Conductivity	16.2	W/m K
	Core diameter	5	mm
	Pitch	3	mm
Holding spring	Pitch	12	mm
	wire diameter	1	mm
Reflector (anodized aluminum)	Rim angle	102	°
	Reflectivity	0.82	-

Air enters the air tube at open end of evacuated glass tube, heated up, while passing from open end to close end through air tube and heated up further while passing from the close end to open end through annulus of air tube and inner glass tube over the turbulator. Hot air is used in the generator of vapour absorption system to separate ammonia and water. The details about physical dimensions, optical properties, and material of various components of the solar collector are given in Table 4.1. Evacuated glass tube dimensions and its optical properties shown in Table 4.1 are taken from the supplier's website. [98].

4.1.1 Thermal modeling

Steady state thermal model has been developed considering various modes of heat transfer between different components of evacuated glass tube based parabolic trough collector. The model has been developed with following assumptions.

- Solar intensity at collector surface is constant throughout the collector.
- Specific heat of working fluid remains constant with respect to temperature change in the system.
- Convective and radiative heat transfer coefficients between outer glass tube and ambient are constant.
- Contact resistance between helical wiry turbulator and evacuated glass tube and between helical wiry turbulator and air tube is neglected.

Thermal network of evacuated glass tube based parabolic trough collector with helical wiry turbulator

Concentrating collectors can work by interposing an optical device between the source of radiation and receiver. In present work, parabolic trough collector is used and evacuated glass tube with helical wiry turbulator is used as receiver. Fig 4.3 shows the cross section of evacuated glass tube with helical wiry turbulator showing different temperatures which influence the heat transfer between different components of the collector. Fig 4.4 shows the thermal network diagram associated with the heat transfer process of the collector. The evacuated tube is heated

69

by solar radiation after concentration by parabolic reflector. The resistances in the network represent the element of collector.
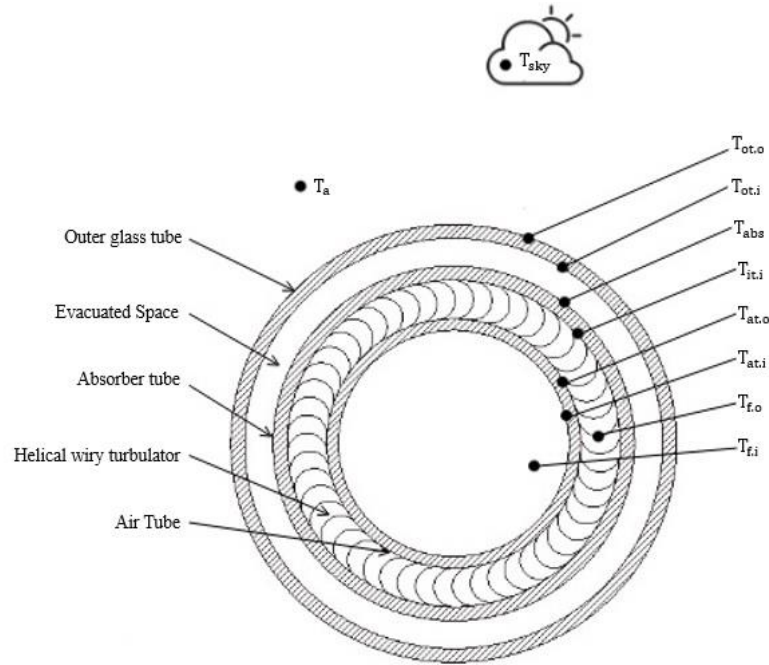
Fig 4.3 Cross section of evacuated glass tube with helical wiry turbulator showing different
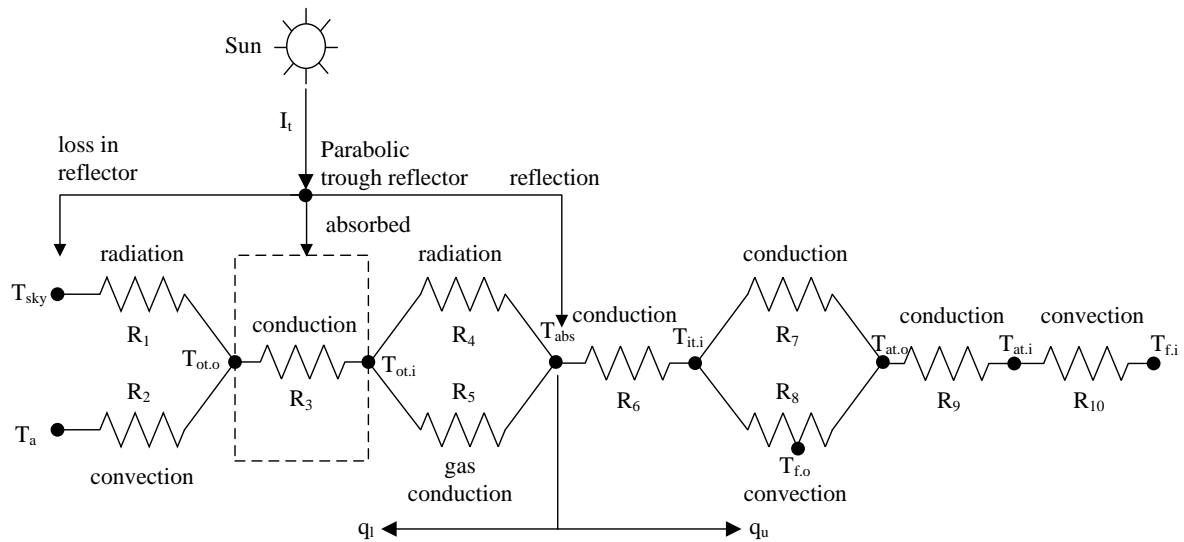
Fig 4.4 Thermal network diagram of evacuated glass tube based parabolic trough collector with helical wiry turbulator

Thermal losses occurs due to radiation and convection from outer glass tube to sky and ambient respectively. Corresponding thermal resistances for radiation and convection heat transfer are

70

denoted by R_1 and R_2 respectively. Thermal resistance to conduction through the outer glass tube is denoted by R_3. Radiation heat exchange take place between the absorber tube and the outer glass tube. Associated thermal resistance for radiation heat transfer is denoted by R_4. R_5 is the thermal resistance due to gas conduction which occurs in the vacuum between two glass tubes. Conduction thermal resistance through absorber tube is denoted by R_6. Conduction takes place between the absorber tube and air tube through helical wiry turbulator. Corresponding thermal resistance is denoted by R_7. Convection heat transfer takes place between inner surface of absorber tube and air passing through annulus of absorber tube and air tube; and between the air and air tube outer surface. Corresponding thermal resistance is denoted by R_8. Helical wiry turbulator augments this convective heat transfer. Conduction resistance of air tube and convective resistance between inner surface of air tube and air passes through air tube is denoted by R_9 and R_{10} respectively.

Essential equations governing heat transfer between various components of the collector and thus required to estimate its efficiency as well as different thermal resistance are given below. Area of absorber tube is calculated by

$$A_{abs} = \pi \times d_{abs} \times l_u \tag{4.1}$$

Area of outer glass tube is given by

$$A_{ot.o} = \pi \times d_{ot.o} \times l_u \tag{4.2}$$

Aperture width of parabola can be calculated by

$$w_{para} = \pi \times d_{abs} \times CR \tag{4.3}$$

The concentration ratio (CR) is defined as the ratio of aperture area to the absorber area. For simulation, different values of CR in the range of 2 to 4 was considered.

Aperture area of parabolic reflector can be calculated by

$$A_{ap} = w_{para} \times l_u \tag{4.4}$$

Solar radiation intercepted can be calculated by

$$Q_i = I_t A_{ap} \tag{4.5}$$

Cross section area of annulus can be calculated by

$$A_{cs.anu} = \frac{\pi}{4} \left(d_{it.i}^2 - d_{at.o}^2 \right) \tag{4.6}$$

Perimeter of annulus can be calculated by

$$p_{anu} = \pi \times \left(d_{it.i} + d_{at.o} \right) \tag{4.7}$$

Hydraulic diameter of annulus is obtained by

$$d_{h.anu} = \frac{4 \times A_{cs.anu}}{p_{anu}}$$ (4.8)

Blockage area due to helical wiry turbulator is given by

$$A_{bl.hwt} = d_{hwt} \times (d_{it.i} - d_{at.o}) \times n_{hwt.p.hs}$$ (4.9)

Free flow area of annulus to calculate velocity of air is given by

$$A_{f.anu} = A_{cs.anu} - A_{bl.hwt}$$ (4.10)

Thermal resistance to radiation heat transfer from outer tube to sky is written as

$$R_1 = \frac{1}{A_{ot.o}\varepsilon_{ot.o}\sigma(T_{ot.o} + T_{sky})(T_{ot.o}^2 + T_{sky}^2)}$$ (4.11)

Where, sky temperature is evaluated by using following equation [99]

$$T_{sky} = 0.0552(T_0 + 273.15)^{1.5} - 273.15$$ (4.12)

Thermal resistance to convection from outer glass tube can be estimated as

$$R_2 = \frac{1}{h_{a.o}A_{ot.o}}$$ (4.13)

Where, outside convective heat transfer coefficient [4] is calculated by either using equation (4.14) or (4.15)

$$h_{a.o} = 5.7 + 3.8 \times v_w$$ (4.14)

$$h_{a.o} = \frac{Nu_{a.o}k_{a.o}}{d_{ot.o}}$$ (4.15)

Nusselt number is evaluated using following equation [99].

$$Nu_{a.o} = \begin{cases} 0.4 + 0.54\,\mathrm{Re}_{a.o}^{0.52} \rightarrow 0.1 < \ \mathrm{Re}_{a.o} \leq 1000 \\ 0.3\,\mathrm{Re}_{a.o}^{0.6} \rightarrow 1000 < \ \mathrm{Re}_{a.o} < 50000 \end{cases}$$ (4.16)

Where, all fluid properties are evaluated at ambient temperature.

Thermal resistance to conduction through the outer glass tube thickness is due to Fourier's law of conduction

$$R_3 = \frac{1}{2\pi k_g l_u} \ln \frac{d_{ot.o}}{d_{ot.i}}$$ (4.17)

Radiation heat transfer between absorber tube and outer glass tube is through following resistance

$$R_4 = \frac{\dfrac{1}{\varepsilon_{abs}} + \left(\dfrac{d_{it.o}}{d_{ot.i}}\right)\left(\dfrac{1}{\varepsilon_{ot}} - 1\right)}{A_{abs}\sigma\left(T_{abs} + T_{ot.i}\right)\left(T_{abs}^2 + T_{ot.i}^2\right)} \tag{4.18}$$

Thermal resistance due to gas conduction in the evacuated space can be written as

$$R_5 = \frac{g + 2p}{k_{air} A_{abs}} \tag{4.19}$$

Where, g is the gap width and p is the mean free path. For air, the mean free path at atmospheric pressure is about 70 μm. If 99 % of the air is removed from a tubular collector, the mean free path increases to 7 mm and conduction heat transfer is affected very little [100].

Thermal resistance to conduction in the absorber tube thickness can be written as

$$R_6 = \frac{1}{2\pi k_g l_u} \ln\frac{d_{it.o}}{d_{it.i}} \tag{4.20}$$

Helical wiry turbulator is held in position between air tube and inner glass tube. It is resilient in contact with both, the outer surface of air tube and the inner surface of absorber tube. Neglecting contact resistance, conductive resistance between absorber tube and air tube is due to helical wiry turbulator as per Fourier's law is given by.

$$R_7 = \frac{d_c}{k_r d_r^2 n_r} \tag{4.21}$$

Thermal resistance due to convection between inner surface of absorber tube and air passing through annulus of absorber tube and air tube; and between the air and air tube outer surface can be written as

$$R_8 = \frac{d_{it.i} - d_{at.o}}{Nu_{anu} k_{anu} \pi d_{it.i} l_u} \tag{4.22}$$

For fully developed transition and turbulent flow, Nusselt number is calculated using Gnielinski [101] correlation as given below

$$Nu_i = \frac{\left(\dfrac{f}{8}\right)(\mathrm{Re}_i - 1000)\mathrm{Pr}_i}{1 + 12.7\sqrt{\dfrac{f}{8}}\left(\mathrm{Pr}_i^{\frac{2}{3}} - 1\right)}\left[1 + \left(\dfrac{d_{at.i}}{l_u}\right)^{\frac{2}{3}}\right]\left(\dfrac{T_m}{T_{it.i}}\right)^{0.45} \rightarrow \begin{cases} \mathrm{Re}_i > 2300 \\ \mathrm{Pr}_i = 0.6 - 10^5 \end{cases} \tag{4.23}$$

Where, f can be calculated by using following formula

$$f = \left[1.82\log_{10}\left(\mathrm{Re}_i\right) - 1.64\right]^{-2} \tag{4.24}$$

All fluid properties in equation (4.23) are evaluated at average fluid temperature in annulus.

Nusselt number for fully developed laminar flow with constant heat flux is given by

$$Nu_{anu} = 4.36 \tag{4.25}$$

Convective heat transfer coefficient calculated using Equation 4.23 or 4.25 is assumed to be augmented by 50% due to turbulator based on work of Bhatt [102].

$$h_{a.hwt} = e_{hwt} \times h_{a.anu} \tag{4.26}$$

Thermal resistance due to conduction through air tube thickness can be written as

$$R_9 = \frac{1}{2\pi k_{at} l_u} \ln \frac{d_{at.o}}{d_{at.i}} \tag{4.27}$$

Thermal resistance due to convection between inner surface of air tube and air passes through air tube can be written as

$$R_{10} = \frac{1}{\pi Nu_i k_i l_u} \tag{4.28}$$

Where, Nusselt number is calculated using Equation 4.23 or 4.25 based on the Reynolds number of air inside the tube. Air tube inner diameter is taken as hydraulic diameter for the calculations. Heat absorbed by absorber tube is given by

$$Q_{a.abs} = \left(Q_i - Q_{a.ot} - Q_{r.ot} - Q_{a.ref} \right) \times \alpha_{abs} \tag{4.29}$$

Due to multiple absorption and reflection effective emissivity is calculated from following equation

$$\varepsilon_{eff} = \left[\frac{1}{\varepsilon_{abs}} + \left(\frac{d_{it.o}}{d_{ot.i}} \right) \left(\frac{1}{\varepsilon_{gc}} - 1 \right) \right]^{-1} \tag{4.30}$$

Radiation losses from absorber tube is given by

$$Q_{rl.abs} = \varepsilon_{eff} \times \sigma \times A_{abs} \times \left(T_{abs.av}^4 - T_{gc.av}^4 \right) \tag{4.31}$$

Useful heat gain by the air is the difference between heat absorbed by absorber tube to the radiation losses from absorber tube and it is calculated by

$$Q_u = Q_{a.abs} - Q_{rl.abs} \tag{4.32}$$

Heat absorbed in outer glass tube is given by

$$Q_{a.ot} = \alpha_{gc} \times I_t \times d_{ot.o} \times l_u \times \left(1 + \left((\pi \times CR - 1) \times \gamma_{ref} \right) \right) \tag{4.33}$$

Heat reflected from outer glass tube is given by

$$Q_{r.ot} = \lambda_{gc} \times I_t \times d_{ot.o} \times l_u \times \left(1 + \left((\pi \times CR - 1) \times \gamma_{ref} \right) \right) \tag{4.34}$$

Heat absorbed by reflector is given by

$$Q_{a.ref} = I_t \times d_{abs} \times l_u \times \left(\left(\pi \times CR - 1\right) \times \left(1 - \gamma_{ref}\right)\right) \tag{4.35}$$

Radiation and convection losses from outer glass tube is calculated from following equations.

$$Q_{rad.ot} = \varepsilon_{gc} \sigma A_{gc} \left(T_{gc.av}^4 - T_{sky}^4\right) \tag{4.36}$$

$$Q_{conv.ot} = h_o A_{gc} \left(T_{gc.av} - T_{amb}\right) \tag{4.37}$$

Average glass cover temperature is calculated iteratively from equations (4.31), (4.33), (4.36) and (4.37)

Efficiency of solar collector is evaluated by following equation

$$\eta_{sc} = \frac{Q_u}{Q_i} \tag{4.38}$$

Calculation of thermal resistance

All the thermal resistances discussed earlier in section 3 were calculated for CR=3, I_t = 900 W/m^2, T_{in} = 35ºC, T_{out} = 170ºC and T_{amb} = 35ºC, which are listed in Table 4.2. From the table it was inferred that thermal resistance to radiation (R_4) and gas conduction (R_5) between absorber tube and outer glass tube were significantly higher and therefore heat energy can easily be transferred to the working fluid. Heat loss from outer tube to ambient and sky represent overall heat loss from the collector. Due to higher values of the resistance R_4 and R_5 and lower value of resistance R_3, temperature of outer glass tube was sufficiently lower than absorber temperature and close to ambient temperature. Hence overall heat loss from the collector was less and thermal efficiency of the collector was on higher side. It can further be noted that convection resistance between absorber tube and air passing through annulus of absorber and air tube was comparative lower. This was due to helical wiry turbulator which helps to reduce temperature difference between the absorber tube and the air, which reduces absorber temperature for required air outlet temperature. Convection resistance (R_{10}) between air and inner surface of air tube was about four times that of between absorber tube and air (R_8). This ensures that air temperature when it enters the annulus space at closed end was comparatively lower which ensure lower average absorber temperature.

Table 4.2 Values of thermal resistances of Fig 4.4

Thermal resistance	Value (K/W)
Radiation thermal resistance from outer glass tube (R_1)	0.523
Convection thermal resistance from outer glass tube (R_2)	0.2455
Conduction thermal resistance from outer glass tube (R_3)	0.00596
Radiation thermal resistance from absorber tube to outer glass tube (R_4)	3.784
Gas conduction thermal resistance (R_5)	22.28
Conduction thermal resistance from absorber tube thickness (R_6)	0.00656
Conduction thermal resistance between absorber and air tube from helical wiry turbulator (R_7)	0.218
Convection thermal resistance between absorber and air passing from annulus of absorber and air tube (R_8)	0.0664
Conduction thermal resistance from air tube thickness (R_9)	0.000364
Convection thermal resistance between inner surface of air tube and air passes from air tube (R_{10})	0.2524

As expected, all the conduction resistance (except gas conduction) are very small. Thermal resistance due to gas conduction, which is considered in present case is very high and hence can be neglected for all practical purposes.

4.1.2 Simulation of evacuated glass tube based parabolic trough collector with helical wiry turbulator

To understand the effect of solar radiation on efficiency and required mass flow rate for desired air outlet temperature in the range of 150 to 190ºC, simulation was carried out for solar radiation between 500 and 1100 W/m^2, assuming air inlet temperature of 35ºC. Fig 4.5 shows the effect of solar insolation on efficiency of solar collector for different air outlet temperatures. Simulation results show that collector efficiency increases with increase in solar insolation for desired air outlet temperature. With increase in solar insolation, radiation intercepted increases and hence useful heat gain increases significantly. While heat loss from the collector does not increase significantly due to same air inlet and outlet temperatures.

It was also observed from simulation results that at same value of solar insolation, efficiency of the collector is lower for the higher air outlet temperature. This is due to the fact that heat loss from the collector is propositional to average absorber temperature. With increase in air outlet temperature for same air inlet temperature, average absorber temperature increases and therefore efficiency of the collector decreases.
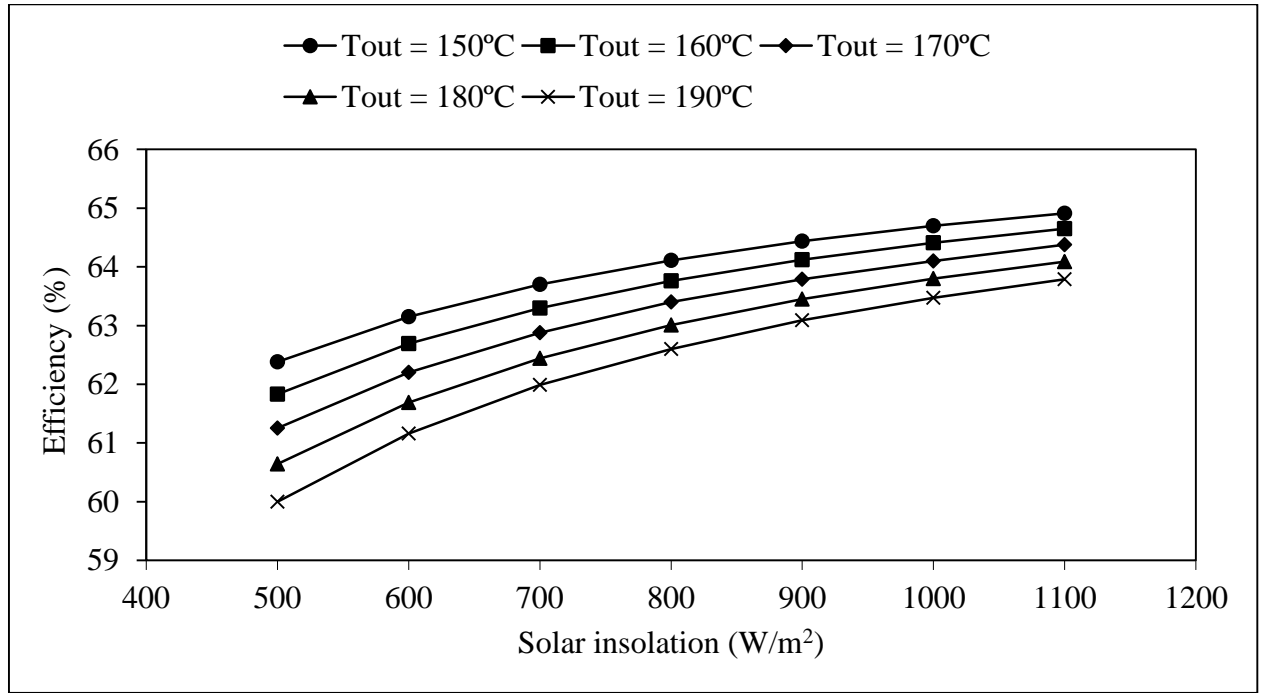
Fig 4.5 Effect of solar insolation on efficiency for different air outlet temperatures

Fig 4.6 shows the effect of solar insolation on mass flow rate for different air outlet temperatures. It was observed that with increase in solar insolation, mass flow rate required for desired air outlet temperature increases. This is due to increase in collector efficiency with increase in solar insolation for fixed air inlet and outlet temperatures. It is also seen that for the same solar insolation and fixed air inlet temperature, higher mass flow rate is required at lower air outlet temperature. At lower air outlet temperature, collector efficiency and hence useful heat gain is higher which demands for higher mass flow rate of air.
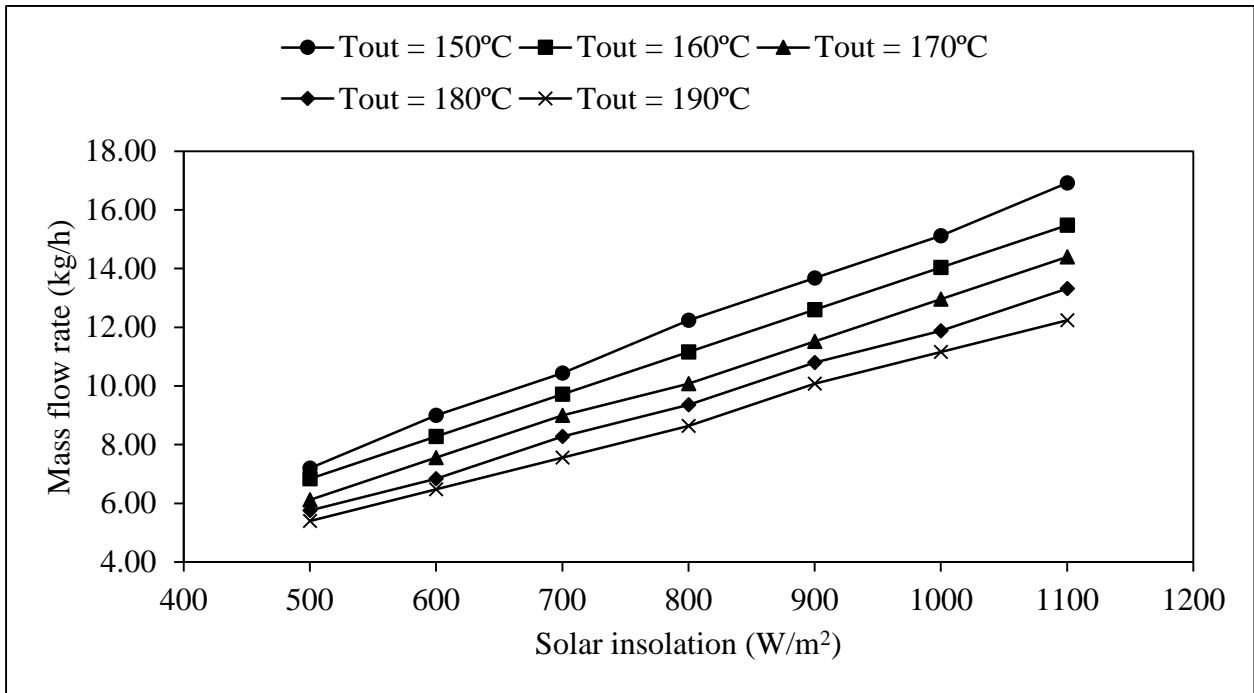
Fig 4.6 Effect of Solar insolation on required mass flow rate of air for different air outlet temperatures
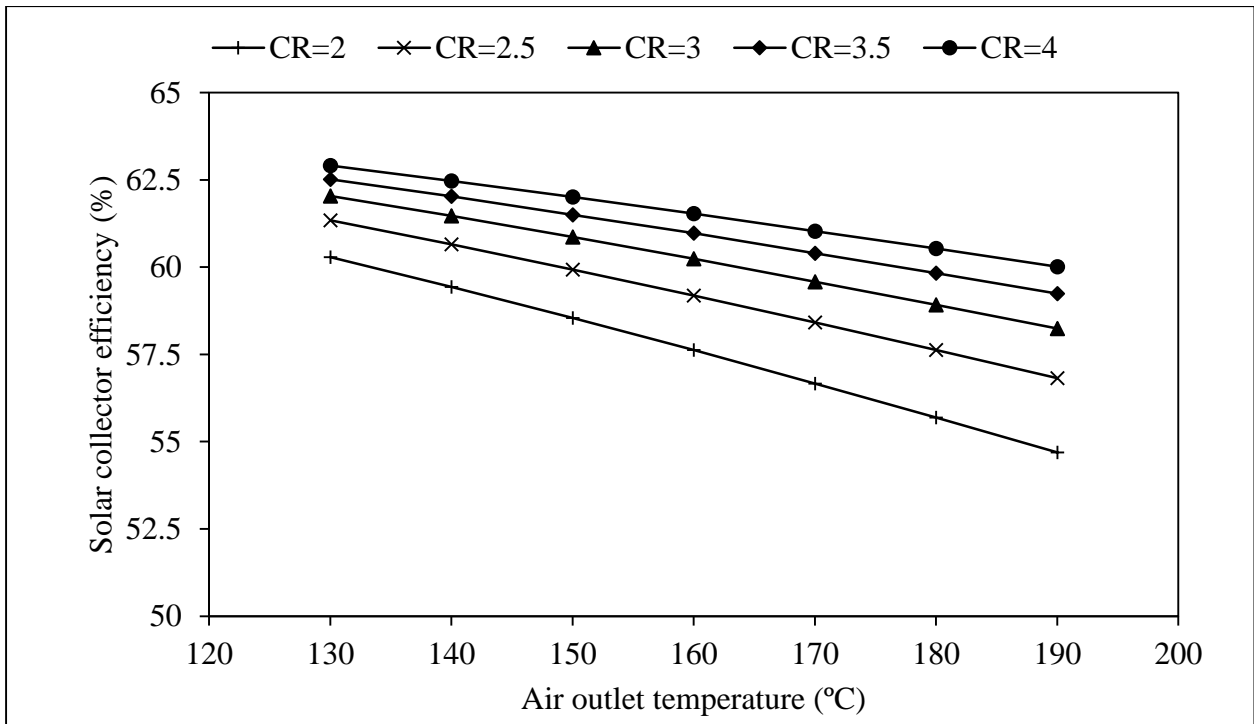
Fig 4.7 Effect of air outlet temperature on solar collector efficiency for different values of CR

Fig 4.7 shows the effect of air outlet temperature on solar collector efficiency for different concentration ratio. It is observed that as air outlet temperature increases solar collector

efficiency decreases for all values of CR. It is also observed that solar collector efficiency is higher at higher concentration ratio for the same value of air outlet temperature due to interception of more solar radiation. At higher CR the slope of the curves decrease, however due to decrease in acceptance angle, the tilt angle needs to be adjusted more than once over a day.

4.2 Simulation of absorption refrigeration system coupled with evacuated glass tube based parabolic trough collector with helical wiry turbulator

The evacuated glass tube based parabolic trough collector with helical wiry turbulator was considered to be coupled with the absorption refrigeration system described in Chapter 3. The effect of generator temperature on Solar COP was studied. Solar COP is a product of solar collector efficiency and COP of the absorption refrigeration system.
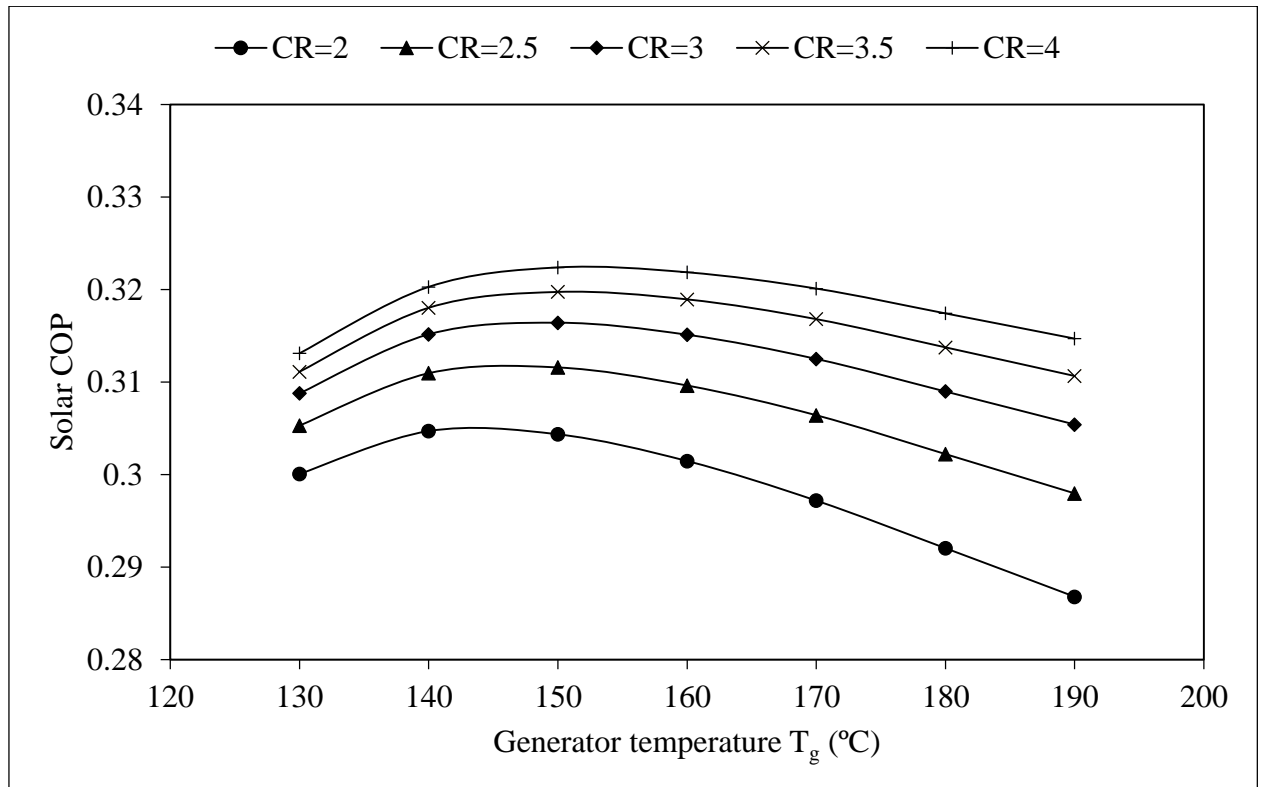
Fig 4.8 Effect of generator temperature on Solar COP for different values of CR

Fig 4.8 shows the effect of generator temperature on Solar COP for different values of concentration ratio. From simulation results it is observed that Solar COP first increases with increase in generator temperature, reaches a maximum value and then decreases with further increase in generator temperature due to lower collector efficiency at higher temperature and lower COP due to increase in irreversibility in the system. Solar COP is higher for the high concentration ratio at same generator temperature. In present study, the solar collector with concentration ratio of 3 was selected to power the ARS, as with increase of CR, acceptance angle decreases which demands for frequent or continuous tracking of the collector. It was also observed that for the concentration ratio of 3, maximum Solar COP is 0.3164 at optimum generator temperature of 150ºC. For the concentration ratio 3 an aperture width of 443 mm, height of 132 mm and length of 1710 mm were considered. Aperture area per tube was 0.757 m^2.

Chapter 5

Development of evacuated glass tube based parabolic trough collector

Evacuated glass tube based parabolic trough collector with helical wiry turbulator as described in Chapter 4 was fabricated and tested under the sun. In order to evaluate the thermal performance of evacuated glass tube based parabolic trough collector with helical wiry turbulator of concentration ratio 3, an experimental set up was constructed as illustrated in Fig 5.1. Fig 5.2 shows the photograph of complete experimental setup. In order to evaluate the performance improvement using the turbulator, two identical collectors, one with turbulator and the other without turbulator were constructed and tested under outdoor field conditions at Rajkot, Gujarat, India (latitude 22.3039º N, longitude 70.8022º E). The parabolic trough collector was mounted on a stand with focal axis E-W and horizontal. The aperture plane was tilted at an angle β towards the south. The tilt of the collector was adjusted once in a day i.e. at

the beginning of the day such that incident solar radiation was normal to the collector aperture at solar noon on that day. In the experimental work air was used as heat transfer fluid.
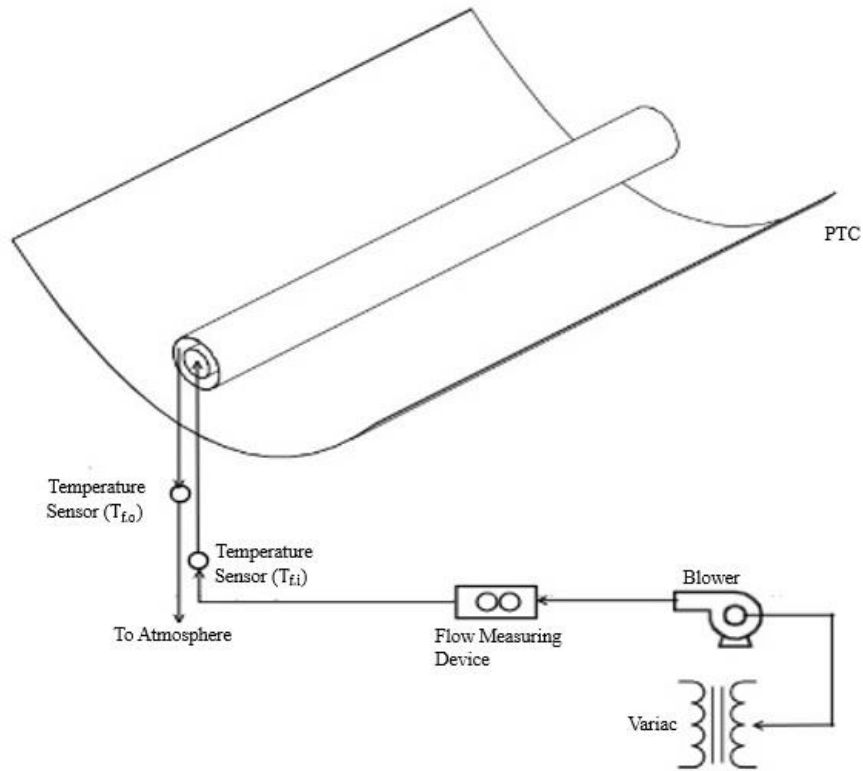
Fig 5.1 Experimental set up of evacuated glass tube based parabolic trough collector
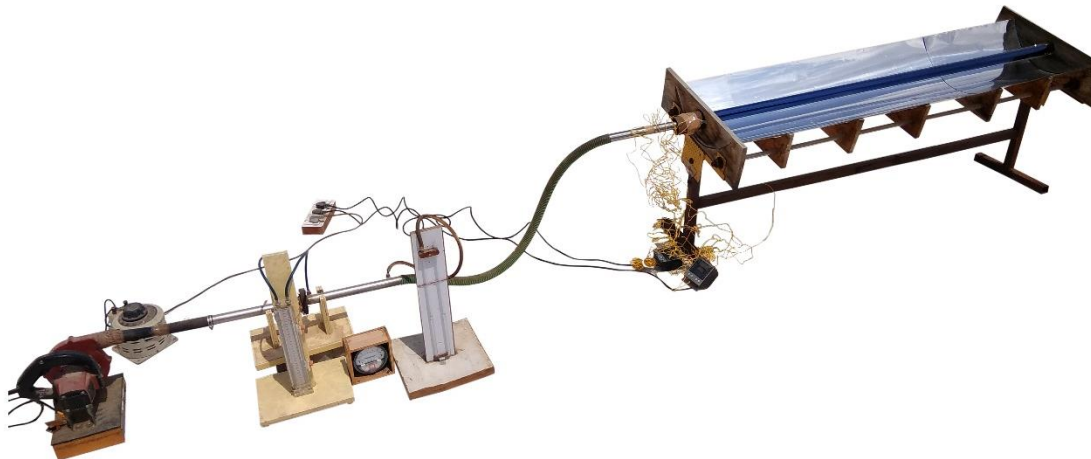
Fig 5.2 Photograph of experimental set up

Fig 5.3 to 5.6 shows the development of evacuated glass tube based parabolic trough collector with and without turbulator.

82

Fig 5.3 ETC with turbulator and air tube

Fig 5.4 Fabrication work of solar collector structure

Two identical prototypes of parabolic trough collector one with turbulator and the other without turbulator with concentration ratio of 3 were tested under outdoor field conditions for the different mass flow rates (4.32, 6.12, 7.56, 8.86, 9.72, 10.8, 11.52, 12.34, 12.96 and 13.68 kg/h) to investigate the thermal performance of the collectors. To evaluate daily thermal performance,

the collectors were tested from 9.00 to 16.30 h (local time) at particular mass flow rate. Each experiment was repeated three times to check the repeatability of the results.

Fig 5.5 Photograph of experimental set up (only collectors)

Fig 5.6 Photograph of experimental set up (arrangement of air flow circulation and measurement)

To investigate the thermal performance of evacuated glass tube based parabolic trough collector, various operating parameters like solar insolation, air outlet temperatures, air inlet temperatures, volume flow rate of air and pressure drop for different flow rates were recorded during the entire experimental period at regular interval. Air was sucked from the ambient and caused to move through the collector by a centrifugal blower. A variac was connected to the blower to regulate the air flow through the collector. An orifice meter with U-tube manometer/Magnehelic pressure gauge was installed between the blower and the collector to measure volume flow rate of air.

Various temperatures were measured by k-type of thermocouples. Total eight thermocouples were used to measure outlet temperature of air and three thermocouples were used to measure inlet temperature of air. Outlet and inlet temperatures were recorded by taking average of eight and three thermocouples temperatures respectively. Pyranometer was used for the measurement of solar irradiation.

Table 5.1 Specifications and accuracy of instruments used

Instrument	Parameter	Value	Accuracy
Pyranometer	Radiation (W/m^2)	0 to 2000	± 10 W/m^2 or $\pm 5\%$ (whichever is greater)
k-type thermocouple	Inlet and outlet fluid temperature (ºC)	-200 to 670	± 1ºC
U-tube manometer	Pressure head (mm of water)	0 to 450 mm of water	± 1 mm of water
Magnehelic pressure gauge	Pressure head (mm of water)	0 to 10 mm of water	± 0.2 mm of water
Flow meter	Diameter	15 mm	± 0.02 mm
Scale	Length and width of parabola	Length = 1710 mm Width = 443 mm	± 1 mm

Table 5.1 shows the specification and accuracy of instruments which were used in the fabrication work. U-tube manometer was used to measure the velocity head for mass flow rate of air from 13.68 to 7.56 kg/h and Magnehelic pressure gauge was used for the mass flow rate of air from 6.12 and 4.32 kg/h to get the more accuracy at lower mass flow rate.

5.1 Results and discussion

Experiments were carried out for the different mass flow rates of air. Results were recorded for air inlet temperature, air outlet temperature, solar insolation, velocity head and pressure drop across the collector for the different mass flow rates. Experiments were carried out for the mass flow rate in the range of 13.68 kg/h to 4.32 kg/h. Experiments were carried out to obtain air outlet temperature of 170ºC for duration of at least 6 h a day. Fig 5.7 to 5.16 shows the air temperature (inlet and outlet) with and without turbulator and solar insolation over a time of the day. It indicates that from morning to noon solar insolation increases, which is maximum approximately at solar noon, and then it starts decreases. Air outlet temperature is also increases from morning to noon and then it also starts to decreases.
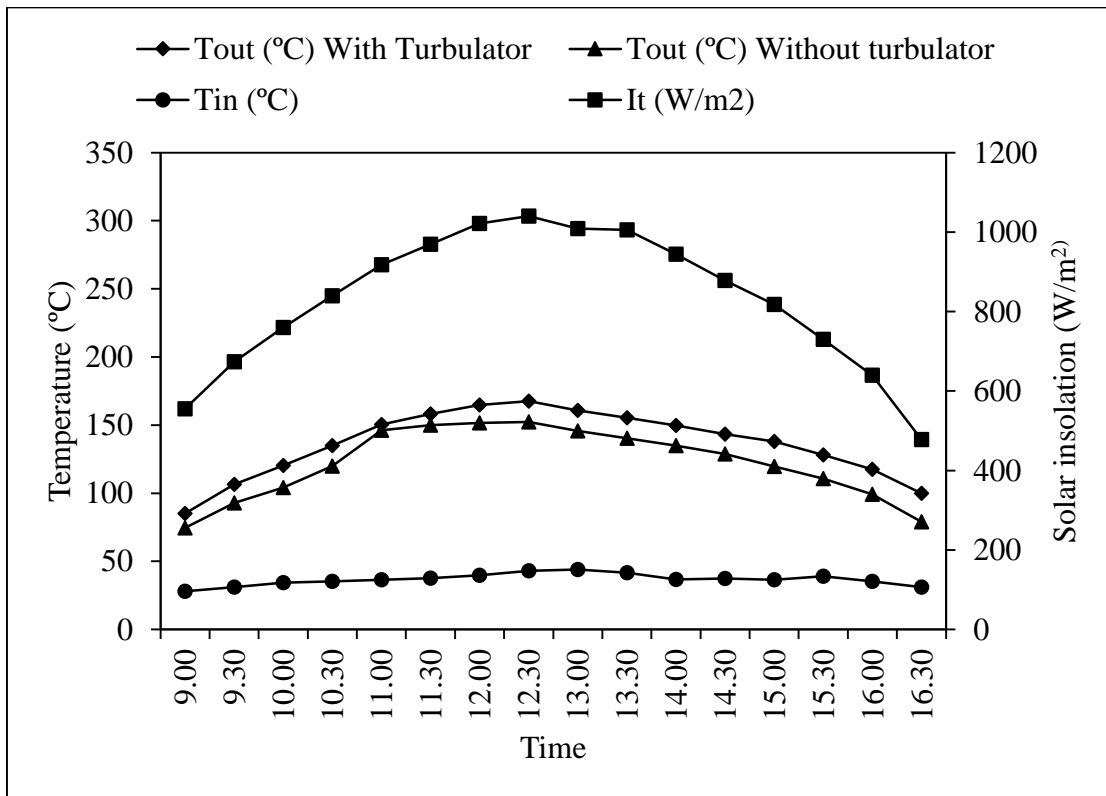
Fig 5.7 Experimental results for mass flow rate of 13.68 kg/h (Date: 11.04.2018)
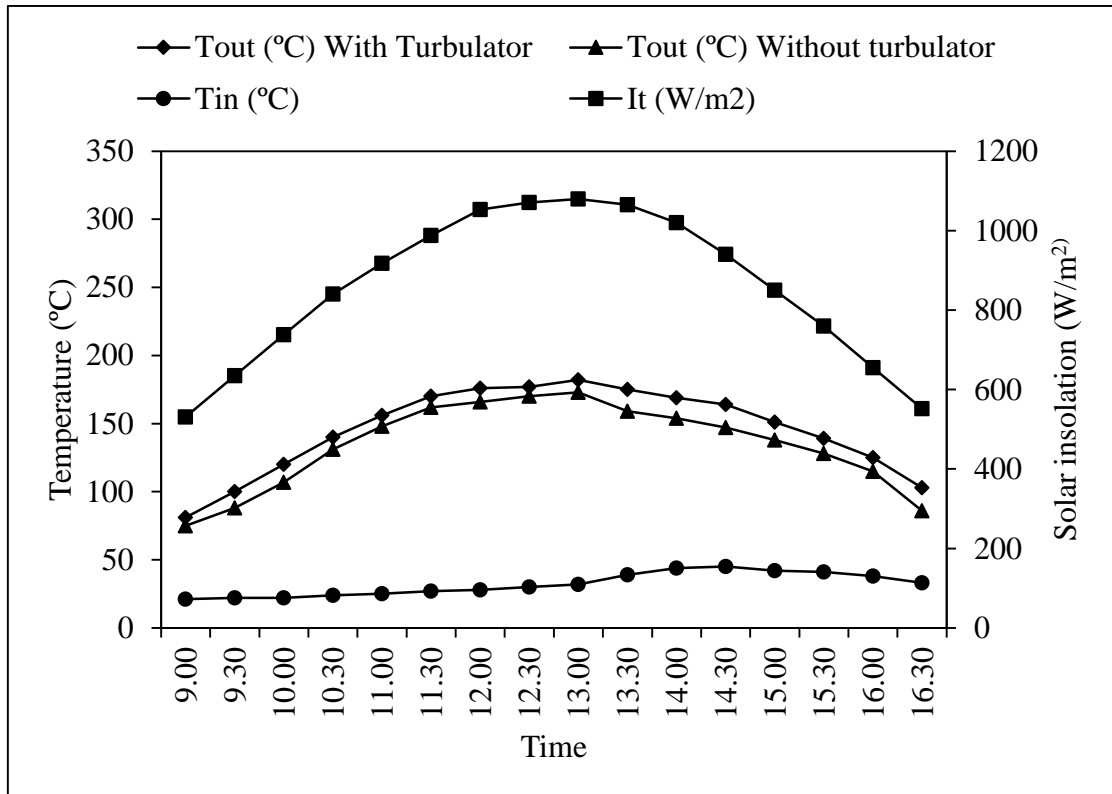
Fig 5.8 Experimental results for mass flow rate of 12.96 kg/h (Date: 14.04.2018)
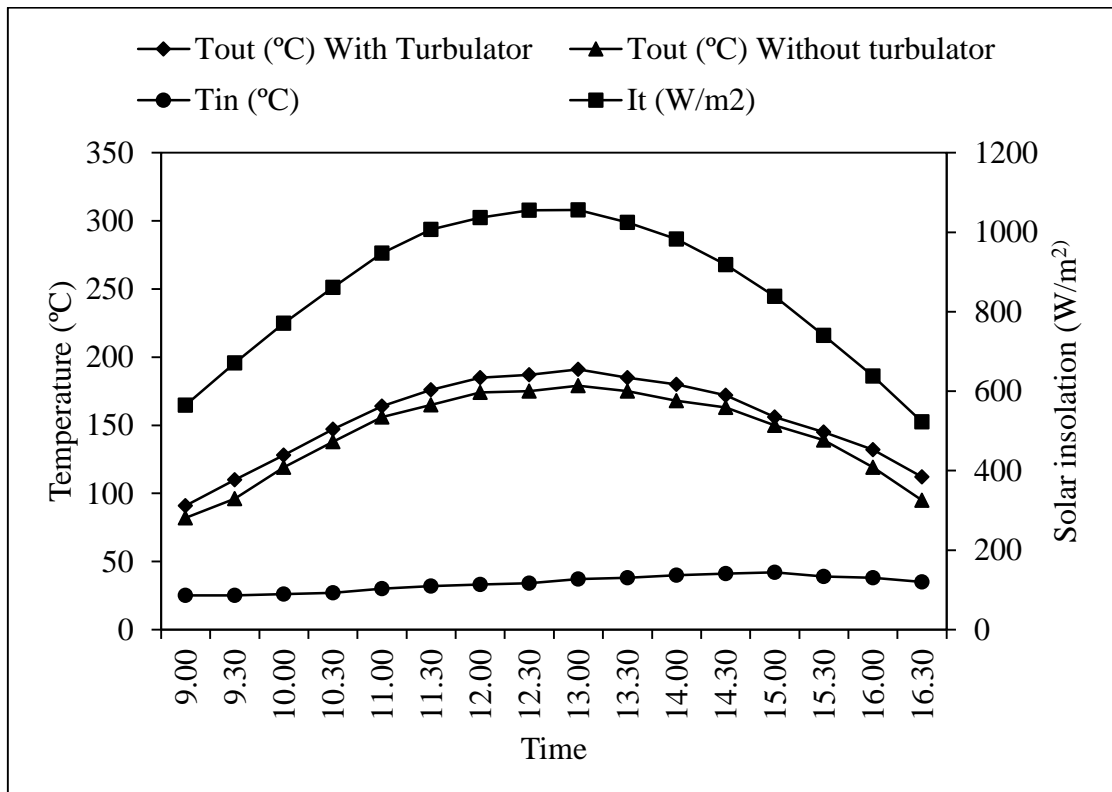
Fig 5.9 Experimental results for mass flow rate of 12.24 kg/h (Date: 17.04.2018)
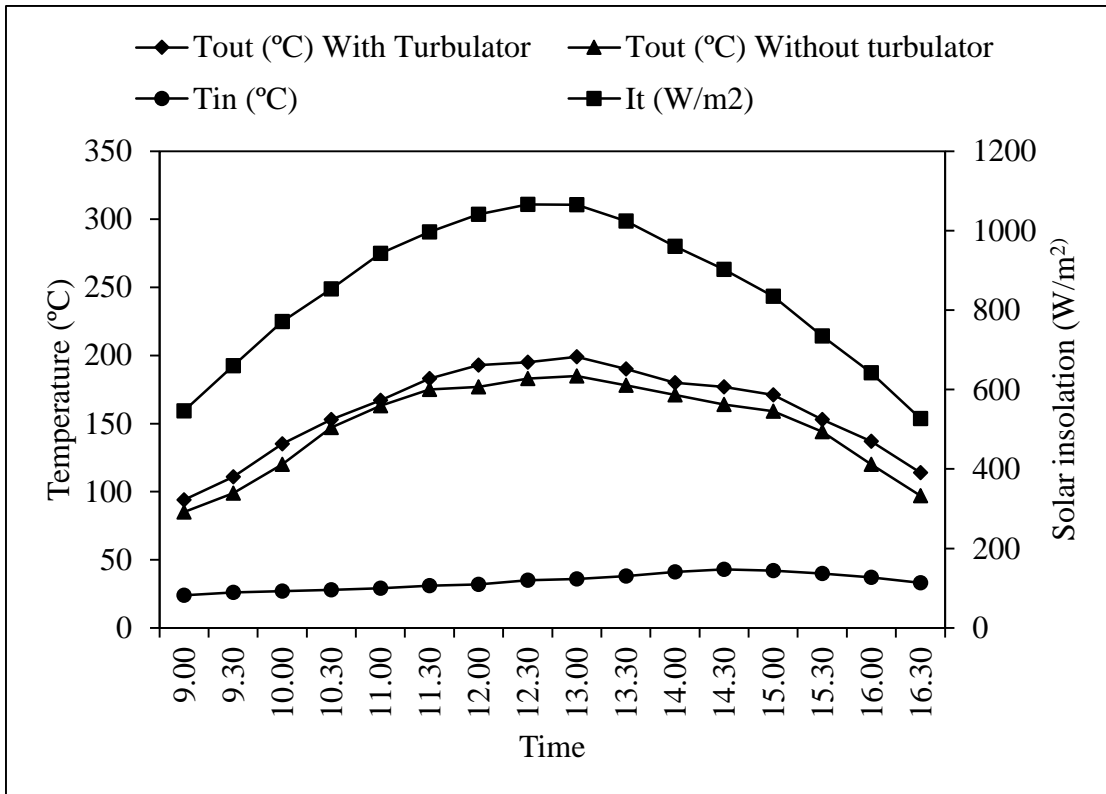
Fig 5.10 Experimental results for mass flow rate of 11.52 kg/h (Date: 20.04.2018)
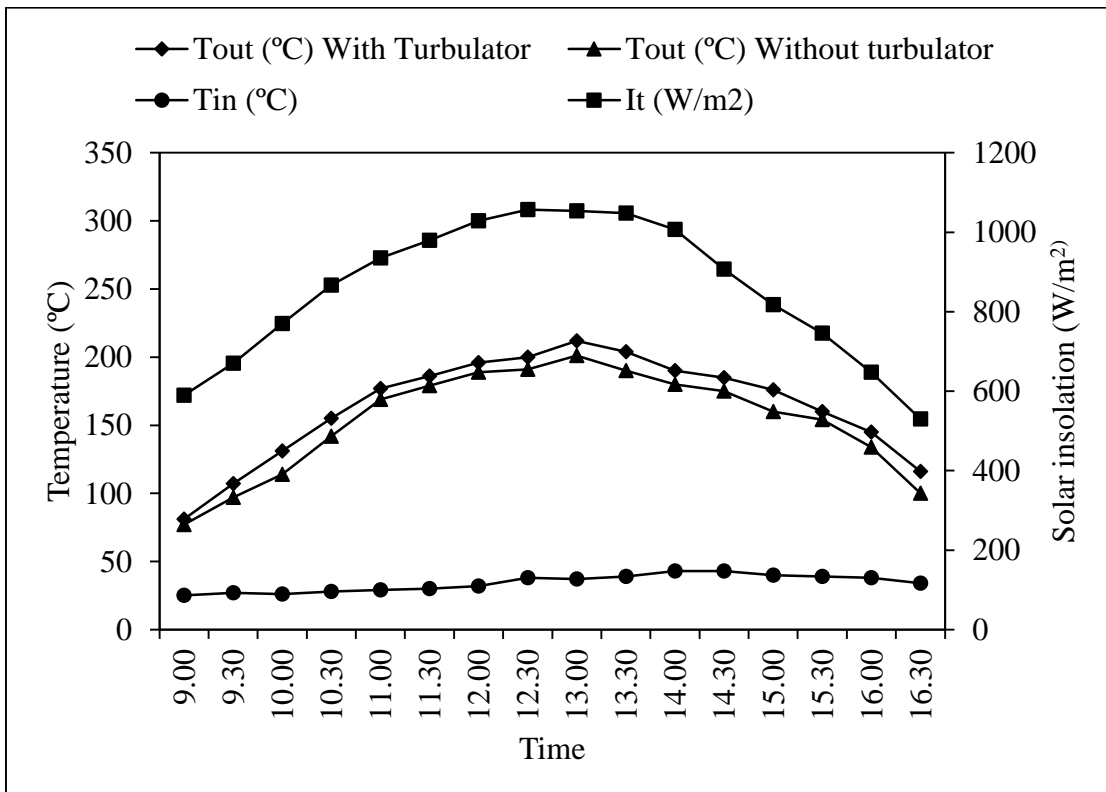
Fig 5.11 Experimental results for mass flow rate of 10.8 kg/h (Date: 23.04.2018)
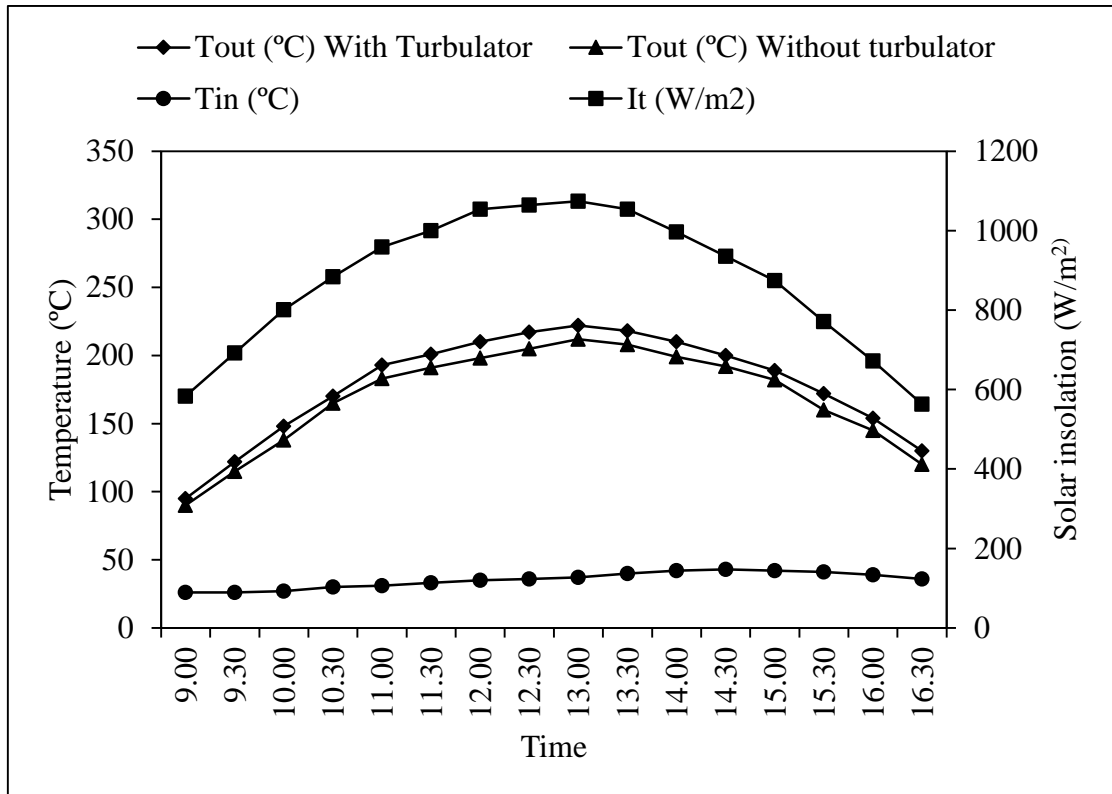
Fig 5.12 Experimental results for mass flow rate of 9.72 kg/h (Date: 26.04.2018)
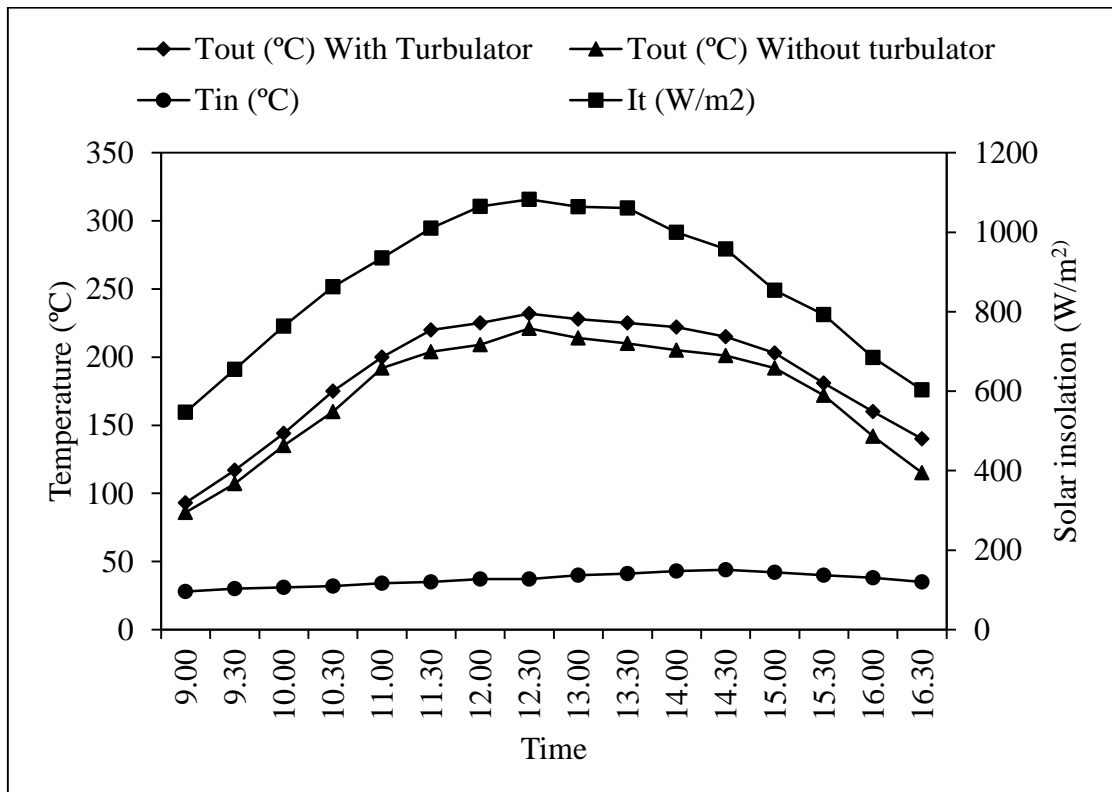
Fig 5.13 Experimental results for mass flow rate of 8.64 kg/h (Date: 29.04.2018)
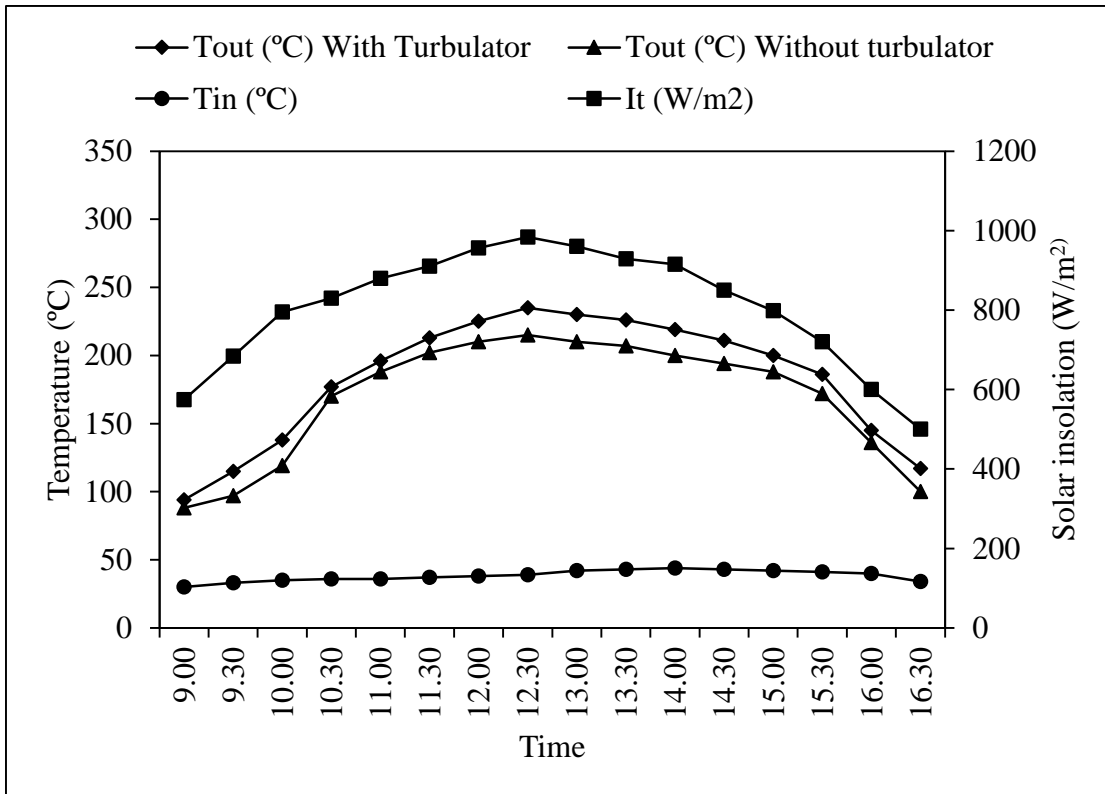
Fig 5.14 Experimental results for mass flow rate of 7.56 kg/h (Date: 02.05.2018)
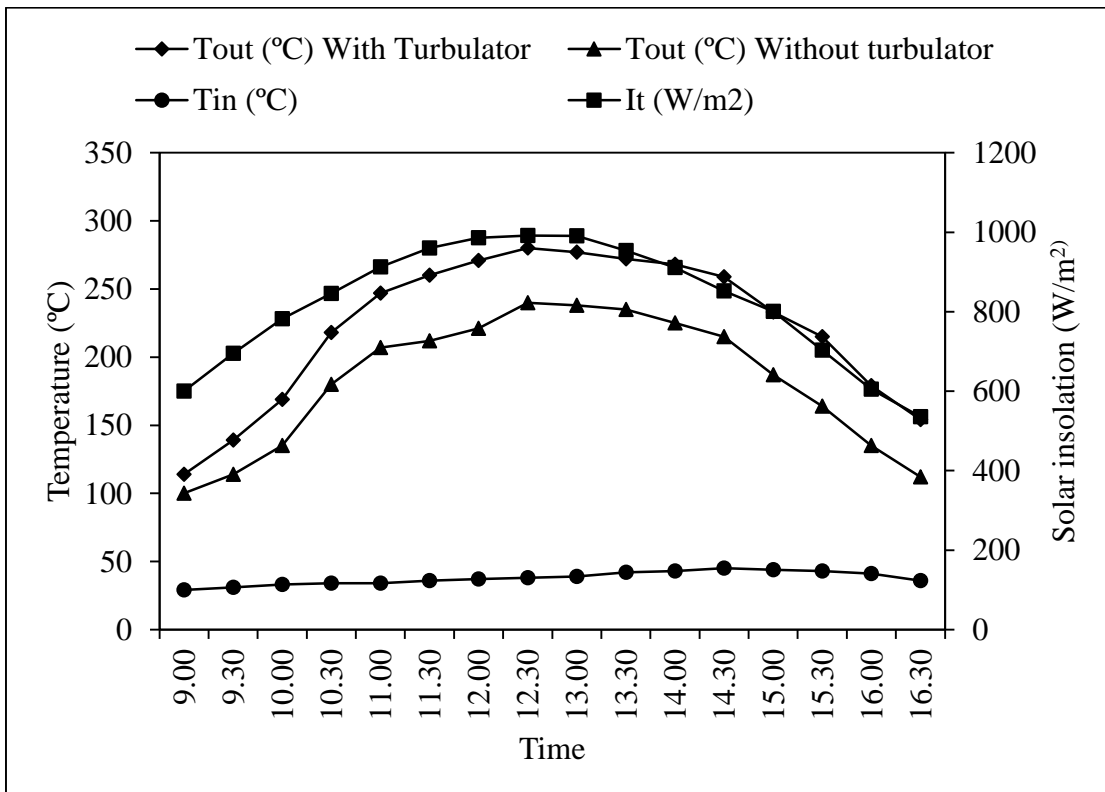
Fig 5.15 Experimental results for mass flow rate of 6.12 kg/h (Date: 05.05.2018)
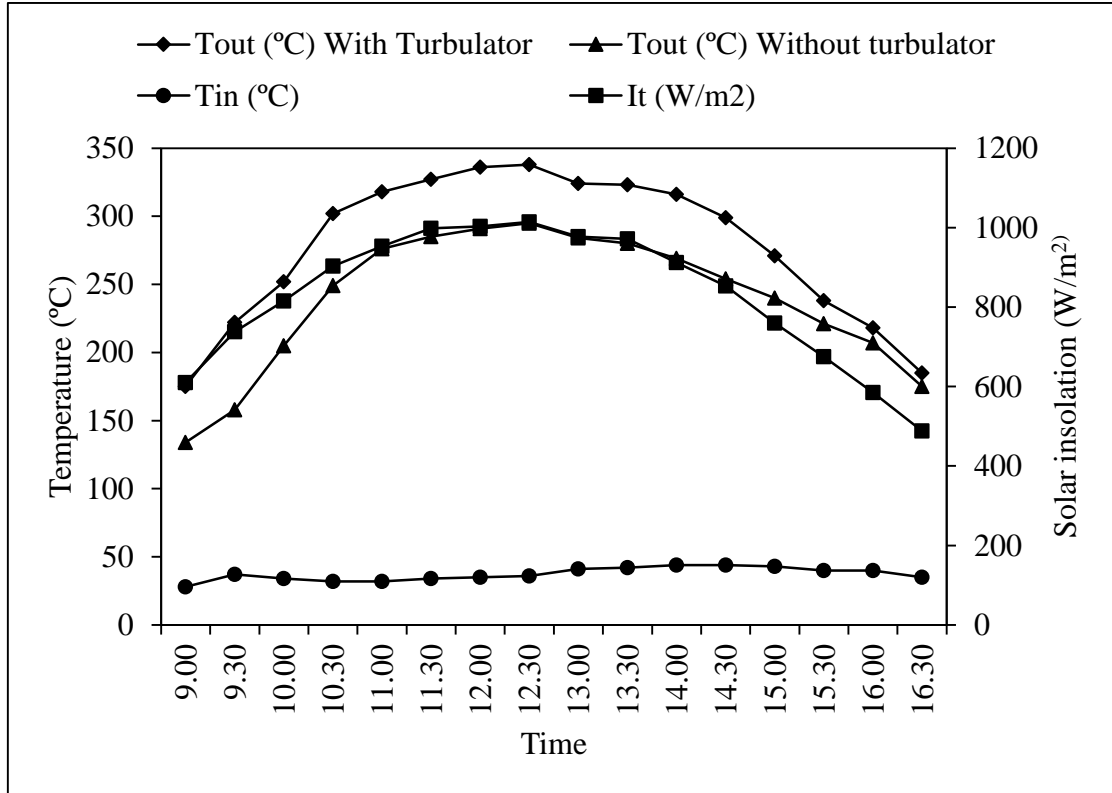
Fig 5.16 Experimental results for mass flow rate of 4.32 kg/h (Date: 08.05.2018)

5.1.1 Validation of results

Table 5.2 and 5.3 shows the validation of theoretical results for outlet temperature and efficiency at $I_t = 900$ W/m^2 and Fig 5.17 is graphical representation of the same. Due to increase in heat capacity of air, air outlet temperature decreases with increase in mass flow rate. Due to higher heat removal rate and lower average air temperature, average absorber temperature and average glass cover temperature reduces with increase in mass flow rate, which results in increase in collector efficiency. For all values of mass flow rate, efficiency and outlet temperature with turbulator is higher compared to those without turbulator. Average absorber temperature without turbulator is higher than that of with turbulator, which leads to lower efficiency of the collector without turbulator.

Table 5.2 Validation of results for outlet temperature with and without turbulator

m_a (kg/h)	T_{out} with turbulator (theo.)	T_{out} without turbulator (theo.)	T_{out} with turbulator (exp.)	T_{out} without turbulator (exp.)	% variation in T_{out} (with turbulator)	% variation in T_{out} (without turbulator)
4.32	342.8	279.4	299.0	249.0	14.65	12.21
6.12	271.7	217.8	240.0	197.0	13.21	10.56
7.56	232.7	218.4	209.0	198.0	11.34	10.30
8.64	210.7	199.8	192.0	183.0	9.74	9.18
9.72	192.9	184.5	179.0	171.5	7.77	7.58
10.8	178.3	171.6	167.4	162.0	6.51	5.93
11.52	170	164.2	162.0	156.5	4.94	4.92
12.24	162.5	157.4	157.0	152.1	3.50	3.48
12.96	155.8	151.4	152.3	148.0	2.30	2.30
13.68	149.8	145.8	148.2	144.2	1.08	1.11

Table 5.3 Validation of results for efficiency with and without turbulator

m_a (kg/h)	η with turbulator (theo.)	η without turbulator (theo.)	η with turbulator (exp.)	η without turbulator (exp.)	% variation in η (with turbulator)	% variation in η (without turbulator)
4.32	54.55	43.31	47.00	37.85	16.06	14.43
6.12	59.42	45.89	51.60	40.60	15.16	13.03
7.56	61.31	56.88	54.10	50.50	13.33	12.63
8.64	62.27	58.41	55.80	52.50	11.59	11.26
9.72	62.96	59.61	57.40	54.40	9.69	9.58
10.8	63.49	60.52	58.80	56.20	7.98	7.69
11.52	63.8	61.06	60.00	57.60	6.33	6.01
12.24	64.02	61.46	61.20	58.90	4.61	4.35
12.96	64.22	61.88	62.50	60.20	2.75	2.79
13.68	64.42	62.18	63.70	61.50	1.13	1.11
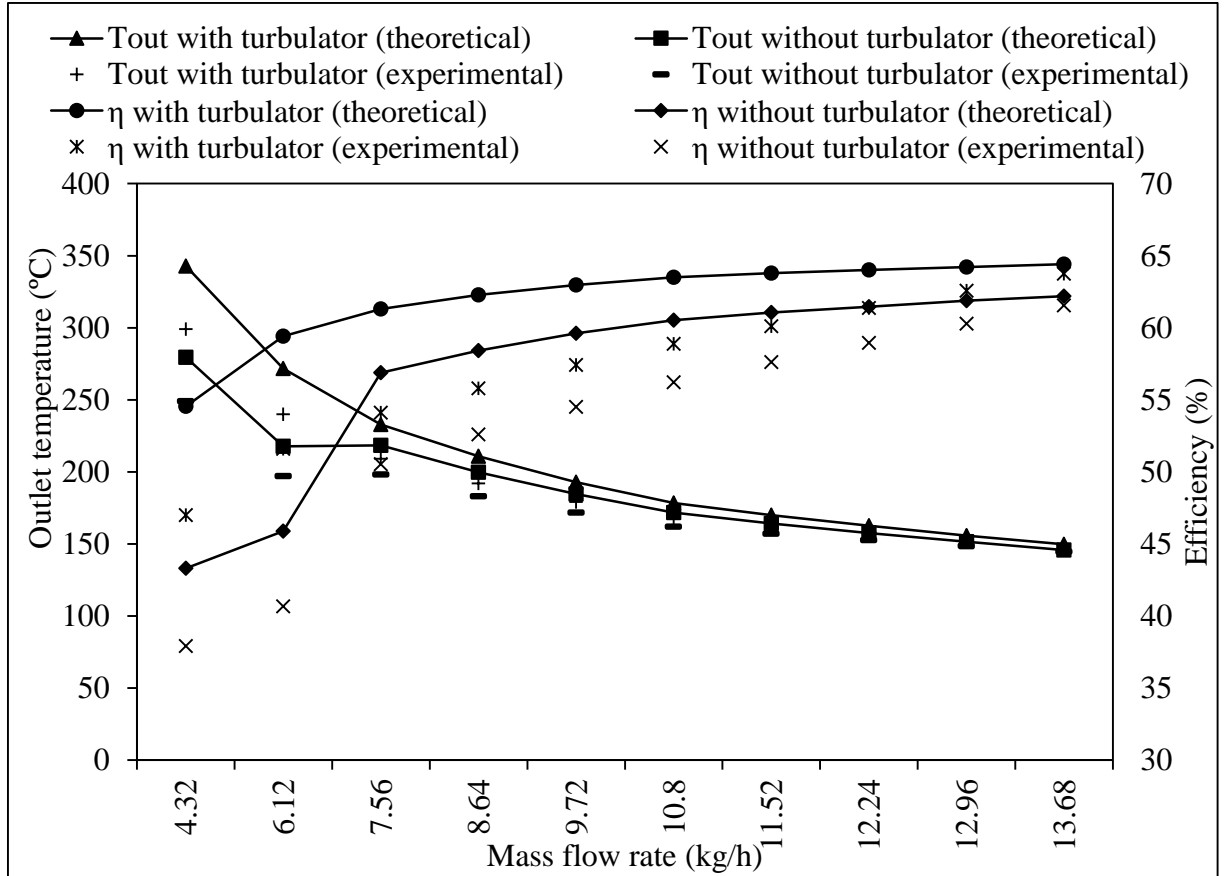
Fig 5.17 Validation of results for I_t = 900 W/m^2

The flow is laminar for mass flow rate of 4.32 kg/h for the collector with turbulator and for mass flow rates of 4.32 and 6.12 kg/h for the collector without turbulator. For mass flow rates of 4.32 kg/h and 6.12 kg/h, efficiency of collector with turbulator is about 24% higher compared to that without turbulator, while for mass flow rates of 10.8 kg/h and 13.68 kg/h, efficiency of collector with turbulator is 4.73% and 3.57% higher compared to without turbulator. Thus use of helical wiry turbulator is justified at low Reynolds number. For same mass flow rate of air Reynolds number with turbulator is higher compared to that without turbulator due to blockage area of turbulator. Maximum pressure drop was 0.255 and 0.069 kPa at mass flow rate of 4.32 kg/h with and without turbulator respectively and 1.73 and 0.333 kPa at mass flow rate of 13.65 kg/h with and without turbulator respectively. Thermo-hydraulic performance of the collector was evaluated by calculating effective efficiency of the collector as given by Mittal and Varshney[103]. For solar insolation of 900 W/m^2 and air outlet and inlet temperatures of 299°C and 34°C, effective efficiency of 46.5% was calculated for the collector with turbulator at mass flow rates of 4.32 kg/h. For the same insolation and mass flow rate, effective efficiency of 37.8% was calculated for the collector without turbulator with air outlet and inlet temperatures

of 249°C and 34°C respectively. For solar insolation of 900 W/m^2 and air outlet and inlet temperatures of 148.5°C and 35°C, effective efficiency of 59.5% was calculated for the collector with turbulator at mass flow rates of 13.68 kg/h. For the same insolation and mass flow rate, effective efficiency of 61.04% was calculated for the collector without turbulator with air outlet and inlet temperatures of 144.5°C and 35°C respectively. Thus turbulator is desirable at lower mass flow rates only. To cater to the need of ARS, it was necessary that evacuated glass tube based parabolic trough collector deliver heat above 170°C for a period of more than 6 h a day. Table 5.4 shows the duration for which air outlet temperature was higher than 170°C at different mass flow rates for the collector with turbulator and without turbulator. Experimental results shows that mass flow rates 4.32 and 6.12 kg/h are suitable to obtain desirable air outlet temperature with CR 3.

Table 5.4 Duration for which air outlet temperature was higher than 170°C

Mass flow rate (kg/h)	Duration for the collector with turbulator (h)	Duration for the collector without turbulator (h)
4.32	7	6.5
6.12	6	5.5
7.56	5.5	5
8.64	5	4.5
9.72	4.5	4
10.8	4	3.5
11.52	3.5	2.5
12.24	3	2
12.96	2.5	1
13.68	0	0

5.2 Uncertainty analysis

A precise method of estimating uncertainty in experimental results was presented by Kline and McClintock [104]. Uncertainty analysis of experimental results of present study was done using Kline-McClintock method which is presented in this section. Different dimensions of all

components are taken from chapter 4, section 4.1. As mentioned earlier volume flow rate of air was measured using U-tube manometer and Magnehelic pressure gauge. To measure the velocity head from 13.68 to 7.56 kg/h of mass flow rate of air, U-tube manometer was used. Magnehelic differential pressure gauge was used for the mass flow rate of 6.12 and 4.32 kg/h for higher accuracy at lower mass flow rates. Following equations are used to calculate uncertainty in the calculation of efficiency of the solar collector using Magnehelic pressure gauge. All calculations were carried out for the reading taken at 10.30 h on 08/05/2018.

Orifice meter was used to measure flow rate of air through the solar collectors. Diameter of orifice meter was selected as 0.015 m.

For the 5 mm of water deflection in Magnehelic pressure gauge, 5 mm of water = 4.363 m of air. Velocity of air through orifice meter can be calculated by

$$v_{fm} = \sqrt{2 \times g \times h_a} \tag{5.1}$$

Where, h_a is m of air

Therefore, $v_{fm} = \sqrt{2 \times 9.81 \times 4.363}$

$v_{fm} = 9.252$ m/s

Cross section area of orifice meter is calculated by

$$A_{cs.fm} = \frac{\pi}{4} d_{fm}^2 \tag{5.2}$$

$$A_{cs.fm} = \frac{3.14}{4} \times (0.015)^2$$

$A_{cs.fm} = 1.767 \times 10^{-4}$ m^2

Now, volume flow rate of air is calculated by

$$vol_{fa.in} = C_d \times A_{fm} \times v_{fm} \tag{5.3}$$

$vol_{fa.in} = 1.0463 \times 10^{-3}$ m^3/s

Mass flow rate of air can be calculated by

$$m_a = \rho_a \times vol_{fa.fm} \tag{5.4}$$

Where, density of air is taken at air inlet temperature

$m_a = 1.146 \times 1.0463 \times 10^{-3}$

$m_a = 1.199 \times 10^{-3}$ kg/s

Heat collected can be calculated by using following equation

$$Q_u = m_a \times c_{pa} \times (T_{out} - T_{in}) \tag{5.5}$$

$$Q_u = 1.199 \times 10^{-3} \times 1005 \times (299 - 32)$$

Where, outlet and inlet temperatures are taken from experimental readings at 900 W/m² and for 5 mm of water pressure head.

$$Q_u = 321.7 \text{ W}$$

Aperture area of solar collector can be calculated by

$$A_{ap} = w_{para} \times l_u \tag{5.6}$$

$$A_{ap} = 0.443 \times 1.71$$

$$A_{ap} = 0.757 \text{ m}^2$$

Heat intercepted can be calculated by

$$Q_i = I_t A_{ap} \tag{5.7}$$

$$Q_i = 900 \times 0.757$$

$$Q_i = 681.3 \text{ W}$$

Solar collector efficiency can be calculated by

$$\eta_{sc} = \frac{Q_u}{Q_i} \tag{5.8}$$

$$\eta_{sc} = \frac{321.7}{681.3}$$

$$\eta_{sc} = 47.22 \%$$

Error in velocity of air can be calculated by

$$ev_{fm} = \left[\left\{ \left(\frac{d}{dh_a} \sqrt{2 \times g \times h_a} \right) eh_a \right\}^2 \right]^{0.5} \tag{5.9}$$

$$ev_{fm} = 0.1855 \text{ m/s}$$

Percentage error in velocity of air can be calculated by

$$ev_{fm}\% = \frac{ev_{fm}}{v_{fm}} \tag{5.10}$$

$$ev_{fm}\% = \frac{0.1855}{8.252}$$

$$ev_{fm}\% = 2.01 \%$$

Error in cross section area of flow meter

$$eA_{cs.fm} = \left[\left\{\left(\frac{d}{d_{fm}}\left(\frac{\pi}{4}d_{fm}^2\right)\right)ed_{fm}\right\}^2\right]^{0.5} \tag{5.11}$$

$$eA_{cs.fm} = 4.7124\times10^{-7} \ \text{m}^2$$

Percentage error in cross section area of flow meter can be calculated by

$$eA_{cs.fm}\% = \frac{eA_{cs.fm}}{A_{cs.fm}} \tag{5.12}$$

$$eA_{cs.fm}\% = \frac{4.7124\times10^{-7}}{1.767\times10^{-4}}$$

$$eA_{cs.fm}\% = 0.267 \ \%$$

Error in volume flow rate of air can be calculated by

$$evol_{fa.fm} = \left[\left[\left[\frac{d}{d_{A_{cs.fm}}}\left(0.64\times A_{cs.fm}\times v_{fm}\right)\right]eA_{cs.fm}\right]^2 + \left[\left[\frac{d}{dv_{fm}}\left(0.64\times A_{cs.fm}\times v_{fm}\right)\right]ev_{fm}\right]^2\right]^{0.5} \tag{5.13}$$

$$evol_{fa.fm} = 2.1162\times10^{-5} \ \text{m}^3/\text{s}$$

Percentage error in volume flow rate of air can be calculated by

$$evol_{fa.fm}\% = \frac{evol_{fa.fm}}{vol_{fa.fm}} \tag{5.14}$$

$$evol_{fa.fm}\% = \frac{2.1162\times10^{-5}}{1.0463\times10^{-3}}$$

$$evol_{fa.fm}\% = 2.023 \ \%$$

Error in mass flow rate of air can be calculated by

$$em_a = \left[\left\{\left(\frac{d}{dvol_{fa.fm}}\left(\rho_a\times vol_{fa.fm}\right)\right)evol_{fa.fm}\right\}^2\right]^{0.5} \tag{5.15}$$

$$em_a = 2.4252\times10^{-5} \ \text{kg/s}$$

Percentage error in mass flow rate of air can be calculated by

$$em_a\% = \frac{em_a}{m_a} \tag{5.16}$$

$$em_a\% = \frac{2.4252\times10^{-5}}{1.199\times10^{-3}}$$

$$em_a\% = 2.023 \ \%$$

Error in heat collected can be calculated by

$$eQ_u = \left[\left[\left\{ \frac{d}{dm_a} \left(m_a \times c_{pa} \times (T_{out} - T_{in}) \right) \right\} em_a \right]^2 + \left[\left\{ \frac{d}{dT_{out}} \left(m_a \times c_{pa} \times (T_{out} - T_{in}) \right) \right\} eT_{out} \right]^2 + \left[\left\{ \frac{d}{dT_{in}} \left(m_a \times c_{pa} \times (T_{out} - T_{in}) \right) \right\} eT_{in} \right]^2 \right]^{0.5}$$

(5.17)

$$eQ_u = 6.7271 \ W$$

Percentage error in heat collected can be calculated by

$$eQ_u \% = \frac{eQ_u}{Q_u}$$

(5.18)

$$eQ_u \% = \frac{6.7271}{321.7}$$

$$eQ_u \% = 2.087 \ \%$$

Error in aperture area can be calculated by

$$eA_{ap} = \left[\left\{ \left(\frac{d}{dl_u} (l_u \times w_{sc}) \right) el_u \right\}^2 + \left\{ \left(\frac{d}{dw_{sc}} (l_u \times w_{sc}) \right) ew_{sc} \right\}^2 \right]^{0.5}$$

(5.19)

$$eA_{ap} = 1.766 \times 10^{-3} \ m^2$$

Percentage error in aperture area can be calculated by

$$eA_{ap} \% = \frac{eA_{ap}}{A_{ap}}$$

(5.20)

$$eA_{ap} \% = \frac{1.766 \times 10^{-3}}{0.757}$$

$$eA_{ap} \% = 0.233 \ \%$$

Error in radiation intercepted can be calculated by

$$eQ_i = \left[\left\{ \left(\frac{d}{dA_{ap}} (A_{ap} \times I_t) \right) eA_{ap} \right\}^2 + \left\{ \left(\frac{d}{dI_t} (A_{ap} \times I_t) \right) eI_t \right\}^2 \right]^{0.5}$$

(5.21)

$$eQ_i = 1.761 \ W$$

Percentage error in radiation intercepted can be calculated by

$$eQ_i \% = \frac{eQ_i}{Q_i}$$

(5.22)

$$eQ_i \% = \frac{1.761}{681.7}$$

$eQ_i\% = 0.258\ \%$

Error in solar collector efficiency can be calculated by

$$e\eta_{sc} = \left[\left\{ \left(\frac{d}{dQ_u} \left(Q_u \times Q_i^{-1} \right) \right) eQ_u \right\}^2 + \left\{ \left(\frac{d}{dQ_i} \left(Q_u \times Q_i^{-1} \right) \right) eQ_i \right\}^2 \right]^{0.5} \tag{5.23}$$

$e\eta_{sc} = 9.943 \times 10^{-3}\ \%$

Percentage error in solar collector efficiency can be calculated by

$$e\eta_{sc}\% = \frac{e\eta_{sc}}{\eta_{sc}} \tag{5.24}$$

$$e\eta_{sc}\% = \frac{9.943 \times 10^{-3}}{0.4722}$$

$$e\eta_{sc}\% = 2.10\ \%$$

Table 5.5 shows results of error analysis for the reading taken at 10.30 h on 08/05/2018. It may be noted that Magnehelic pressure gauge was used to measure velocity of air through orifice meter. For comparison the errors were also calculated if U-tube manometer was used to measure the velocity.

Table 5.5 Results of error analysis

Parameter	Error using Magnehelic pressure gauge (%)	Error using U-tube manometer (%)
Velocity of air	2.01	10.00
Cross section area	0.27	0.27
Volume flow rate	2.02	10.01
Mass flow rate	2.02	10.01
Heat collected	2.09	10.00
Aperture area	0.23	0.23
Radiation intercepted	0.26	0.26
Solar collector efficiency	2.10	10.01

Chapter 6

Conclusions

In present work, thermodynamic analysis of ammonia-water absorption refrigeration system with and without ejector has been carried out. Due to increased refrigerant circulation rate through refrigerant circuit and reduction of generator heat duty and pump work, cycle COP of combined ejector absorption refrigeration cycle is higher than conventional absorption refrigeration cycle. However combined ejector absorption cycle suffers from a practical limitation of requirement of higher pressure ratio solution pump. First and second law analysis and optimization of ammonia-water absorption refrigeration system with SHE and RHE has been carried out to study the effect of generator temperature on COP, total entropy generation and exergetic efficiency. Optimum generator temperature for maximum COP has been computed considering condenser temperature of 50ºC and evaporator temperature of 10ºC for the application of summer air conditioning. To supply heat to the ammonia-water absorption refrigeration system at the optimum generator temperature, evacuated glass tube based parabolic trough collector with helical wiry turbulator was conceived and simulation results of evacuated glass tube based parabolic trough collector has been presented. ARS was considered to be coupled with evacuated glass tube based parabolic trough collector. Coupled system was

simulated and Solar COP was obtained for the different values of CR of the solar collector in the range of 2 to 4. Effect of generator temperature on solar COP for the different values of CR was also studied. Based on the simulation result, two identical evacuated glass tube based parabolic trough collectors with concentration ratio of 3, one with helical wiry turbulator and the other without the turbulator were constructed and tested under outdoor field conditions at Rajkot, Gujarat, India (latitude 22.3039ºN, longitude 70.8022ºE). From the research work following conclusions have been drawn.

- Compared to conventional cycle combined ejector-absorption refrigeration cycle results in higher COP in the range of 14.66% to 30.1% for various combinations of condenser temperature in the range of 35°C to 45°C, evaporator temperature in the range of 5°C to 15°C and entrainment ratio in the range of 0.04 to 0.14.

- However it is observed that at lower evaporator and higher condenser temperatures ejector inlet pressure is more than twice of that of conventional ammonia-water absorption refrigeration system even for lower entrainment ratio. For entrainment ratio of 0.14, the ejector inlet pressure is as high as 45 bar for condenser and evaporator temperatures of 45°C and 5°C respectively. Therefore a higher pressure solution pump is required for combined-ejector absorption cycle which is presently not available in the market.

- It is found that for given application, higher evaporator temperature, lower condenser temperature, higher SHE and RHE effectiveness of conventional absorption refrigeration cycle are desirable for the higher COP.

- For conventional absorption refrigeration cycle total entropy generation and exergetic efficiency is higher at low evaporator temperature for the same value of generator temperature. Also exergetic efficiency is higher and total entropy generation is lower at low condenser temperature for the same value of generator temperature.

- Exergetic efficiency increases and total entropy generation decreases with increase in effectiveness of SHE and RHE. Maximum entropy generation is associated with the absorber and generator, 39.64% and 16.55% of total entropy generation respectively.

- For comfort air conditioning with $T_e = 10$ºC, $T_c = T_a = 50$ºC, $\varepsilon_{RHE} = 0.7$ and $\varepsilon_{SHE} = 0.7$, maximum COP of the ARS is computed as 0.525 at optimum generator temperature of 170ºC.

- Optimum COP is 0.65 at $T_c = 35$°C, $T_e = 10$°C, $T_g = 150$°C, $\varepsilon_{RHE} = \varepsilon_{SHE} = 0.75$ and optimum exergetic efficiency is 23.94% at $T_c = 35$°C, $T_e = -5$°C, $T_g = 120$°C, $\varepsilon_{RHE} = \varepsilon_{SHE} = 0.6$ for the selected Taguchi design.

- Based on SN analysis, optimum COP is 0.6612 at $T_c = 35$°C, $T_e = 10$°C, $T_g = 150$°C, $\varepsilon_{RHE} = 0.6$ and $\varepsilon_{SHE} = 0.75$ and optimum exergetic efficiency is 24.74% at $T_c = 35$°C, $T_e = -5$°C, $T_g = 120$°C, $\varepsilon_{RHE} = 0.6$ and $\varepsilon_{SHE} = 0.75$.

- To power the absorption refrigeration cycle, an evacuated glass tube based parabolic trough collector is conceived. Thermal model is developed to predict the useful heat collected and efficiency of the collector. Simulation results for fixed inlet air temperature show that efficiency of the collector is proportional to solar insolation, CR and mass flow rate of the air and inversely proportional to air outlet temperature.

- Analysis of the solar powered absorption refrigeration cycle reveals that solar COP increases with increase in generator temperature, reaches to its maximum value at optimum generator temperature and then decreases.

- It is seen that solar COP increases with increase in CR. Solar COP is maximum between 140°C and 150°C generator temperature for the CR in the range of 2 to 4. Solar COP of 0.3164 is computed at optimum generator temperature of 150°C with CR of the collector equal to 3.

- Considering temperature difference of 20°C between solution in generator and collector heat transfer fluid (air in present case), the evacuated glass tube based parabolic trough collector was tested under outdoor field condition to achieve the air outlet temperature of 170°C for 6 h of solar operation. A helical wiry turbulator is inserted in the annulus of inner glass tube and air tube to enhance heat removal rate from the collector and thus to achieve higher collector efficiency.

- Experiments were performed at 10 different mass flow rates in the range of 4.32 to 13.68 kg/h. For mass flow rates of 6.12 kg/h and lower, the collector with turbulator is capable of delivering heat at temperature higher than 170°C for more than 6 h per day.

- Experimental results show that air outlet temperature increases with increase in solar radiation at fixed mass flow rate through collector.

- Air outlet temperature with turbulator is higher for all values of mass flow rate compared to that without turbulator. For mass flow rates of 4.32 kg/h and 6.12 kg/h, efficiency of collector with turbulator is about 24% higher compared to that without turbulator, while

for mass flow rates of 10.8 kg/h and 13.68 kg/h, efficiency of collector with turbulator is 4.73% and 3.57% higher compared to without turbulator.

- Thus evacuated glass tube based parabolic trough collector is technically viable option to cater to heat energy requirement of widely used conventional ammonia-water absorption refrigeration system. This will not only reduce the fast depleting fossil fuel resources but also address the critical environmental issue of global warming.

Recommendation for Future Work

- One may develop complete absorption refrigeration system coupled with evacuated glass tube based parabolic trough collector and test outdoor field condition.
- Techno-economic optimization of the solar power absorption refrigeration system can also be worked out.
- One may also can try to evaluate the performance of solar powered absorption refrigeration system using other working fluid pairs.

Appendix I

Data points of various graphs for Chapter 3

Table AI.1 Data points for Fig 3.3

T_g	COP			
(°C)	$T_c = 45°C, T_e = 5°C$	$T_c = 45°C, T_e = 15°C$	$T_c = 35°C, T_e = 5°C$	$T_c = 35°C, T_e = 15°C$
80	-	-	0.5278	0.6757
90	-	-	0.5705	0.6794
100	0.4374	0.5844	0.5757	0.6638
110	0.4706	0.5849	0.5815	0.6593
120	0.4886	0.5847	0.5742	0.6477
130	0.4864	0.5746	0.5724	0.642
140	0.4835	0.5661	0.568	0.6355
150	0.4816	0.5608	-	-

Table AI.2 Data points for Fig 3.4

T_g	COP					
(°C)	$\mu=0.04$	$\mu=0.06$	$\mu=0.08$	$\mu=0.1$	$\mu=0.12$	$\mu=0.14$
130	0.5787	0.57995	0.5812	-	-	-
140	0.5912	0.6038	0.6048	0.6124	0.6218	0.635
150	0.5783	0.591	0.5926	0.6103	0.6158	0.6246
160	0.5728	0.5877	0.5933	0.61	0.615	0.6228
170	0.5584	0.5693	0.5765	0.6016	0.6126	0.6156

Table AI.3 Data points for Fig 3.5

T_g	COP					
(°C)	$\mu=0.04$	$\mu=0.06$	$\mu=0.08$	$\mu=0.1$	$\mu=0.12$	$\mu=0.14$
120	0.6223	0.6358	0.6445	0.6532	0.6642	0.621
130	0.628	0.6414	0.65555	0.6697	0.67445	0.6792
140	0.6056	0.6253	0.645	0.6647	0.6672	0.6697
150	0.5916	0.6115	0.6314	0.6513	0.65545	0.6596
160	0.5841	0.6025	0.62095	0.6394	0.64475	0.6501

Table AI.4 Data points for Fig 3.6

T_g (°C)	COP					
	μ=0.04	μ=0.06	μ=0.08	μ=0.1	μ=0.12	μ=0.14
100	0.5984	0.6167	0.635	0.6533	0.6568	0.6603
110	0.629	0.641	0.65305	0.6651	0.6701	0.6751
120	0.6203	0.6309	0.64155	0.6522	0.6614	0.6706
130	0.6141	0.6252	0.63635	0.6475	0.65445	0.6614
140	0.6126	0.6199	0.6272	0.6345	0.6444	0.6543
150	0.5867	0.6	0.61335	0.6267	0.6354	0.6441

Table AI.5 Data points for Fig 3.7

T_g (°C)	COP					
	μ=0.04	μ=0.06	μ=0.08	μ=0.1	μ=0.12	μ=0.14
90	0.66	0.6826	0.70525	0.7279	0.7515	0.7751
100	0.6694	0.6941	0.71885	0.7436	0.7614	0.7792
110	0.6584	0.6791	0.69985	0.7206	0.7385	0.7564
120	0.6562	0.6726	0.689	0.7054	0.7208	0.7362
130	0.6551	0.6655	0.67595	0.6864	0.70685	0.7273
140	0.6414	0.653	0.66465	0.6763	0.69495	0.7136

Table AI.6 COP, Total entropy generation and exergetic efficiency at T_c=50°C, T_e=10°C, Effectiveness of SHE & RHE=0.7

T_g (°C)	COP	Total Entropy Generation (W/K)	Exergetic Efficiency (%)
130	0.4977	18.45	11.39
140	0.5127	19.05	11.04
150	0.5199	19.88	10.57
160	0.5231	20.82	10.1
170	0.5245	21.77	9.656
180	0.5244	22.75	9.243
190	0.5244	23.69	8.875

Table AI.7 COP, Total entropy generation and exergetic efficiency at T_c=45°C, T_e=10°C, Effectiveness of SHE & RHE=0.7

T_g (°C)	COP	Total Entropy Generation (W/K)	Exergetic Efficiency (%)
110	0.5238	15.01	14.02
120	0.5501	15.42	13.64
130	0.5598	16.26	12.93
140	0.563	17.25	12.19
150	0.5636	18.25	11.52
160	0.563	19.28	10.9
170	0.5617	20.28	10.37

Table AI.8 COP, Total entropy generation and exergetic efficiency at T_c=40°C, T_e=10°C, Effectiveness of SHE & RHE=0.7

T_g (°C)	COP	Total Entropy Generation (W/K)	Exergetic Efficiency (%)
100	0.585	12.07	17.42
110	0.6018	12.87	16.34
120	0.6064	13.87	15.16
130	0.6065	14.92	14.09
140	0.6045	16.00	13.14
150	0.602	17.04	12.33

Table AI.9 COP, Total entropy generation and exergetic efficiency at T_c=35°C, T_e=10°C, Effectiveness of SHE & RHE=0.7

T_g (°C)	COP	Total Entropy Generation (W/K)	Exergetic Efficiency (%)
90	0.6447	9.673	21.74
100	0.653	10.68	19.69
110	0.6531	11.76	17.87
120	0.6502	12.87	16.34
130	0.6461	13.96	15.06
140	0.6418	15.03	13.99

Table AI.10 COP, Total entropy generation and exergetic efficiency at T_c=35°C, T_e=5°C, Effectiveness of SHE & RHE=0.7

T_g (°C)	COP	Total Entropy Generation (W/K)	Exergetic Efficiency (%)
90	0.5676	11.11	24.94
100	0.5981	11.72	23.63
110	0.607	12.69	21.82
120	0.6087	13.78	20.1
130	0.6076	14.87	18.63
140	0.6052	15.95	17.37
150	0.6025	17.02	16.28

Table AI.11 COP, Total entropy generation and exergetic efficiency at T_c=35°C, T_e=0°C, Effectiveness of SHE & RHE=0.7

T_g (°C)	COP	Total Entropy Generation (W/K)	Exergetic Efficiency (%)
100	0.5303	13.32	25.98
110	0.5558	13.92	24.87
120	0.5652	14.87	23.27
130	0.5684	15.92	21.74
140	0.5687	17.00	20.36
150	0.5679	18.07	19.16
160	0.5667	19.10	18.13

Table AI.12 COP, Total entropy generation and exergetic efficiency at T_c=35°C, T_e=-5°C, Effectiveness of SHE & RHE=0.7

T_g (°C)	COP	Total Entropy Generation (W/K)	Exergetic Efficiency (%)
110	0.4965	15.67	26.67
120	0.5186	16.26	25.71
130	0.528	17.17	24.33
140	0.532	18.19	22.98
150	0.5337	19.24	21.72
160	0.5343	20.27	20.62
170	0.5342	21.28	19.63

Table AI.13 COP, Total entropy generation and exergetic efficiency at T_c=50°C, T_e=10°C, T_g=170°C and Effectiveness of RHE=0.7

ε_{SHE}	COP	Total Entropy Generation (W/K)	Exergetic Efficiency (%)
0.6	0.5	22.82	9.21
0.65	0.5119	22.29	9.428
0.7	0.5245	21.77	9.656
0.75	0.5376	21.24	9.895
0.8	0.5514	20.71	10.15

Table AI.14 COP, Total entropy generation and exergetic efficiency at T_c=50°C, T_e=10°C, T_g=170°C and Effectiveness of SHE=0.7

ε_{RHE}	COP	Total Entropy Generation (W/K)	Exergetic Efficiency (%)
0.6	0.5197	21.98	9.568
0.65	0.5221	21.87	9.612
0.7	0.5245	21.77	9.656
0.75	0.5268	21.67	9.7
0.8	0.5292	21.57	9.744

Table AI.15 Entropy generation in (W/K) for different components of absorption refrigeration system at Tc = 50ºC, Te = 10ºC, εRHE = 0.7, εSHE = 0.7

Component	$T_g =$ 130ºC	$T_g =$ 140ºC	$T_g =$ 150ºC	$T_g =$ 160ºC	$T_g =$ 170ºC	$T_g =$ 180ºC	$T_g =$ 190ºC
Absorber	6.902	7.221	7.646	8.124	8.631	9.166	9.717
Pump	0.3024	0.2381	0.2002	0.1759	0.1583	0.1454	0.1353
SHX	2.536	2.437	2.429	2.467	2.524	2.643	2.705
Generator Absorber	1.718	2.219	2.711	3.173	3.603	3.952	4.298
Throttle Valve	0.2226	0.164	0.1275	0.104	0.08715	0.07475	0.06496
Rectifier	1.443	1.444	1.443	1.444	1.444	1.444	1.444
Condenser	2.386	2.388	2.387	2.388	2.387	2.388	2.387
RHX	0.074	0.07405	0.07401	0.07405	0.07403	0.07404	0.07402
Exp.Valve	0.3072	0.3074	0.3073	0.3074	0.3073	0.3074	0.3073
Evaporator	2.556	2.557	2.556	2.557	2.557	2.557	2.557
Total entropy generation	18.45	19.05	19.88	20.82	21.77	22.75	23.69

Table AI.16 State points at $T_c = 50$ºC, $T_e = 10$ºC, $\varepsilon_{RHE} = 0.7$, $\varepsilon_{SHE} = 0.7$, $T_g = 130$ºC

State Point	h (kJ/kg)	m (kg/s)	P (kPa)	s (kJ/kg K)	T (ºC)	v (m³/kg)	x (kg/kg sol)
1	-13.67	0.05355	524.9	0.5859	50	0.00121	0.447
2	-10.01	0.05355	2036	0.5915	50.56	0.00121	0.447
3	197.5	0.05355	2036	1.191	95.94	0.001294	0.447
4	377.8	0.04413	2036	1.626	130	0.001289	0.329
5	126	0.04413	2036	0.9559	75.27	0.001182	0.329
6	126	0.04413	524.9	0.9609	73.27	0.003089	0.329
7	1495	0.009989	2036	4.638	104.3	0.08141	0.9682
8	237.7	0.000567	2036	1.299	104.3	0.00134	0.447
9	1293	0.009422	2036	4.066	53.08	0.06345	0.9996
10	241	0.009422	2036	0.8137	50	0.001785	0.9996
11	169.9	0.009422	2036	0.5883	35.77	0.001711	0.9996
12	169.9	0.009422	524.9	0.6209	5.501	0.0291	0.9996
13	1284	0.009422	524.9	4.605	10	0.2472	0.9996
14	1355	0.009422	524.9	4.838	37.38	0.2745	0.9996

Table AI.17 State points at $T_c = 50ºC$, $T_e = 10ºC$, $\varepsilon_{RHE} = 0.7$, $\varepsilon_{SHE} = 0.7$, $T_g = 140ºC$

State Point	h (kJ/kg)	m (kg/s)	P (kPa)	s (kJ/kg K)	T (ºC)	v (m³/kg)	x (kg/kg sol)
1	-13.67	0.04216	524.9	0.5859	50	0.00121	0.447
2	-10.01	0.04216	2036	0.5915	50.56	0.00121	0.447
3	208.7	0.04216	2036	1.221	98.29	0.0013	0.447
4	437.4	0.03273	2036	1.751	140	0.001282	0.2878
5	155.8	0.03273	2036	1.014	78.45	0.001166	0.2878
6	155.8	0.03273	524.9	1.019	78.69	0.001167	0.2878
7	1495	0.009996	2036	4.638	104.3	0.08141	0.9682
8	237.7	0.000567	2036	1.299	104.3	0.00134	0.447
9	1293	0.009429	2036	4.066	53.08	0.06345	0.9996
10	241	0.009429	2036	0.8137	50	0.001785	0.9996
11	169.9	0.009429	2036	0.5883	35.77	0.001711	0.9996
12	169.9	0.009429	524.9	0.6209	5.501	0.0291	0.9996
13	1284	0.009429	524.9	4.605	10	0.2472	0.9996
14	1355	0.009429	524.9	4.838	37.38	0.2745	0.9996

Table AI.18 State points at T_c = 50ºC, T_e = 10ºC, ε_{RHE} = 0.7, ε_{SHE} = 0.7, T_g = 150ºC

State Point	h (kJ/kg)	m (kg/s)	P (kPa)	s (kJ/kg K)	T (ºC)	v (m³/kg)	x (kg/kg sol)
1	-13.67	0.03545	524.9	0.5859	50	0.00121	0.447
2	-10.01	0.03545	2036	0.5915	50.56	0.00121	0.447
3	218.5	0.03545	2036	1.248	100.4	0.001305	0.447
4	499.7	0.02603	2036	1.873	150	0.001276	0.2469
5	188.5	0.02603	2036	1.073	81.65	0.00115	0.2469
6	188.5	0.02603	524.9	1.078	81.88	0.001151	0.2469
7	1495	0.009991	2036	4.638	104.3	0.08141	0.9682
8	237.7	0.000567	2036	1.299	104.3	0.00134	0.447
9	1293	0.009424	2036	4.066	53.08	0.06345	0.9996
10	241	0.009424	2036	0.8137	50	0.001785	0.9996
11	169.9	0.009424	2036	0.5883	35.77	0.001711	0.9996
12	169.9	0.009424	524.9	0.6209	5.501	0.0291	0.9996
13	1284	0.009424	524.9	4.605	10	0.2472	0.9996
14	1355	0.009424	524.9	4.838	37.38	0.2745	0.9996

Table AI.19 State points at $T_c = 50ºC$, $T_e = 10ºC$, $\varepsilon_{RHE} = 0.7$, $\varepsilon_{SHE} = 0.7$, $T_g = 160ºC$

State Point	h (kJ/kg)	m (kg/s)	P (kPa)	s (kJ/kg K)	T (ºC)	v (m³/kg)	x (kg/kg sol)
1	-13.67	0.03114	524.9	0.5859	50	0.00121	0.447
2	-10.01	0.03114	2036	0.5915	50.56	0.00121	0.447
3	226.9	0.03114	2036	1.27	102.1	0.001309	0.447
4	562.9	0.02171	2036	1.99	160	0.001269	0.207
5	223	0.02171	2036	1.13	84.77	0.001135	0.207
6	223	0.02171	524.9	1.135	85.01	0.001136	0.207
7	1495	0.009996	2036	4.638	104.3	0.08141	0.9682
8	237.7	0.000567	2036	1.299	104.3	0.00134	0.447
9	1293	0.009429	2036	4.066	53.08	0.06345	0.9996
10	241	0.009429	2036	0.8137	50	0.001785	0.9996
11	169.9	0.009429	2036	0.5883	35.77	0.001711	0.9996
12	169.9	0.009429	524.9	0.6209	5.501	0.0291	0.9996
13	1284	0.009429	524.9	4.605	10	0.2472	0.9996
14	1355	0.009429	524.9	4.838	37.38	0.2745	0.9996

Table AI.20 State points at $T_c = 50^{\circ}C$, $T_e = 10^{\circ}C$, $\varepsilon_{RHE} = 0.7$, $\varepsilon_{SHE} = 0.7$, $T_g = 170^{\circ}C$

State Point	h (kJ/kg)	m (kg/s)	P (kPa)	s (kJ/kg K)	T (ºC)	v (m³/kg)	x (kg/kg sol)
1	-13.67	0.03545	524.9	0.5859	50	0.00121	0.447
2	-10.01	0.03545	2036	0.5915	50.56	0.00121	0.447
3	218.5	0.03545	2036	1.248	100.4	0.00131	0.447
4	499.7	0.02603	2036	1.873	150	0.00128	0.2469
5	188.5	0.02603	2036	1.073	81.65	0.00115	0.2469
6	188.5	0.02603	524.9	1.078	81.88	0.00115	0.2469
7	1495	0.00999	2036	4.638	104.3	0.08141	0.9682
8	237.7	0.00057	2036	1.299	104.3	0.00134	0.447
9	1293	0.00942	2036	4.066	53.08	0.06345	0.9996
10	241	0.00942	2036	0.8137	50	0.00179	0.9996
11	169.9	0.00942	2036	0.5883	35.77	0.00171	0.9996
12	169.9	0.00942	524.9	0.6209	5.501	0.0291	0.9996
13	1284	0.00942	524.9	4.605	10	0.2472	0.9996
14	1355	0.00942	524.9	4.838	37.38	0.2745	0.9996

Table AI.21 State points at $T_c = 50ºC$, $T_e = 10ºC$, $\varepsilon_{RHE} = 0.7$, $\varepsilon_{SHE} = 0.7$, $T_g = 180ºC$

State Point	h (kJ/kg)	m (kg/s)	P (kPa)	s (kJ/kg K)	T (ºC)	v (m³/kg)	x (kg/kg sol)
1	-13.67	0.02575	524.9	0.5859	50	0.00121	0.447
2	-10.01	0.02575	2036	0.5915	50.56	0.00121	0.447
3	242.4	0.02575	2036	1.311	104.6	0.001551	0.447
4	696.3	0.01632	2036	2.211	180	0.001248	0.1278
5	298.1	0.01632	2036	1.238	91.13	0.001103	0.1278
6	298.1	0.01632	524.9	1.242	91.38	0.001104	0.1278
7	1495	0.009995	2036	4.638	104.3	0.08141	0.9682
8	237.7	0.000567	2036	1.299	104.3	0.00134	0.447
9	1293	0.009428	2036	4.066	53.08	0.06345	0.9996
10	241	0.009428	2036	0.8137	50	0.001785	0.9996
11	169.9	0.009428	2036	0.5883	35.77	0.001711	0.9996
12	169.9	0.009428	524.9	0.6209	5.501	0.0291	0.9996
13	1284	0.009428	524.9	4.605	10	0.2472	0.9996
14	1355	0.009428	524.9	4.838	37.38	0.2745	0.9996

Table AI.22 State points at T_c = 50ºC, T_e = 10ºC, ε_{RHE} = 0.7, ε_{SHE} = 0.7, T_g = 190ºC

State Point	h (kJ/kg)	m (kg/s)	P (kPa)	s (kJ/kg K)	T (ºC)	v (m³/kg)	x (kg/kg sol)
1	-13.67	0.02396	524.9	0.5859	50	0.00121	0.447
2	-10.01	0.02396	2036	0.5915	50.56	0.00121	0.447
3	248.2	0.02396	2036	1.326	104.9	0.001816	0.447
4	762.2	0.01453	2036	2.306	190	0.001233	0.08857
5	336.4	0.01453	2036	1.28	94.1	0.001086	0.08857
6	336.4	0.01453	524.9	1.285	94.35	0.001087	0.08857
7	1495	0.009993	2036	4.638	104.3	0.08141	0.9682
8	237.7	0.000567	2036	1.299	104.3	0.00134	0.447
9	1293	0.009426	2036	4.066	53.08	0.06345	0.9996
10	241	0.009426	2036	0.8137	50	0.001785	0.9996
11	169.9	0.009426	2036	0.5883	35.77	0.001711	0.9996
12	169.9	0.009426	524.9	0.6209	5.501	0.0291	0.9996
13	1284	0.009426	524.9	4.605	10	0.2472	0.9996
14	1355	0.009426	524.9	4.838	37.38	0.2745	0.9996

Appendix II

Data points of various graphs for Chapter 4

Table AII.1 Data points for Fig 4.2

I_t (W/m²)	η_{sc}				
	$T_{out} = 150°C$	$T_{out} = 160°C$	$T_{out} = 170°C$	$T_{out} = 180°C$	$T_{out} = 190°C$
500	62.38	61.83	61.25	60.64	60
600	63.15	62.69	62.2	61.69	61.16
700	63.7	63.3	62.88	62.44	61.99
800	64.11	63.76	63.4	63.01	62.6
900	64.44	64.12	63.79	63.45	63.09
1000	64.7	64.41	64.1	63.8	63.47
1100	64.91	64.65	64.38	64.09	63.79

Table AII.2 Data points for Fig 4.3

I_t (W/m²)	Mass flow rate (kg/h)				
	$T_{out} = 150°C$	$T_{out} = 160°C$	$T_{out} = 170°C$	$T_{out} = 180°C$	$T_{out} = 190°C$
500	7.20	6.84	6.12	5.76	5.40
600	9.00	8.28	7.56	6.84	6.48
700	10.44	9.72	9.00	8.28	7.56
800	12.24	11.16	10.08	9.36	8.64
900	13.68	12.60	11.52	10.80	10.08
1000	15.12	14.04	12.96	11.88	11.16
1100	16.92	15.48	14.40	13.32	12.24

Table AII.3 Data points for Fig 4.4

T_{out} (°C)	η_{sc}				
	CR=2	CR=2.5	CR=3	CR=3.5	CR=4
130	60.29	61.34	62.04	62.51	62.91
140	59.43	60.65	61.47	62.03	62.47
150	58.54	59.93	60.86	61.5	62.01
160	57.63	59.19	60.24	60.97	61.53
170	56.66	58.42	59.58	60.4	61.03
180	55.69	57.63	58.92	59.83	60.53
190	54.69	56.82	58.24	59.24	60.01

Table AII.4 Data points for Fig 4.5

T_g (ºC)	Solar COP				
	CR=2	CR=2.5	CR=3	CR=3.5	CR=4
130	0.3001	0.30529	0.30877	0.31111	0.3131
140	0.3047	0.31095	0.31516	0.31803	0.32028
150	0.3043	0.31158	0.31641	0.31974	0.32239
160	0.3015	0.30962	0.31512	0.31893	0.32186
170	0.2972	0.30641	0.3125	0.3168	0.3201
180	0.2920	0.30221	0.30898	0.31375	0.31742
190	0.2868	0.29796	0.30541	0.31065	0.31469

Appendix III

Data points of various graphs for Chapter 5

Table AIII.1 Data points for Fig 5.8

Time	I_t (W/m^2)	T_{out} (°C) with turbulator	T_{out} (°C) without turbulator	T_{in} (°C)	η_{sc} (%) with turbulator	η_{sc} (%) without turbulator
9.00	555	85	75	28	51.71	41.73
9.30	674	107	93	31	56.77	45.57
10.00	760	120	104	34	56.97	46.37
10.30	840	135	120	35	59.94	50.95
11.00	918	151	146	36	63.07	60.33
11.30	969	158	150	38	62.35	58.19
12.00	1022	165	152	40	61.58	55.18
12.30	1040	168	152	43	60.51	53.25
13.00	1009	161	146	44	58.38	50.90
13.30	1006	155	140	42	56.55	49.05
14.00	944	150	135	37	58.67	50.67
14.30	878	143	129	37	60.21	52.18
15.00	818	138	120	36	62.17	51.09
15.30	730	128	111	39	60.69	49.66
16.00	640	118	99	35	65.30	50.35
16.30	478	100	79	31	72.68	50.56

Table AIII.2 Data points for Fig 5.9

Time	I_t (W/m^2)	T_{out} (°C) with turbulator	T_{out} (°C) without turbulator	T_{in} (°C)	η_{sc} (%) with turbulator	η_{sc} (%) without turbulator
9.00	531	81	75	21	53.97	48.57
9.30	635	100	88	22	58.67	49.65
10.00	738	120	107	22	63.43	55.01
10.30	840	140	131	24	65.96	60.84
11.00	918	156	148	25	68.16	64.00
11.30	988	170	162	27	69.13	65.27
12.00	1053	176	166	28	67.13	62.60
12.30	1071	177	170	30	65.56	62.44
13.00	1080	182	173	32	66.34	62.36
13.30	1065	175	159	39	61.00	53.82
14.00	1020	169	154	44	58.54	51.51
14.30	940	164	147	45	60.47	51.83
15.00	850	151	138	42	61.25	53.95
15.30	760	139	128	41	61.59	54.68
16.00	655	125	115	38	63.44	56.15
16.30	552	103	86	33	60.57	45.86

Table AIII.3 Data points for Fig 5.10

Time	I_t (W/m^2)	T_{out} (°C) with turbulator	T_{out} (°C) without turbulator	T_{in} (°C)	η_{sc} (%) with turbulator	η_{sc} (%) without turbulator
9.00	565	91	82	25	52.60	45.43
9.30	671	110	96	25	57.05	47.65
10.00	771	128	119	26	59.58	54.32
10.30	861	147	138	27	62.76	58.06
11.00	947	164	156	30	63.72	59.92
11.30	1007	176	165	32	64.40	59.48
12.00	1037	185	174	33	66.01	61.23
12.30	1055	187	175	34	65.31	60.19
13.00	1056	191	179	37	65.67	60.56
13.30	1025	185	175	38	64.58	60.19
14.00	983	180	168	40	64.14	58.64
14.30	918	172	163	41	64.26	59.85
15.00	839	156	150	42	61.19	57.97
15.30	740	145	139	39	64.51	60.86
16.00	638	132	119	38	66.35	57.17
16.30	523	112	95	35	66.30	51.66

Table AIII.4 Data points for Fig 5.11

Time	I_t (W/m^2)	T_{out} (ºC) with turbulator	T_{out} (ºC) without turbulator	T_{in} (ºC)	η_{sc} (%) with turbulator	η_{sc} (%) without turbulator
9.00	546	94	85	24	54.01	47.06
9.30	660	111	99	26	54.25	46.59
10.00	771	135	120	27	59.01	50.81
10.30	853	153	147	28	61.73	58.77
11.00	943	167	163	29	61.65	59.86
11.30	997	183	175	31	64.22	60.84
12.00	1041	193	177	32	65.15	58.67
12.30	1066	195	183	35	63.23	58.48
13.00	1065	199	185	36	64.47	58.93
13.30	1024	190	178	38	62.53	57.59
14.00	960	180	171	41	60.99	57.04
14.30	902	177	164	43	62.58	56.51
15.00	835	171	159	42	65.08	59.02
15.30	735	153	144	40	64.76	59.60
16.00	642	137	120	37	65.61	54.46
16.30	527	114	97	33	64.75	51.16

Table AIII.5 Data points for Fig 5.12

Time	I_t (W/m^2)	T_{out} (°C) with turbulator	T_{out} (°C) without turbulator	T_{in} (°C)	η_{sc} (%) with turbulator	η_{sc} (%) without turbulator
9.00	590	81	77	25	37.02	34.37
9.30	670	107	97	27	46.57	40.75
10.00	770	131	114	26	53.18	44.57
10.30	867	155	142	28	57.13	51.28
11.00	935	177	169	29	61.73	58.40
11.30	980	186	179	30	62.08	59.30
12.00	1029	196	189	32	62.16	59.50
12.30	1057	200	191	38	59.77	56.45
13.00	1054	212	201	37	64.75	60.68
13.30	1048	204	190	39	61.40	56.19
14.00	1007	190	180	43	56.93	53.06
14.30	907	185	175	43	61.06	56.76
15.00	818	176	160	40	64.84	57.21
15.30	746	160	154	39	63.26	60.12
16.00	648	145	134	38	64.40	57.78
16.30	530	116	100	34	60.34	48.57

Table AIII.6 Data points for Fig 5.13

Time	I_t (W/m^2)	T_{out} (°C) with turbulator	T_{out} (°C) without turbulator	T_{in} (°C)	η_{sc} (%) with turbulator	η_{sc} (%) without turbulator
9.00	583	95	90	26	42.14	39.08
9.30	692	122	115	26	49.39	45.79
10.00	801	148	138	27	53.78	49.34
10.30	884	170	165	30	56.38	54.37
11.00	959	193	183	31	60.14	56.43
11.30	1000	201	191	33	59.81	56.25
12.00	1054	210	198	35	59.11	55.06
12.30	1064	217	205	36	60.56	56.55
13.00	1074	222	212	37	61.33	58.01
13.30	1054	218	208	40	60.12	56.75
14.00	997	210	199	42	59.99	56.06
14.30	935	200	192	43	59.78	56.73
15.00	874	189	182	42	59.88	57.03
15.30	771	172	160	41	60.49	54.95
16.00	672	154	145	39	60.93	56.16
16.30	563	130	120	36	59.44	53.12

Table AIII.7 Data points for Fig 5.14

Time	I_t (W/m²)	T_{out} (°C) with turbulator	T_{out} (°C) without turbulator	T_{in} (°C)	η_{sc} (%) with turbulator	η_{sc} (%) without turbulator
9.00	547	93	86	28	37.84	33.76
9.30	655	117	107	30	42.30	37.43
10.00	764	144	135	31	47.10	43.35
10.30	863	175	160	32	52.76	47.23
11.00	935	200	192	34	56.53	53.81
11.30	1010	220	204	35	58.33	53.28
12.00	1065	225	209	37	56.21	51.43
12.30	1083	232	221	37	57.34	54.10
13.00	1064	228	214	40	56.26	52.07
13.30	1061	225	210	41	55.22	50.72
14.00	1000	222	205	43	57.00	51.59
14.30	958	215	201	44	56.84	52.19
15.00	854	203	192	42	60.03	55.93
15.30	793	181	172	40	56.62	53.00
16.00	685	160	142	38	56.71	48.35
16.30	603	140	115	35	55.45	42.25

Table AIII.8 Data points for Fig 5.15

Time	I_t (W/m^2)	T_{out} (ºC) with turbulator	T_{out} (ºC) without turbulator	T_{in} (ºC)	η_{sc} (%) with turbulator	η_{sc} (%) without turbulator
9.00	574	94	88	30	30.75	27.87
9.30	684	115	97	33	33.06	25.80
10.00	795	138	119	35	35.73	29.14
10.30	830	177	170	36	46.85	44.52
11.00	880	196	188	36	50.14	47.63
11.30	910	213	202	37	53.34	50.00
12.00	956	225	210	38	53.94	49.62
12.30	984	235	215	39	54.93	49.32
13.00	960	230	210	42	54.00	48.26
13.30	929	226	207	43	54.32	48.68
14.00	915	219	200	44	52.74	47.02
14.30	850	211	194	43	54.50	48.99
15.00	798	200	188	42	54.60	50.45
15.30	720	186	172	41	55.54	50.17
16.00	600	145	136	40	48.26	44.12
16.30	500	117	100	34	45.78	36.40

Table AIII.9 Data points for Fig 5.16

Time	I_t (W/m^2)	T_{out} (ºC) with turbulator	T_{out} (ºC) without turbulator	T_{in} (ºC)	η_{sc} (%) with turbulator	η_{sc} (%) without turbulator
9.00	600	114	100	29	31.90	26.64
9.30	695	139	114	31	34.99	26.89
10.00	782	169	135	33	39.16	29.37
10.30	846	218	180	34	48.97	38.86
11.00	913	247	207	34	52.53	42.67
11.30	960	260	212	36	52.54	41.28
12.00	986	271	221	37	53.44	42.02
12.30	992	280	240	38	54.93	45.85
13.00	991	277	238	39	54.08	45.21
13.30	954	272	235	42	54.28	45.55
14.00	911	268	225	43	55.61	44.98
14.30	852	259	215	45	56.56	44.93
15.00	801	233	187	44	53.13	40.20
15.30	703	215	164	43	55.09	38.76
16.00	605	179	135	41	51.36	34.98
16.30	536	154	112	36	49.57	31.93

Table AIII.10 Data points for Fig 5.17

Time	I_t (W/m^2)	T_{out} (°C) with turbulator	T_{out} (°C) without turbulator	T_{in} (°C)	η_{sc} (%) with turbulator	η_{sc} (%) without turbulator
9.00	610	175	134	28	38.37	27.67
9.30	738	222	158	37	39.91	26.10
10.00	815	252	205	34	42.59	33.41
10.30	903	302	249	32	47.61	38.26
11.00	953	318	276	32	47.78	40.76
11.30	998	327	285	34	46.74	40.04
12.00	1003	336	291	35	47.78	40.64
12.30	1014	338	295	36	47.42	40.67
13.00	977	324	284	41	46.12	39.60
13.30	972	323	280	42	46.03	38.98
14.00	912	316	269	44	47.49	39.28
14.30	853	299	254	44	47.60	39.20
15.00	760	271	240	43	47.76	41.27
15.30	675	238	221	40	46.70	42.69
16.00	585	218	207	40	48.45	45.45
16.30	488	185	175	35	48.94	45.68

References

[1]   Demirbas A. Global renewable energy projections. Energy Sources 2009; 4:212–24.

[2]   Energy statistics. Central statistics office. Ministry of statistics and programme implementation. Government of India. New Delhi. 2018.

[3]   Variable Renewable Energy Sources Integration. Energy 4.0: Energy transition towards 2030. February 2018.

[4]   Sukhatme SP, Nayak JK. Solar Energy Principles of Thermal Collection and Storage. McGraw Hill 2011; 3rd Edition.

[5]   Kalogirou SA. Solar Energy Engineering– Process and Systems. Academic Press; 2009.

[6]   Garg HP, Prakash J. Solar Energy Fundamentals and Applications. Tata McGrew Hill 2011:282.

[7]   Hassan HZ, Mohamad AA. A review on solar cold production through absorption technology. Renewable and Sustainable Energy Reviews 2012; 16:5331–48.

[8]   Anisur MR, Mahfuz MH, Kibria MA, Saidur R, Metselaar IHSC, Mahlia TMI. Curbing global warming with phase change materials for energy storage. Renewable and Sustainable Energy Reviews 2013; 18:23–30.

[9]   Hassan HZ and Mohamad AA. A review on solar-powered closed physisorption cooling systems. Renewable and Sustainable Energy Reviews 2013; 16:2516-38.

[10]   Ullah KR, Saidur R, Ping HW, Akikur RK, Shuvo NH. A review of solar thermal refrigeration and cooling methods. Renewable and Sustainable Energy Reviews 2013; 24:499–513.

[11]   Li ZF, Sumathy K. Technology development in the solar absorption air-conditioning systems. Renewable and Sustainable Energy Reviews 2000; 4: 267–93.

[12]   Srikhirin P, Aphornratana S, Chungpaibulpatana S. A review of absorption refrigeration Technologies. Renewable and Sustainable Energy Review 2001; 5:343-72.

[13]   Ataer OE, Gogus Y. Comparative study of irreversibilities in an aqua-ammonia absorption refrigeration system. International Journal of Refrigeration 1991; 14:86-92.

[14]   Dincer I, Dost S. Energy analysis of an ammonia-water absorption refrigeration system. Energy Sources 1996; 18:727-33.

[15]   Chuaa HT, Toh HK, Ng KC. Thermodynamic modeling of an ammonia–water absorption chiller. International Journal of Refrigeration 2002; 25:896–906.

[16] Sahoo PK, Misra RD, Gupta A. Exergoeconomic optimization of an aqua-ammonia absorption refrigeration system. International Journal of Exergy 2004; 1:82-93.

[17] Adewusi SA, Zubair SM. Second law based thermodynamic analysis of ammonia–water absorption systems. Energy Conversion and Management 2004; 45:2355–69.

[18] Ezzine NB, Barhoumi M, Mejbri K, Bellagi A. Second Law Study of Ammonia-Water Double Effect Absorption Chiller. International Refrigeration and Air Conditioning Conference at Purdue 2004:12-15.

[19] Boer D, Medrano M, Nogues M. Exergy and Structural Analysis of an Absorption Cooling Cycle and the Effect of Efficiency Parameters. International Journal of Thermodynamics 2005; 8:191-98.

[20] Kim B, Park J. Dynamic simulation of a single-effect ammonia-water absorption chiller. International Journal of Refrigeration 2007; 30:535-45.

[21] Hasabnis YC, Bhagwat SS. Performance evaluation of ammonia absorption refrigeration cycle based on exergetic coefficient of performance. International Journal of Exergy 2007; 4:19-37.

[22] Darwish NA, Al-Hashimi SH, Al-Mansoori AS. Performance analysis and evaluation of a commercial absorption–refrigeration water–ammonia (ARWA) system. International Journal of Refrigeration 2008; 31:1214-23.

[23] Sathyabhama A, Ashokbabu TP. Thermodynamic simulation of ammonia-water absorption refrigeration system. Thermal Science 2008; 12 (3):45-53.

[24] Barhoumi M, Ben Ezzine N, Bellagi A. Exergy analysis of an ammonia-water absorption system. International Journal of Exergy 2009; 6:698-714.

[25] Kong D, Liu J, Zhang L, He H, Fang Z. Thermodynamic and Experimental Analysis of an ammonia-Water Absorption Chiller. Energy and Power Engineering 2010; 2:298-305.

[26] Matawala VK, Prabhakaran P. Exergoeconomic analysis of industrial brine chilling unit using aqua-ammonia vapour absorption refrigeration system. International Journal of Exergy 2011; 8:333-58.

[27] Ouadha A, El-Gotni Y. Integration of an ammonia-water absorption refrigeration system with a marine Diesel engine: A thermodynamic study. Procedia Computer Science 2013; 19: 754 – 61.

[28] Rashidi AMM, Habibzadeh BA, Rezaie CSS. Study of an Absorption Machine for an ammonia-water system Decentralized Trigenation. Journal of Fundamental Applied Science 2016; 8:552-68.

[29] Anand S, Gupta A, Anand Y, Tyagi SK. Use of process steam in vapor absorption refrigeration system for cooling and heating applications: An exergy analysis. Cogent Engineering 2016; 3.

[30] Lamp P, Ziegler F. European research on solar-assisted air conditioning. International journal of refrigeration 1998; 21 (2):89-99.

[31] Sarbu I, Sebarchievici C. Review of solar refrigeration and cooling systems. Energy and Buildings 2013; 67:286–97.

[32] Li z, Ye X, Liu J. Optimal temperature of collector for solar double effect LiBr/H_2O absorption cooling system in subtropical city based on a year round meteorological data. Applied Thermal Engineering 2014; DOI: 10.1016/j.applthermaleng.2014.04.039.

[33] Abdulateef JM, Murad NM, Alghoul MA, Zaharim A, Sopian K. Experimental Study On Combined Solar-Assisted Ejector Absorption Refrigeration System. Solar Energy Research Institute. Universiti Kebangsaan Malaysia. 43600 Bangi Selangor, MALAYSIA: 162-66.

[34] Sirwan R, Ali Y, Zaharim A, Sopian K. Effect of adding flash tank on the evaporator's thermal load of the combined ejector-absorption cooling system. 10th WSEAS International Conference on System Science &Simulation in Engineering 2011:124-27.

[35] Staicovici MD. Polybranched regenerative GAX cooling cycles. International journal of refrigeration 1995; 18 (5):318–29.

[36] Staicovici MD. An autonomous solar ammonia–water refrigeration system. Solar Energy 1986; 36 (2):115–24.

[37] Alvares SG, Trepp C. Simulation of a solar driven aqua-ammonia absorption refrigeration system part-1 mathematical description and system optimization. International Journal of Refrigeration 1987; 10:40-48.

[38] Kaushik SC, Rao SK, Kumari R. Dynamic simulation of an aqua-ammonia absorption cooling system with refrigerant storage. Energy Conservation and Management 1991; 32 (3):197-206.

[39] De Francisco A, Illanes R, Torres JL, Castillo M, De Blas M, Prieto E, Garcıa A. Development and testing of a prototype of low power water–ammonia absorption equipment for solar energy applications. Renewable Energy 2002; 25:537–44.

[40] Adel A. Al-Hemiri, Ahmed DN. The use of direct solar energy in absorption refrigeration employing NH_3-H_2O system. Iraqi journal of chemical and petroleum engineering 2010; 11 (4):13-21.

[41] Shankar R, Srinivas T. Solar thermal based power and vapour absorption refrigeration system. Procedia Engineering 2012; 38:730 – 36.

[42] Anand S, Gupta A, Tyagi SK. Renewable energy powered evacuated tube collector refrigerator system. Mitig Adapt Strateg Glob Change 2013; DOI 10.1007/s11027-013-9461-3.

[43] Siddiqui FR, El-Shaarawi MAI, Said SAM. Exergo-economic analysis of a solar driven hybrid storage absorption refrigeration cycle. Energy Conversion and Management 2014; 80: 165–72.

[44] Khan MMA, Ibrahim NI, Saidur R, Mahbubul IM, Al-Sulaiman FA. Performance assessment of a solar powered ammonia-water absorption refrigeration system with storage units. Energy Conservation and Management 2016; 126:316-28.

[45] Stanciu C, Stanciu D, Gheorghian A. Thermal analysis of a solar powered absorption cooling system with fully mixed thermal storage at startup. Energies 2017; 10.

[46] Nakahara N, Miyakawa Y, Yamamoto M. Experimental study on house cooling and heating with solar energy using flat plate collector. Solar Energy 1977; 19 (6):657–62.

[47] Hammad M, Audi M. Performance of a solar LiBr-water absorption refrigeration system. Renew Energy 1992; 2:275-82.

[48] Hammad M, Zurigat Y. Performance of a second generation solar cooling unit. Solar Energy 1998; 62:79-84.

[49] Chen G, Hihara E. A new absorption refrigeration cycle using solar energy. Solar Energy 1999; 66 (6):479-82.

[50] Syed A, Izquierdo M, Rodriguez P, Maidmet G, Missenden J, Lecuona A, Tozer R. A novel experimental investigation of a solar cooling system in Madrid. International Journal of Refrigeration 2005; 28 (6):859–71.

[51] Arora S, Chitkara S, Udayakumar R, Ali M. Thermal analysis of evacuated solar tube collectors. Journal of Petroleum and Gas Engineering 2011; 2(4):74-82.

[52] Raja VB, Shanmugam V. A review and new approach to minimize the cost of solar assisted absorption cooling system. Renewable and sustainable energy reviews 2012; 16:6725-31.

[53] Wu C, Chen L, Sun F. Optimization of solar absorption refrigerator. Applied Thermal Engineering 1997; 17 (2):203-08.

[54] Abdulateef JM, Sopian KZ, Alghoul MA, Sulaiman MY, Zaharim A, Ahmad I. Solar absorption refrigeration system using new working fluid pairs. International Journal of Energy 2007; 1 (3): 82-87.

[55] Kim DS, Infante Ferreira CA. Solar refrigeration options – a state-of-the-art review. International Journal of Refrigeration 2008; 31:3-15.

[56] Kalogirou S. The potential of solar industrial process heat applications. Applied Energy 2003; 76: 337–61.

[57] Mohammadkarim A, Kasaeian A, Kaabinejadian A. Performance investigation of solar evacuated tube collector using TRNSYS in Tehran. International journal of renewable energy research 2014; 4 (2):497-503.

[58] Milani D, Abbas A. Multiscale modeling and performance analysis of evacuated tube collectors for solar water heaters using diffuse flat reflector. Renewable Energy 2016; 86:360-74.

[59] Pei G, Li G, Zhou X, Ji J, Su Y. Comparative experimental analysis of the thermal performance of evacuated tube solar water heater systems with and without a mini-compound parabolic concentrating (CPC) Reflector($C < 1$). Engineers 2012; 5:911-24.

[60] Ong KS, Tong Wl. System performance of U-tube and heat pipe solar water heaters. Journal of Applied Science and Engineering 2012; 15 (2):105-10.

[61] Ayompe LM, Duffy A. Thermal performance analysis of a solar water heating system with heat pipe evacuated tube collector using data from a field trial. Solar Energy 2013; 90:17–28.

[62] Chow SP, Harding GL, Zhiqlang Y. Optimization of evacuated tubular solar collector arrays with diffuse reflectors. Solar energy 1984; 33 (3/4):277-82.

[63] Ma L, Lu Z, Zhang J, Liang R. Thermal performance analysis of the glass evacuated tube solar collector with U-tube. Building and Environment 2010; 45:1959-67.

[64] Sharma N, Diaz G. Performance model of a novel evacuated-tube solar collector based on minichannels. Solar Energy 2011; 85:881–90.

[65] Demianiuk A, Adam Sorko S. Analysis of flow and thermal phenomena in evacuated tube collectors. acta mechanica et automatic 2012; 6 (4):5-10.

[66] Jradi M, Riffat S. Medium temperature concentrators for solar thermal applications. International Journal of Low-Carbon Technologies 2014; 9:214-24.

[67] Sabiha MA, Saidur R, Mekhilef S, Mahian O. Progress and latest developments of evacuated tube solar collectors. Renewable and Sustainable Energy Reviews 2015; 51:1038–54.

[68] Kiran Naik B, Varshney A, Muthukumar P, Somayaji C. Modelling and performance analysis of U type evacuated tube solar collector using different working fluids. Energy Procedia 2016; 90:227- 37.

[69] Picon-Nunez M, Martinez-Rodriguez G, Fuentes-Silva AL. Targeting and design of evacuated tube solar collector networks. Chemical engineering transactions 2016; 52:859-64.

[70] Kim Y, Seo T. Thermal performances comparisons of the glass evacuated tube solar collectors with shapes of absorber tube. Renewable Energy 2007; 32:772–95.

[71] Zambolin E, Del Col D. Experimental analysis of thermal performance of flat plate and evacuated tube solar collectors in stationary standard and daily conditions. Solar energy 2010; 84:1382-96.

[72] Hayek M, Assaf J, Lteif W. Experimental investigation of the performance of evacuated-tube solar collectors under eastern Mediterranean climatic conditions. Energy Procedia 2011; 6:618–26.

[73] Nkwetta DN, Smyth M. Performance analysis and comparison of concentrated evacuated tube heat pipe solar collectors. Applied Energy 2012; 98:22-32.

[74] Umayal Sundari AR, Neelamegam P, Subramanian CV. Performance of evacuated tube collector solar dryer with and without heat sources. Iranica Journal of Energy & Environment 2013; 4:336-42.

[75] Li X, Dai YJ, Li Y, Wang RZ. Comparative study on two novel intermediate temperature CPC solar collectors with the U-shape evacuated tabular absorber. Solar Energy 2013; 93:220-34.

[76] Ricci M, Bocci E, Michelangeli E, Micangeli A, Villarini M, Naso V. Experimental tests of solar collectors prototypes systems. Energy Procedia 2015; 82:744–51.

[77] Ghoneim AA, Shabana HM, Shaaban MS, Mohammedein AM. Performance analysis of evacuated tube collector in hot climate. European International Journal of Science and Technology 2016; 5 (3):8-20.

[78] Cabanillas RE, Estrada CA, Avila F. A device for measuring the angular distribution of incident radiation on tubular solar collectors. Renewable energy 1995; 6 (7):843-47.

[79] Ghoneim AA, Mohammedein AM, Kandil KA. Performance analysis of parabolic trough collector in hot climate. British Journal of Applied Science & Technology 2014; 4 (14):2038-58.

[80] Bellos E, Tzivanidis C, Antonopoulos KA. A detailed working fluid investigation for solar parabolic trough collectors. Applied Thermal Engineering 2016; DOI: 10.1016/ l.applthermaleng.2016.11.201.

[81] Arora CP. Refrigeration and air conditioning. McGraw Hill education, Third edition 2009: 401-06.

[82] Park Y, Sonntag R. Thermodynamic properties of ammonia-water mixtures: a generalized equation-of-state approach. ASHRAE Trans 1990; 96:150-59.

[83] McNeely L. Thermodynamic properties of aqueous solutions of lithium bromide. ASHRAE Trans 1979; 85:413-34.

[84] Lee R, DiGuilio R, Jeteter S, Teja A. Properties of lithium bromide-water solutions at high temperatures and concentrations-part II: density and viscosity. ASHRAE Trans 1990; 96:709-14.

[85] Lenard J, Jeter S, Teja A. Properties of lithium bromide-water solutions at high temperatures and concentrations-part IV vapor pressure. ASHRAE Trans 1992; 98:167-72.

[86] Jeter S, Moran J, Teja A. Properties of lithium bromide-water solutions at high temperatures and concentrations-part III: specific heat. ASHRAE Trans 1992; 98:137-49.

[87] Patek J, Klomfar J. Simple functions for fast calculations of selected thermodynamic properties of ammonia-water system, International journal of refrigeration 1995; 18 (4):228-34.

[88] Bennani N, Prevost M, Coronas A. Absorption heat pump cycle: performance analysis of water glycerol mixture. Heat Recovery System and CHP 1989; 9 (3):257–63.

[89] Grover GS, Eisa MAR, Holland FA. Thermodynamic design data for absorption heat pump system operating on water-lithium chloride: part I cooling. Heat Recovery System and CHP 1988; 8 (1):33–41.

[90] Idema P. D. Simulation of stationary operation and control of a LiBr/ZnBr$_2$/CH$_3$OH absorption heat pump system, directly fired heat pump. Procs. Int. Conf. University of Bristol 1984: paper 2.1.

[91] Best R, Porras L, Holland FA. Thermodynamic design data for absorption heat pump system operating on ammonia-nitrate: part I cooling. Heat Recovery System and CHP 1991; 11 (1):49–61.

[92] ASHRAE Handbook Fundamentals 2009:29.4-29.6.

[93] Sun DW, Eames IW, Aphornratana S. Evaluation of a novel combined ejector-absorption refrigeration cycle: computer simulation. International Journal of Refrigeration 1996; 19 (3):172-180.

[94] Kherris S, Makhlouf M, Zebbar D, Sebbane O. Contribution study of the thermodynamics properties of the ammonia-water mixture. Thermal science 2013; 17 (3):891-902.

[95] Cengle YA, Boles MA. Thermodynamics An engineering Approach. McGraw-Hill publications.

[96] Huang FF. Engineering Thermodynamics Fundamentals and Applications. Macmillan Publishing Company; 1989.

[97] Roy RK. A Primer on the Taguchi Method. Second Edition; 2010.

[98] www.apricus.com

[99] Duffie JA, Beckman WA. Solar engineering of thermal processes. John Wiley & Sons, New York 2006.

[100] Ali M El-Nashar. Renewable energy systems and desalination. Vol. II. Evacuated tube collectors.

[101] Gnielinski V. New equations for heat and mass transfer in turbulent pipe and channel flow. International chemical engineering 1976; 16 (2):359–63.

[102] Bhatt NM. Investigation for improving techno economic liability of solar cold store for potato with emphasis on solar collector. PhD thesis, IIT, Bombay; 2007.

[103] Mittal MK, Varshney L. Optimal thermodynamic performance of a wire mesh packed solar air heater. Solar Energy 2006; 80:1112-1120.

[104] Kline SJ, McClintock FA. Describing uncertainty in single-sample experiments. Mech. Eng. 1953: 3.